SAPIENZA
UNIVERSITÀ DI ROMA

DOTTORATO DI RICERCA IN BIOCHIMICA
CICLO XXVI (A.A. 2010-2013)

EXPLORING THE MICROGLIA PROTEOME IN AN ALZHEIMER'S DISEASE CELLULAR MODEL

DOTTORANDA
VIRGINIA CORREANI

TUTOR
PROF.SSA M. EUGENIA SCHININÀ

COORDINATORE
PROF. FRANCESCO MALATESTA

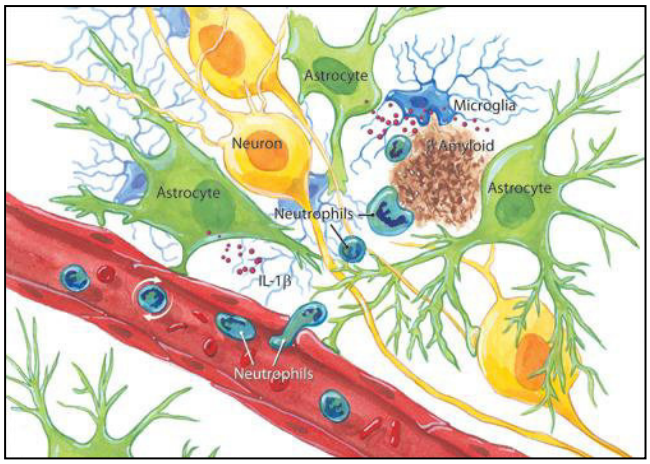

DICEMBRE 2013

SAPIENZA
UNIVERSITÀ DI ROMA

DOTTORATO DI RICERCA IN BIOCHIMICA
CICLO XXVI (A.A. 2010-2013)

EXPLORING THE MICROGLIA PROTEOME IN AN ALZHEIMER'S DISEASE CELLULAR MODEL

DOTTORANDA
VIRGINIA CORREANI

TUTOR
PROF.SSA M. EUGENIA SCHININÀ

COORDINATORE
PROF. FRANCESCO MALATESTA

DICEMBRE 2013

Cover image from:
R&D System
(http://www.rndsystems.com/Cytokine_cb08i2_IL1betaNeuroinflammation.aspx)

TABLE OF CONTENTS

CHAPTER 1
INTRODUCTION

1.1 Microglia

Microglial cells represent one of the three glial sub-population of the Central Nervous System (CNS).They have been described for the first time in 1899 by Franz Nissl, who named them “rod cell” because of the shape of the rod-shaped cell body. However, only many years later, Pio del Rio-Hortega, using the silver carbonate staining, identified these cells as a population independent from astrocytes and oligodendrocytes and coined the term “microglia”. Based on morphological similarity with macrophages, he hypothesized that microglial cells derive from circulating blood monocytes and that they have the ability to transform from resting cells to activated macrophages. Indeed, unlike the other cells of the nervous system, microglia originate from hematopoietic stem cells in the fetal yolk sac. During the early phases of the embryonic development, before the formation of the blood brain barrier, the myeloid progenitors of microglia migrate toward the developing brain where they differentiate into mature microglial cells (Ransohoff & Cardona, 2010). At the end of the fetal development, microglia have settled in all regions of the nervous system, including the retina. In the adult brain,microglia represent about 12% of the nervous cells and are distributed differently among brain regions: predominantly in the gray matter, with the highest concentration in hippocampus, olfactory telencephalon, basal ganglia and *substantia nigra* (Lawson *et al*., 1990).

In the mature brain, microglial cells are generally found in quiescent form, characterized by a branched shape. However, morphological studies, based on the silver carbonate staining, have shown the existence of other types of morphology: an amoeboid and some intermediate forms. This morphological classification is also used to describe the state of activation of the microglia: the quiescent highly ramified cells undergo reversible morphological transitions (Fig. 1.1) toward an active and phagocytic state, characterized by an amoeboid morphology, getting through to “primed” states with an intermediate shape between ramified and amoeboid (Kim & de Vellis, 2005).

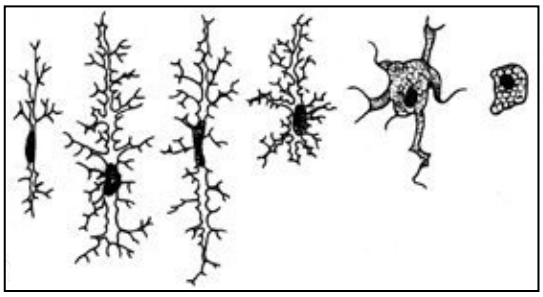

Fig. 1.1 Transformation of resting microglia (left end) into activated (right end; Kreutzberg, 1996).

1.1.a Resting microglia

In healthy brain, microglia are in a resting state characterized by a highly ramified morphology. However, these cells are not really inactive. *In vivo* studies on transgenic mice brain by two- photon microscopy have shown that the cellular processes of microglia are highly motile and in continuous remodeling. These membranous processes sample randomly the extracellular environment and remove metabolites and cellular debris accumulated in the parenchyma. This activity of perception and interpretation of environmental signals is essential for the establishment of a fast response to pathogens and brain lesions (Nimmerjahn *et al*., 2005).

Usually, the microglial activation is triggered by the recognition of exogenous factors not present in the nervous system under normal conditions (*e.g.* microbial structures and serum components), factors usually present in low concentration (*e.g.* intracellular constituents), and molecules present in an abnormal state (*e.g.* aggregated proteins; Hanisch & Kettenmann, 2007).
In order to detect and interpret all these potential insults, microglia constitutively express different kind of receptors: the Toll like receptors (TLRs) family; scavenger receptors (*e.g.* CD36 and MARCO); integrin receptors (*e.g.* MAC1); IgG superfamily receptors (*e.g* .receptor for advanced glycation end products); other receptors for chemokines, cytokines, complement factors and immunoglobulins (Block *et al*., 2007).

Interestingly, the brain evolved various safety measures to keep microglia in a resting state. These kind of regulatory mechanisms allow neurons to inhibit microglial activation until tissue homeostasis is perturbed. For example, various secreted neurotransmitters, such as dopamine and noradrenaline, show modulatory effects on microglia (Faber & Kettenmann, 2005). Furthermore, CD200, a membrane glycoprotein expressed by neurons, interacts with its cognate receptor on microglia (CD200R) to deliver regulatory signals (Hoek *et al*., 2000). Also some chemokines produced by neurons, as fractalkine (CX3CL1), can restrict microglial activity when bound their receptors (Cardona *et al*., 2006). The loss of these signals, due to the impairment of neurons, triggers microglial response and activation.

1.1.b Activated microglia functions

Beyond morphological changes, the activation process is characterized by an increased proliferation, migration toward the lesion and some dramatic changes in their function. In fact, microglia adjust the response according to environmental changes and to the nature of injury that affect the CNS (Ransohoff & Perry, 2009).

Depending on the environment in which microglia are activated, they can either take on a "classically activated" (also called M1) phenotype or an "alternatively activated" (also called M2) phenotype (Mantovani *et al.*, 2004). M2 microglia are typically considered less inflammatory than M1 cells and are characterized by reduced nitric oxide production and increased anti-inflammatory cytokine production (Lucin & Wiss-Coray, 2009). A brief description of the principal microglial functions is reported below.

Phagocytosis

An efficient phagocytic process is necessary for the maintenance of tissue homeostasis. Antigens (*i.e.* cellular debris, apoptotic cells, viruses, bacteria, abnormal proteins and peptides) may be recognized by receptors directly. Some of these receptors serve to tether the phagocyte and the target together; others trigger internalization, such as TLRs and scavenger receptors (Underhill & Goodridge, 2012; Sierra *et al*., 2013). In addition, engulfment can also triggered by soluble opsonins that bind to receptors and send an internalization signal. Antibodies and proteins of the complement system bind to phagocyte Fc receptors and complement receptor, respectively, and mediate phagocytosis. Particles are thus incorporated into a coated vesicle, the phagosome, which in turn merges with lysosomes. Inside the lysosomal compartment, the swallowed material is subjected to phagocytic oxidase, which promotes the production of oxygen free radicals (ROS), and to inducible nitric oxide synthase (iNOS), and it is digested by means of numerous lysosomal proteases.

Oxidative Burst

Microglia can release a variety of cytotoxic substances. Indeed, microglial cells are a potent source of free radicals. The protein complex involved in the production of extracellular ROS is NADPH oxidase, an enzymatic complex composed of different cytoplasmic and membrane subunits, which catalyzes the conversion of oxygen to superoxide when activated in response to different environmental stimuli (Babior, 1999). Following microglia activation, the regulatory subunits dispersed into the cytosol translocate on the membrane to form the active enzymatic complex through the binding of catalytic subunits (Wilkinson & Landreth, 2006).

Furthermore, NADPH oxidase seems to be crucial for microglial cell signaling. Indeed, the increase of superoxide and intracellular ROS are thought to be involved in the modification of gene expression by means of kinase cascades and the activation of transcription factors. These events culminate in the acquisition of an activated morphology, proliferation and production of pro-inflammatory molecules, such as nitric oxide (NO) by expression of iNOS (Qin *et al*., 2004). Both ROS and NOS (Nitric Oxide Species), can directly damage cells and lead to neuronal cell

death. The cytotoxic secretion is addressed to destroy infected neurons, viruses and bacteria, but can also cause many collateral damage to healthy neurons.

Innate immune response

Other molecules are secreted by activated microglia, such asinterleukin-1 (IL-1) and tumor necrosis factor α (TNF-α), are necessary for the establishment of the inflammatory process. These two cytokines act both in an autocrine way, through the activation and recruitment of local glia (microglia and astrocytes), and in a paracrine way, attracting leukocytes, monocytes and other cells of the immune system. Nevertheless, it has been demonstrated that elevated levels of these two cytokines can cause neuronal death supporting the hypothesis that a chronic inflammatory response can lead to neural damage on a large scale, as microglial cells impair the brain in an attempt to eliminate the infection (Harry & Kraft, 2008).
Microglial cells, like macrophages, also secrete other pro-inflammatory cytokines, such as IL-6 and IL-8, which attract T lymphocytes and promote the growth and differentiation of B lymphocytes, and immunomodulatory cytokines, such as IL-12 (Town *et al*., 2005).

Adaptive immune response and antigen presentation

Activated microglia can also work as antigen presenting cells (APC) similarly to peripheral macrophages, dendritic cells and lymphocytes B.
In fact, after the recognition, microglia can swallow and process the antigen in order to rapidly present it to T lymphocytes through the major histocompatibility complex (MHC) types I and II (O'Keefe *et al*., 2002; Beauvillain *et al*., 2008). The MHC-I, potentially expressed by all nucleated cells, is able to present antigen to CD8+ cytotoxic T lymphocytes; the MHC-II, expressed by professional APC cells and macrophages, is recognized by CD4+ helper T lymphocytes. Then T lymphocytes, after passing the blood-brain barrier, are physically in contact with the antigen and co-stimulatory molecules (*i.e.* CD40 and B7) on the surface of reactive microglia. This process results in a full activation, differentiation and proliferation of lymphocyte cells specific for a certain antigen. The activated lymphocytes fulfill different tasks: the CD4+ cells (helper) recruit macrophages and eosinophils; the CD8+ cells secrete proteins able to create pores in the plasma membrane of target cells and induce apoptosis.

Suppression of inflammation and tissue repair

In the appropriate microenvironment, microglia can also produce anti-inflammatory cytokines, such as IL-10, IL-4 and TGF-β, in order to prevent a too long lasting inflammatory response. Furthermore, they can inhibit phagocytosis, proliferation, cell migration and chemotaxis of macrophages (Strle *et al*., 2002; Boche *et al*., 2006; Harry & Kraft, 2008).

At the same time, microglia undertakes a series of actions to facilitate the regrowth of nerve tissue through the secretion of neurotrophic growth factors (*e.g.* brain-derived neurotrophic factor and glial cell-derived neurotrophic factor), stripping of synapses and removal of extracellular glutamate (Trapp *et al.*, 2007; Hanish & Kettenmann, 2007).

1.2 Microglia and neurodegeneration

Since neurons have limited proliferative and regenerative capacities, the nervous system is extremely vulnerable to sustained inflammatory processes (Fanfara *et al.*, 2008; Gao & Hong, 2008; Khoury & Luster, 2008). A large number of data indicates that an excessive and uncontrolled inflammatory processes may contribute to the loss of neurons during neurodegenerative diseases, but how and how much inflammation is involved in the chronic progression of these diseases remains largely unknown (Perry *et al.*, 2010).

The role of inflammation has been demonstrated in part by stimulation of the cells with environmental stimuli (*e.g.* aggregated proteins): in these cases, it is often observed that a robust secretion of cytotoxic and/or inflammatory factors can accelerate neuronal death (Liu & Hong, 2003). Moreover, the persistent microglial activation was studied using different neurotoxins, such as MPP+ (1-methyl-4-phenylpyridine) and MnEBDC (manganese ethylene bisdithiocarbamate): neuronal sensitivity increases proportionally with the quantity of microglia added to neuron cell cultures (Zhou *et al.*, 2005). Furthermore, treatment with anti-inflammatory drugs (*e.g.* aminopiridazine and glucocorticoids), which suppress the activation of microglial cells, inhibits neurodegeneration (Craft *et al.*, 2004; Sugama *et al.*, 2009).

The extent of immune system reaction depends on the level of injury, its duration, the genetic predisposition of an individual and contemporary events (*e.g.* other diseases or stress); the combined effects of these events could determine the role, if neuroprotective or neurotoxic, should have the microglia. If an inflammatory reaction is temporally regulated and the antigen is removed, the inflammation has a beneficial effect. However, if the insult exceeds the threshold then a chronic inflammatory process is established (Gao & Hong, 2008). Therefore, the microglial activity during neurodegenerative diseases could represent a “double-edged sword”: in the early phase, their role is essential for the removal of neurotoxic peptides; however, with the progression of the disease, it is observed a progressive dysfunction of the microglia, which reduces its phagocytic ability and increases its pro-inflammatory and neurotoxic functions, up-regulating the production of cytokines and ROS (Hickman *et al.*, 2008; Aguzzi *et al.*, 2013).

1.2.a Microglia in Alzheimer's disease

Alzheimer's disease (AD) is an age-related neurodegenerative disorder characterized by a progressive loss of neurons and synapses mostly in the cerebral cortex (Uylings & de Brabander, 2002). These events are associated with the presence of extracellular plaques and of intracellular neurofibrillary tangles.

The latter are made up of the microtubule-associated protein Tau that, following hyperphosphorylation, dissociates from microtubules and aggregates in the cytoplasm. This event lead to microtubule network destabilization and cell dysfunction (Fig. 1.2; Chun *et al*., 2007).

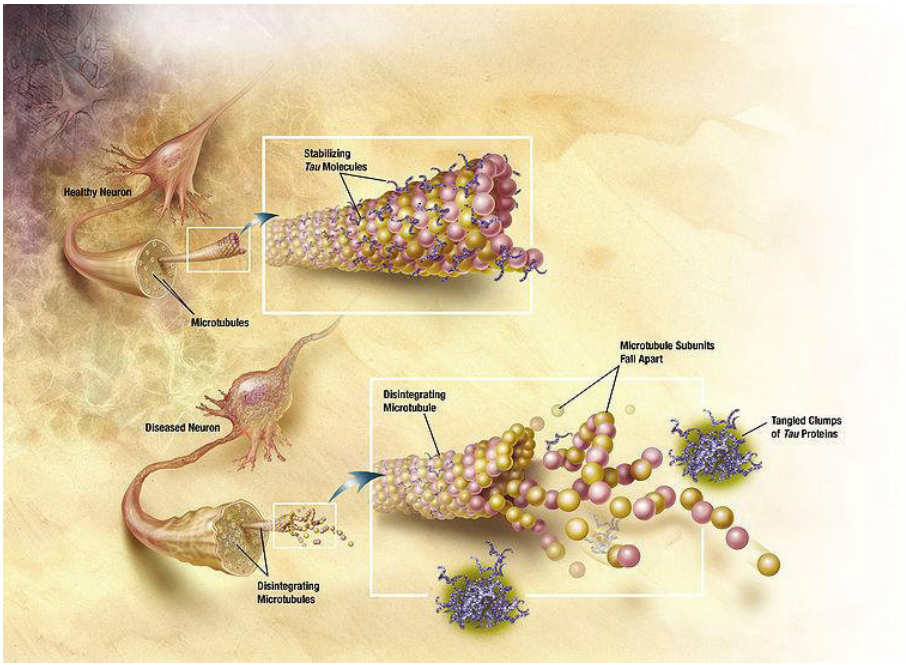

Fig. 1.2 Representation of microtubules disintegration induced by Tau hyperphosphorylation and aggregation during Alzheimer's disease (from "Alzheimer's Disease Education and Referral Center, a service of the National Institute on Aging").

The extracellular senile plaques consist of insoluble proteinaceous deposits of aggregated amyloid β peptides (Aβ) in particular the 42- ($A\beta_{1-42}$) and 40-residues ($A\beta_{1-40}$) species (Maler *et al*., 2007). These peptides are generated by the sequential action of two proteases, the β-secretase and the γ-secretase (Esch *et al*., 1990), which cleave the "Amyloid Precursor Protein" (APP), an integral plasma membrane protein (Fig. 1.3; Goedert & Spillantini, 2006). Mutations of the APP gene are associated to a familiar form of Alzheimer's disease characterized by an autosomal dominant inheritance and early onset, usually before age 65 (Blennow *et al*., 2006). All the known mutations are located in the cleavage sites of secretases and increase

amyloid production (Selkoe, 1997), particularly of $A\beta_{1-42}$, the amyloid species more prone to aggregation. However, the majority of AD cases are sporadic rather than familial. The best known genetic risk factor is represented by the inheritance of the ε4 allele of the apolipoprotein E (APOE) gene (Mahley *et al*., 2006); this allele increase the probability to develop AD by three times in heterozygotes and 15 times in homozygotes.

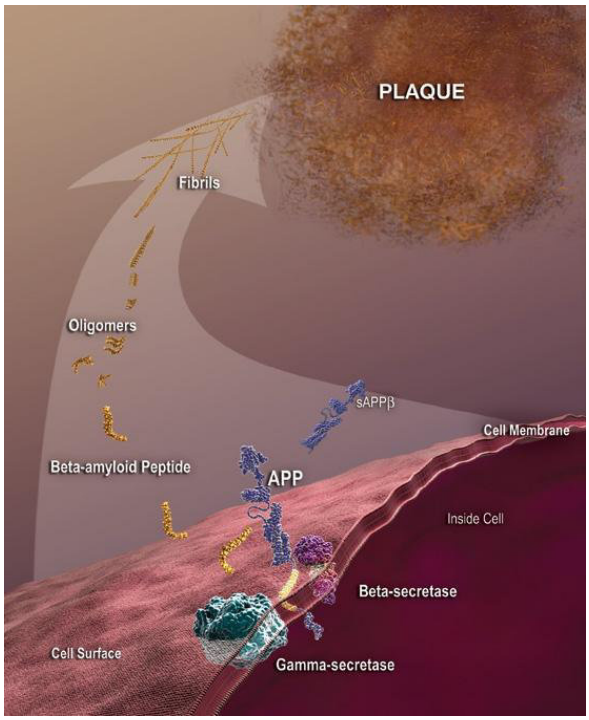

Fig. 1.3 Representation of β amyloid plaque formation (from "Alzheimer's Disease Education and Referral Center, a service of the National Institute on Aging").

The amyloid fibrils and plaque, have long been thought to be responsible of neurodegeneration observed in AD (Hardy & Higgins, 1992; Lansbury & Lashuel, 2006). Recently, clear evidences point to the role of soluble amyloid oligomers as the major cause of neurotoxicity (Hardy & Selkoe, 2002; Haass & Selkoe, 2007). However, it is not fully understood how these sopramolecular species prime intracellular toxic effects but several evidence suggest that they interact with receptors or specific proteins on the plasma membrane of neuronal cells changing the intracellular environment (Larson & Lesné, 2012).

Immunohistochemical studies demonstrated that microglia in a healthy brain are uniformly distributed between gray matter and white matter, while they are grouped around the amyloid deposits in an AD diseased brain (McGeer *et al*., 1987; Heneka

& O'Banion, 2007). Furthermore, in transgenic mouse models of AD, microglia are observed to accumulate within the core of amyloid plaques (Fig. 1.4; Frautschy *et al*., 1998), where they are able to phagocyte amyloid β deposits (D'Andrea *et al*., 2004).

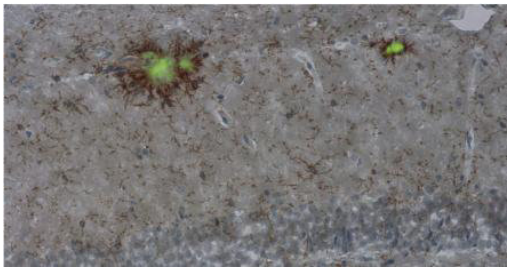

Fig. 1.4 Microglia seem to be clustered around amyloid deposits in brain of transgenic mice. Microglia (brown) were stained with anti-CD11b antibody, while senile-like plaques (green) were stained with Thioflavin-S (Khoury & Luster, 2008).

Several data have shown that amyloid β peptides may act on microglia as inflammatory stimuli to elicit a cellular-mediated response, leading to the release of immunomodulators (Akiyama *et al*., 2000; Eikelenboom *et al*., 2008). The majority of these factors is believed to induce or exacerbate neurodegeneration by causing neuronal apoptosis through mechanisms not yet fully understood (Serrano-Pozo *et al*., 2011).

1.2.b Oxidative stress

Oxidative stress is a pathological condition arising when the production of oxidizing species (*i.e.* ROS and NOS) overcomes the capacity of the antioxidant defences to remove the reactive intermediates or damaged molecules. This redox unbalance could play a critical role in the onset and progression of neurodegenerative pathologies, including AD (Praticò, 2008; von Bernhardi & Eugenín, 2012). Indeed, brain is particularly vulnerable to oxidative stress due to its high aerobic metabolic rate, the paucity of antioxidant defences, the high lipid content, especially polyunsaturated fatty acids, and the post-mitotic nature of neurons. The oxidative stress could be further intensified by concurrent events as mithocondrial dysfunctions, presence of aggregated proteins and activated microglial cells.

The alteration of the normal redox state broadly affects cells and is responsible of covalent modifications of proteins, lipids and nucleic acids (Markesbery *et al*., 1997). Various evidences of damage induced by free radicals have been reported within specific brain region undergoing neurodegeneration. Concerning the AD pathology, markers of lipid peroxidation have been found in the cortex and in the hippocampus (Butterfield *et al*., 2002; Praticò & Sung, 2004); furthermore, markers

of protein oxidation, *i.e.* nitration and carbonylation, resulted increased in the brain of patients affected by AD (Hensley *et al*., 1998; Castegna *et al*., 2003; Boyd-Kimball *et al*., 2005).
However, proteins seems to be the major target of oxidative modifications because of their abundance in biological systems, and their high rate constants of reaction with the free radicals (Davies, 2005).

One of the most relevant redox protein modification is represented by reversible S-thiolation of cysteinyl residues. Even though cysteines are under-represented inside polypeptides, they play a pivotal role in the maintenance of thiol–disulfide homeostasis, protein structure and function. Indeed, cysteinyl residues on the protein surface are the most sensitive to an altered redox potential. The two main factors determining the susceptibility of cysteine residues in redox reactions are: i) the accessibility of the thiol within the protein three-dimensional structure; ii) the reactivity of the cysteine, which is in turn influenced by their enviroment. At a physiological pH, cysteine residues of cytoplasmic proteins have usually a pKa value near to 8.5 and remain in the protonated state in the normal reducing cellular environment. However, in redox-sensitive proteins, there are "active cysteines" showing a lower pKa due to the charge interaction with neighbouring positively charged amino acids; these thiols are more susceptible to oxidative changes (Rhee *et al*., 2000).

Cysteine residues may undergo various modifications on their side chains (Fig. 1.5). Some of these, *i.e.* S-sulfinylation and S-sulfonylation, change irreversibly the chemical-physical properties of the cysteine. Conversely, other modification, such as S-sulfenylation, S-nitrosylation, formation of disulfide bridges or mixed disulfides with glutathione (S-glutathionylation) the major non-enzymatic antioxidant system, are reversible. In particular, this latter modification likely represents the main redox product due to the great abundance of cellular GSH, and to the quick conversion of cysteine-sulfenic acid and S-nitrosocysteine in S-glutathionylcysteine (Mieyal & Gallogly, 2008).

Among these reversible modifications, S-glutathionylation and S-nitrosylation are particularly interesting due to some similarities with phosphorylation, such as enzymatic catalysis and specificity. Indeed, inside the cell, there are enzymes, like thioredoxin or glutaredoxin, able to catalyze the addition/removal of glutathione from target proteins (Lillig & Berndt, 2012; Ghezzi *et al*., 2013). Similar evidences are seen for S-nitrosylation where the level of nitrosocysteines seems to be indirectly regulated by nitrosoglutathione reductase (Janssen-Heininger *et al*., 2008). Furthermore, the oxidative modification of a cysteine is possible only if the chemical environment in which the residue is located determines, as described

above, a decrease in the cysteine pKa that favour deprotonation of its thiol group; this requirement, together with the accessibility of the residue, assures a degree of specificity.

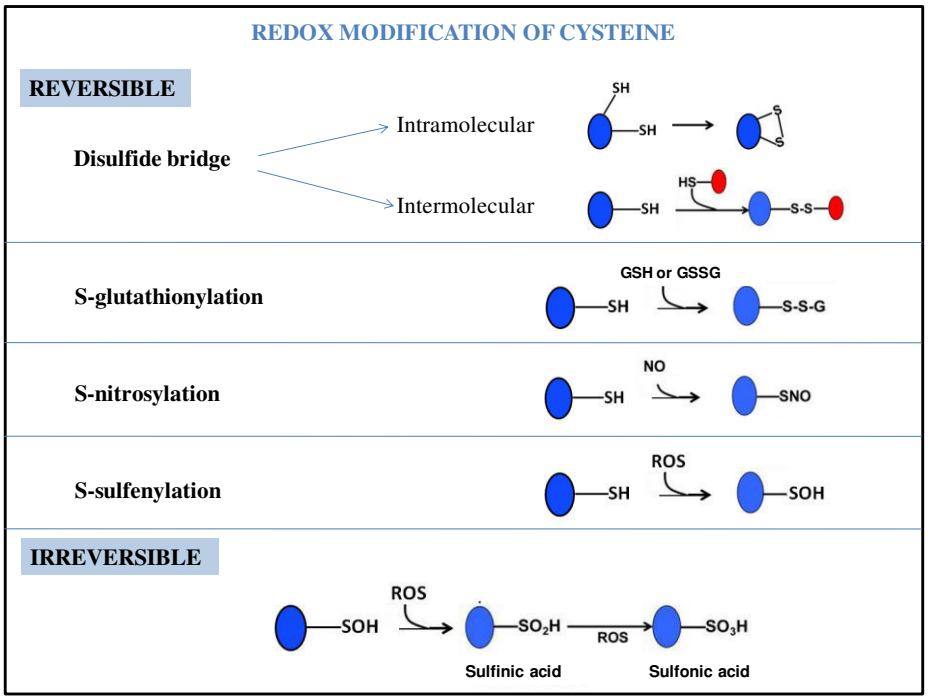

Fig. 1.5 Cysteines in their reduced form could undergo different reversible and irreversible redox modifications by the reaction with ROS, NO radicals or glutathione. ROS can cause vicinal thiols or thiols from different proteins to undergo intra- or intermolecular disulfide bridge formation, respectively. Glutathione, both in reduced and oxidized form, can cause *S*-glutathionylation of protein through two different mechanisms: formation of a mixed disulfide between GSH and protein thiols or disulfide exchange between GSSG and protein thiols. NO cause the *S*-nitrosylation of thiols. ROS cause the *S*-hydroxylation of thiols to form sulfenic acid. Sulfenic acid can further oxidize to sulfinic or sulfonic acids, which represent irreversible oxidations of thiols.

Therefore, S-glutathionylation and S-nitrosylation may, during oxidative stress, not only protect proteins from irreversible modification resulting in their degradation, but may also represent a key mechanism for protein functional regulation and cell signalling both in physiological and pathological conditions (Dalle-Donne *et al*., 2009).

CHAPTER 2
AIM OF THE STUDY

The aim of the present work, which are part of a wide long-term project, is the elucidation of the molecular basis that lead microglia to assume a chronic neuroinflammatory phenotype during neurodegenerative processes. In particular, we focused on the characterization of microglial response during a chronic stimulation with amyloid peptides through the analysis of changes in protein expression levels and the analysis of dynamic post-translational modification (PTM) of proteins.

Thanks to its holistic point of view, proteomics is becoming a suitable approach to expand our understanding of basic biological processes and metabolisms, and their perturbation during pathological conditions. Therefore, proteomics has been extensively used for the study of the complexity of central nervous system and its cell populations in health and disease, with particular regard to neuronal development, activity and injuries (Bajès & Grant, 2009). Despite the growing relevance of microglia due to their involvement in neurodegeneration, only a limited number of genomic and proteomic studies were conducted on microglial activation (Zhou *et al*., 2005; Glanzer *et al*., 2007). When these studies have been carried out using primary microglia cultured from pathological nervous tissues, molecular profiles were able to describe the microglial phenotype at the end point of the pathological activation, but failed to define the genomic or proteomic changes involved in the first steps of the complex pathway leading to the stable activation.

With the aim to highlight molecular pathways involved in the establishment of a stable pro-inflammatory phenotype in microglia during Alzheimer's disease, we used as experimental model an immortalized microglial cell line, named BV2, challenged with the synthetic amyloid β 25-35 peptide ($A\beta_{25-35}$). To achieve a picture of the neuroinflammatory process as global as possible, we collected molecular details on different sub-proteomes (*i.e.* soluble and plasma membrane proteins, and cysteine redox reversible PTMs) applying both classical proteomics approach and new generation quantitative strategies.

CHAPTER 3

EXPERIMENTAL SETUP

3.1 Cell culture conditions

The murine microglial cell line BV2, generated by infecting primary mouse microglial cultures with a v-raf/v-myc oncogene carrying retrovirus (Blasi *et al.*, 1990), were grown in DMEM (Invitrogen) supplemented with penicillin, streptomycin and 10% fetal calf serum (FCS; Sigma Aldrich); cultures were maintained at 37 °C in 5% CO2/95% humidified air atmosphere.
Cell survival was quantified by cell counting using trypan blue exclusion.

3.1.a Stable isotope labeling with amino acids in cell culture (SILAC)

Stable isotope labeling of cultured cells represents a simple and accurate mass spectrometry-based approach for detecting differences in protein abundance among samples. Proteins and peptides of different proteomes can be differentially labeled through the metabolic incorporation of amino acid made of a distinct number of stable isotopic nuclei (*e.g.* ^{13}C, ^{15}N, ^{2}H), introducing a predictable mass difference between peptides from two, or more, experimental conditions (Ong *et al*., 2002; Fig. 3.1).

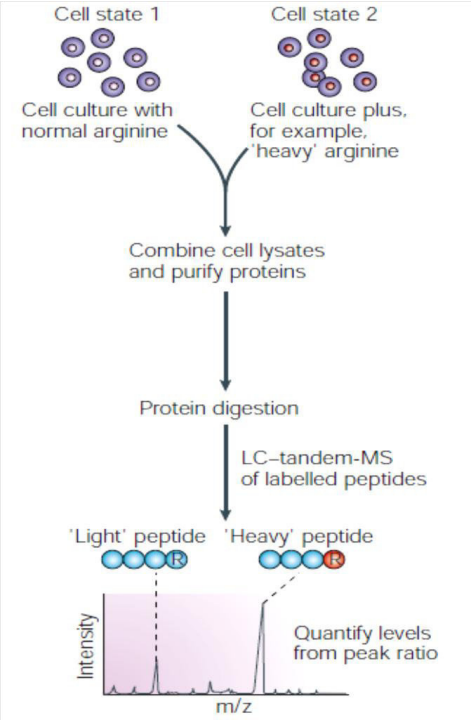

Fig. 3.1 Principle of standard SILAC approach. A stably labelled amino acid in a cell-culture medium (*e.g.* 'heavy' arginine) is fully incorporated into the proteome of one cell population. Relative quantification experiments can easily be carried out using cells that were grown in normal media as the control state. Cell lysates from two conditions can be combined and purified through any number of steps. The proteins are then digested. As the two isotopic forms possess the same chemical-physical properties, the two forms of the peptides co-elute during chromatographic analysis; hence, a peptide ratio can be obtained for each mass spectrum, which allows the protein levels in the two populations to be relatively quantified (Steen & Mann, 2004).

When the SILAC approach was employed for comparative analysis, two different cultured BV2 cells were grown in media (SILAC media) based on arginine, lysine and leucine-free DMEM (Sigma Aldrich) supplemented with 10% dialyzed fetal bovine serum (FBS), 0.8 mM lysine, 0.8 mM leucine, penicillin and streptomycin. However, the two media were distinctive in formulations: one cell population was grown in presence of $^{12}C^{14}N$-arginine (0.28 mM; named "light arginine"), and the other population was grown in presence of $^{13}C_6{}^{15}N_4$-arginine (0.28 mM; named "heavy arginine"). We monitored the incorporation percentage in the proteome of the heavy amino acid by MALDI-TOF mass spectrometry of tryptic digests of selected SDS-PAGE bands (see paragraphs 3.6 b-d).

3.1.b Transient transfection of BV2 cell line

BV2 cells grown in SILAC media were transiently transfected with the expression vector pcDNA3.1/V5-His containing the cDNA of the epsilon isoform of 14-3-3 (kindly supplied by Standaert's group). The protein expressed by this vector was tagged at the C-terminal end with the two epitopes V5 (GKPIPNPLLGLDST) and His_6. The transfection was performed using Lipofectamine® 2000 reagent (Invitrogen) according to the manufacturer.

3.2 $A\beta_{25-35}$ preparation and cell treatment

Synthetic $A\beta_{25-35}$ (GSNKGAIIGLM) and reverse $A\beta_{35-25}$ (MLGIIAGKNSG) peptides (Bachem) were dissolved in sterile, distilled water at a concentration of 1 mM and incubated for 72 h at 37°C to allow aggregation.

BV2 cells were treated for 24 h with 50 μM amyloid peptides.

Regarding the SILAC experiments, only cells grown in presence of $^{13}C_6{}^{15}N_4$-arginine were treated with $A\beta_{25-35}$.

3.3 Characterization of amyloid-induced BV2 activation at cellular level

3.3.a Exocytic activity

Exocytic activity was measured accordingly to the reduction rate of the dye 3-(4,5-dimethylthiazol-2-yl)-2,5-diphenyltetrazolium bromide (MTT) essentially as described (Hansen *et al.*, 1989). This yellow, soluble in water, tetrazolium salt is converted into formazan, insoluble compound of color purple, by the mitochondrial enzyme succinate dehydrogenase, active only in viable cells. Moreover, in amyloid stressed microglia cells, the formed formazan is specifically extruded by exocytosis. Following 24 h treatment with $A\beta_{25-35}$ or $A\beta_{35-25}$, 10 ml of MTT solution (5 mg/ml) was added to each well and the incubation was continued for 3 h. Lysis buffer was prepared by dissolving 40% (w/v) sodium dodecyl sulphate (SDS) in deionised water; an equal volume of N,N-dimethylformamide was then added, and the pH was

adjusted to 4.7. After 3 h incubation with MTT, 100 ml of the lysis buffer was added to each well and the absorbance read at 570 nm on a Microplate Reader. These analysis were kindly performed by Prof. Cinzia Fabrizi (Department of SAIMLAL, Sapienza University of Rome).

3.3.b Pro-inflammatory cytokines expression

Total RNA was purified by $2x10^6$ BV2 cells by a single extraction with Trizol (Invitrogen) and reverse transcribed by oligo$(dT)_{15-18}$ primers and MML-V reverse trascriptase (Invitrogen). The cDNAwas amplified by Taq DNA polymerase in a thermal cycle (PerkinElmer Life Sciences) in the presence of primers for tumor necrosis factor alpha (TNF-α) (5'-primer, GAGCACTGAAAGCATGATCCG; 3'-primer GCAGGTCTACTTTGGGATCATT). Conditions for TNF-α amplifications were as follows: 30 s at 94°C, 30 s at 64°C, 30 s at 72°C. Ten microliters of each PCR product were electrophoresed on 1% agarose gel and then visualized by ethidium bromide staining. The mRNA for GAPDH was used as reference.

Quantitative analysis of the interleukin 1 β (IL-1β) was performed using the ELISA kit (R&D System). These analysis were kindly performed by Prof. Cinzia Fabrizi (Department of SAIMLAL, Sapienza University of Rome).

3.4 Determination of intracellular oxidative stress

3.4.a GSH and GSSG measurements

Thirty microliter of 5% tricloracetic acid (TCA) were added to an aliquot of each cell pellets (~ $1x10^6$ cells); all samples were incubated in ice at 4° C for 2 hr. After centrifugation, these samples were diluted 1:5 with 50 mM phosphate buffer pH 3.0 and filtered through Micron YM-10 centrifugal filter device (Amicon). One microliter of each samples was used for the determination of the levels of GSH and GSSG by a HPLC equipped with electrochemical detector (ECD). The chromatographic analysis was performed using a Waters 626 pump system associated with a Waters 600S controller. The separations were performed by means of a chromatographic column Waters Atlantis (C_{18}, 5 um particle diameter, 100A pore diameter, 4.6 x 250 mm column length) using as mobile phase 100% 50 mM phosphate buffer, pH 3, at a constant flow of 1 ml for minute. The analytes were quantified using a detection system CoulArray electrochemical detector (ESA 5600) equipped with four analytical cells containing electrodes; each cell can record the variation of current over time at a certain constant potential. The potential of each electrode can be controlled independently from -1000 mV to 2000 mV. For the determination of GSH and GSSG were used two cells placed respectively at the potential of 700 mV and 850 mV. Calibration curves for GSH and GSSG were obtained by injecting 10 µl of standard solutions in the concentration range 1 mM -

100 mM. These analysis were kindly performed by Dr. Alberto Macone (Department of Biochemical Sciences, Sapienza University of Rome).

3.4.b Reactive carbonyls measurement

Protein carbonyl measurement was performed after stimulation of microglial cells for 72 h using the method of Cao & Cutler (1995). Briefly, each cell extract was divided into two parts, a test and a blank, with a volume of 1 ml. Four milliliters of 12.5 mM 2,4-dinitrophenylhydrazine (DNPH) in 2.5 M HCl were added to the test while to the blank were added 4 ml of HCl 2.5 M. The two samples were then incubated at room temperature for 1 h, shaking every 10 minutes, precipitated with 10% TCA (final concentration) and subsequently treated with a "strong" or "weak" washing procedures. The "strong" procedure was based on included a strong breaking of the precipitate with a homogenizer before further extraction with 4 ml of ethanol:ethyl acetate (1:1, v/v) for three times. The "weak" washing procedure was based on a weak breaking of the precipitate with a glass rod and an additional wash with 10% TCA prior to extraction with ethanol:ethyl acetate. The final pellets were dissolved in 1 ml of 6 M guanidine-HCl with 20 mM phosphate buffer: trifluoroacetic acid (TFA), pH 2.3, and left for 20 minutes at 37° C under stirring. Any insoluble material was removed by centrifugation. The content of reactive carbonyls (C) was calculated from their peak absorption at 370 nm using a molar absorption coefficient (ε) of 22 M^{-1} cm^{-1}. The final content of protein reactive carbonyls was expressed in nmol carbonyls/mg protein. This analysis was kindly performed by Dr. Alberto Macone (Department of Biochemical Sciences, Sapienza University of Rome).

3.5 Proteome sample preparations

3.5.a Enrichment of the cytosolic and organelle compartments

For the 2-DE-based differential proteomics, lysates from $A\beta_{25-35}$ and $A\beta_{35-25}$ treated BV2 cells, and from untreated control samples underwent a subcellular fractionation by Qproteome Cell Compartment Kit (Qiagen). According to the protocol used, fractions enriched with cytosolic or with membrane proteins and proteins from the lumen of organelles except the nuclear components (named hereafter membrane/organelle proteins), respectively, were obtained from each lysate.

3.5.b Co-immunoprecipitation of 14-3-3ε

To enable elution of 14-3-3ε interactors without antibody contamination, it is recommended to cross link the antibody to the insoluble support. Magnetic beads (~ 32 µl slurry) with recombinant Protein G covalently coupled to the surface (Dynabeads protein G; Invitrogen) were incubated at 4°C overnight with ~ 4 µg of anti-V5 antibody (Invitrogen) on a rotator. After two washes with 0.2 M sodium

borate pH 9, the non covalent complexes beads/antibodies were incubated in 0.2 M sodium borate containing 20 mM dimethyl pimelimidate (DMP) for 1 h at room temperature on a rotator. After two times washes and a further 2 h incubation at room temperature on a rotator in a quenching buffer (0.2 M ethanolamine pH 9), covalently cross-linked complexes anti V5-beads were then resolved from uncovalent ones by sequential washes with 0.1 M glycine pH 2.8 (one time) and with PBS (three times).
BV2 samples (~ $1x10^7$ cells), from $A\beta_{25-35}$ treated (heavy labeled) cells or not (light labeled), were carefully washed 3 times with pre-chilled PBS buffer (1.37 M NaCl, 27 mM KCl, 100 mM Na_2HPO_4, 18 mM KH_2PO_4) by centrifugation at 14000 rpm for 20 min at 4°C; the pellet was then dissolved in a RIPA-slightly modified lysis buffer, containing 50 mM Tris-HCl pH 7.4, 1 mM EGTA, 150 mM NaCl, 1% NP-40, protease (Roche) and phosphatase (5 mM sodium fluoride, 1 mM sodium orthovanadate, 2.5 mM sodium pyrophosphate) inhibitors. Protein concentration was measured with Bradford reagent, on isolated aliquots. An equal amount of proteins (~ 1 mg) from both samples was then mixed and aspecific interactors pre-cleared by treatment with the magnetic beads for 1 h at 4°C on a rotator. The pre-cleared lysates were finally added and incubated with cross-linked antiV5-beads overnight at 4°C on a rotator. Afterward, the beads were washed with the lysis buffer (five times) and with PBS (one time). Then the proteins were eluted by treatment with 0.1 M glycine pH 2.8 for 10 minutes and centrifugation at 14000 rpm at 4°C (3x 10 µl).

3.5.c Enrichment of plasma membrane proteins by sequential two phase systems

The plasma membrane enrichment were performed by two phase partition as previously reported (Schindler *et al.*, 2008). Briefly, two-phase systems were prepared one day prior to usage from stock solutions of 200 mM Tris, adjusted to pH 7.8 with sulfuric acid (Tris/SO_4^{2-}), 40% (w/w) polyethylene glycol (PEG) 3350, and 20% (w/w) dextran T500. The first phase (A) was prepared by mixing 1.035 g of dextran, 0.518 g of PEG, 0.75 g of Tris/SO_4^{2-}, and 0.598 g of water and was incubated overnight at 4°C. Additional six phases (B-G) were prepared by mixing 1.035 g of dextran, 0.518 g of PEG, 0.75 g of Tris/SO_4^{2-}, and 0.698 g of water; also these phases was incubated overnight at 4°C. Prior to the experiment, top phases were removed from bottom phases and stored separately at 4°C.
BV2 cells (~ $7x10^8$), $A\beta_{25-35}$-treated (heavy labeled) and untreated (light labeled), were washed three times with PBS; cell pellets were then resuspended in 50 mM Tris containing protease inhibitors (Roche) and sonicated. The two samples were centrifuged at 1000 rpm for 10 min to remove unbroken cells and nuclei. The resulting supernatants were centrifuged at 14000 rpm for 30 min: the supernatants, containing cytosolic proteins, were quantified using Bradford assay; the pellets, containing plasma membrane-microsome compartment, were resuspended in the top

phase (PEG) A and combined in 1:1 proportion. As shown in figure 3.2, the top phase A was added to the bottom phase (dextran) A; the two resulting two-phase systems were mixed by inverting 20 times, vortexing, and inverting another 20 times. The top phase A was transferred on the bottom phase B and new fresh top phase was added on the bottom phase A. In each of the following steps, all top phases were transferred onto the next bottom phase, and bottom phase A was again re-extracted with a fresh top phase. After each transfer, phases were mixed. The procedure was finished when the seven two phase systems were separated by centrifugation, resulting in a total of 7 top and 7 bottom phases. F and G top phases, both expected as enriched in plasma membrane, were mixed in order to increase the protein yield. Then these combined top phases were sedimented by ultracentrifugation for 1 h at 150000 g. The pellet was resuspended in sample buffer (1 mM Tris-HCl pH 6.8, 4% SDS, 0.1% bromophenol blue, 10% β-mercaptoethanol, 10% glycerol) and proteins were resolved by mono-dimensional gel electrophoresis (see paragraph 3.6.b).

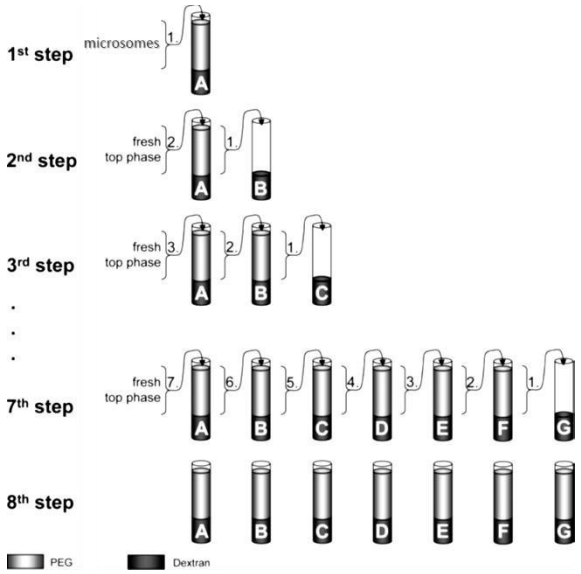

Fig. 3.2 Schematic of the protocol to enrich brain plasma membranes. In the first step, the top phase "A", containing microsomal fraction, were added to the bottom phase "A". After phase separation, the top phase is transferred onto the fresh bottom phase "B", and the bottom phase of the primary two-phase system, "A", is covered with a fresh top phase. In the subsequent steps, the top phases are transferred one bottom phase along, always transferring the latest top phase onto a fresh bottom phase and re-extracting bottom phase "A" with a fresh top phase (for example, in the 3rd step, top phase "B" is transferred onto the fresh bottom phase "C", top phase "A" is then transferred onto bottom phase "B", and bottom phase "A" is finally covered with a fresh top phase). By doing so, 7 two-phase systems ("A"–"G") are obtained after the final 8th step, each containing a top and a bottom phase (adapted from Schindler *et al.*, 2008).

3.5.d Enrichment of the microglia redoxome

BV2 cells, treated with $A\beta_{25-35}$ or not, were washed and centrifuged three times with PBS; the pellet was finally dissolved in a lysis buffer containing 8M urea, 100mM NEM, 50 mM Tris-HCl pH 8.0, 2mM EDTA, 0.1% Triton X-100, protease and phosphatase (5mM sodium fluoride, 1mM sodium orthovanadate, 2.5mM sodium pyrophosphate) inhibitors. Cell extracts were incubated under rotation at 4°C for 15 min and treated for three cycles of sonication/relaxation of 30 sec. Samples were centrifuged at 14000 rpm for 20 min at 4°C. Protein concentration was measured with Bradford reagent on isolated aliquots.

Proteins involved in reversible oxidative modification of cysteines are detected as previously reported (McDonagh *et al*., 2009), with slight modifications. In brief, proteins (500 µg) were precipitated from the cell extracts overnight at -20°C with nine volume of cold ethanol and pellet by centrifugation at 14000 rpm at 4°C for 15 min. Protein pellets were dissolved in 180 µl of denaturing buffer containing 8M urea, 4% CHAPS, 50 mM Tris-HCl pH 8.0 and 2mM EDTA. The reducing agent dithiotreitol (DTT) was then added to the final concentration of 20 mM, and samples were incubated for 45 min on a rotator at room temperature. Proteins were newly ethanol-precipitated in order to remove the remaining DTT. Protein pellet was dissolved in 200 µl of the previous buffer containing 0.5 mM HPDP-biotin, a bifunctional reagent with an alkylating function at one end, and incubated 45 min on a rotator in the dark. Samples were ethanol-precipitated in order to remove the excess of HPDP-biotin and resuspended in 40 µl of 8M urea and 160 µl of 50mM of ammonium bicarbonate; an aliquot of 5 µl was used to measure protein concentration with Bradford assay. An equal amount of proteins from the two samples was tryptic digested (E/S ratio of 1:50) at 37°C overnight. After digestion, was added 200 µl of the denaturing buffer previously described.

An appropriate quantity of 50% slurry streptavidin-agarose resin solution was prepared by two times washes in a binding buffer containing 4M urea, 2% CHAPS, 25 mM Tris-HCl pH 8.0 and 50mM NaCl. Two same aliquots of agarose beads were incubated with each tryptic peptide mixtures overnight at 4°C on a rotator. Then, beads samples were washed once with the binding buffer, twice with wash buffer 1, (8M urea, 4% CHAPS, 25 mM Tris-HCl pH 8.0 and 1mM NaCl), and twice with wash buffer 2 (8M urea, 4% CHAPS, 25 mM Tris-HCl pH 8.0). In order to remove urea, the resin was finally washed four times with wash buffer 3 (5mM ammonium bicarbonate/20% acetonitrile). Peptides were at the same time eluted from streptavidine beads and cleaved from the cystein-HPDP-biotin bait by treatment with 25 µl of elution buffer containing 5mM ammonium bicarbonate/20% acetonitrile and 5% mercaptoethanol at 56°C for 10 min. Peptides were collected by centrifugation at 5000 rpm and stored at -80°C until mass spectrometric analysis.

3.6 Proteomic profilings

3.6.a Bi-dimensional electrophoresis of proteins from the cytosolic and organelle compartments

An equivalent amount (180 μg) from each of the cytosolic and membrane/organelle samples was desalted by precipitation with cold ethanol. The cytosolic pellet was resuspended with rehydration buffer containing 5 M urea, 2 M thiourea, 50 mM DTT, 2% w/v CHAPS, 0,2% v/v ampholytes pH range 3-10 (Bio-Lytes® 3/10, Bio-Rad); the pellet obtained from the organelle fraction was resuspended in the same rehydration buffer described above, added with 2% w/v of amidosulfobetaine-14 (ASB14) to improve the solubilization of membrane proteins. Samples were allowed to solubilize by mixing and incubating for 5 min at room temperature and loaded by passive rehydration on Immobiline linear pH 3-10 IPG^{TM} strips, 11 cm long (Bio-Rad). Isoelectric focusing (IEF) was performed with a Protean IEF Cell (Bio-Rad) at 20°C using the following program: (i) 250 V for 15 min; (ii) 250 to 8000 V in 2.5 h; (iii) 8000 V for 4 h.

After IEF, the proteins on the strip were immediately equilibrated for 2 times for 20 min with 50 mM Tris-HCl, pH 8.8, in 6 M urea, 30% glycerol and 2% SDS. DTT (130 mM) was included in the first and iodoacetamide (135 mM) in the second equilibration step to reduce and alkylate free thiols. Precast SDS gel, 4-12% linear acrylamide gradient Bis-Tris midi gel (BioRad), was used for the second dimension separation by molecular weight. The IEF strip was carefully applied on top of the gel and fixed in position using warm agarose (0.5%) dissolved in MES running buffer [50 mM MES (2-[N-morpholino]ethanesulfonic acid), 50 mM Tris base,1 mM EDTA, 0.1% w/v SDS, pH 7.3]. A standard protein mixture (broad range; BioRad) was applied on a corner of the gel to determine the relative molecular masses of proteins. The gel was electro-run with MES running buffer applying a ramping voltage (from 100 V to 200 V). Proteins were detected by colloidal Coomassie staining. For each cellular fraction three replica were carried out.

Digitized images of 2-DE gels were generated using GS-710 Densitometer (BioRad). Noise reduction, background subtraction, normalization, and quantitative profiling of proteins in 2-D gels were carried out using PDQuest software version 8.0 (BioRad). For spot quantification, spot volumes were calculated with the building feature involving the application of a fixed multiple of Gaussian radius of the spot as a background intensity function. Subsequently, relative spot intensities, defined as percentage of spot volume to the sum of total spot volumes on the parent gel, were extracted from a spreadsheet generated by the software. All of the spots in each samples were matched by the automatic tool in PDQuest software. Where gel and spot quality strongly influenced the matching capabilities of the software used for protein quantitation, the replicate gels were critically reviewed for their

reproducibility. Subsequently, analysis sets were created to identify differentially expressed proteins between control and treated samples. Proteins identified in the majority of the replica and with a two-fold differential level of detection in the majority of the treated samples compared with control ones, were selected for mass spectrometry.

3.6.b SDS-PAGE of immunoprecipitated complexes and plasma membrane enriched fractions

Proteins co-immunoprecipitated with 14-3-3ε were partially resolved by mono-dimensional SDS-PAGE gel in a Tris-glycine buffer system on pre-casted 4-12% polyacrylamide gels (BioRad). Mono-dimensional gels were stained by colloidal Coomassie.

The same procedure was used to resolve and visualize proteins in the plasma membrane enriched fraction.

3.6.c In-gel digestion

Selected spots from the 2-DE and 1-DE were manually excised from the gels and submitted to in-gel digestion using a sequencing grade trypsin. Briefly, the excised gel pieces were destained with a solution of 50 mM ammonium bicarbonate containing 50% acetonitrile, dehydrated with 100% acetonitrile and speed-vac dried. The dried gel pieces were then rehydrated by adding about 10 µl of 25 mM ammonium bicarbonate containing 11 ng/µl of trypsin and incubated on ice. After 30 min, more trypsin buffer was added, if necessary. Gel pieces were then incubate for 16 h at 37 °C.

3.6.d MALDI-TOF analysis of 2-DE spots

A minimal amount (1 µl) of tryptic peptide mixtures derived from the digestion of 2DE spots were analyzed by matrix-assisted laser desorption ionization (MALDI) time of flight (TOF) mass spectrometry by mixing the samples with a α-cyano-4-hydroxycinnamic acid (HCCA) solution saturated in 50% acetonitrile/0.1% TFA in a 1:1 (v/v) ratio. The mixture was loaded onto the MALDI target using the dried droplet technique. MALDI-MS measurements were performed on a Voyager-DE® STR (Applied Biosystems) time of flight (TOF) mass spectrometer, equipped with a 337 nm nitrogen laser and operating in reflector mode. In this analyzer, the ions travel down a flight tube and are turned around an ion mirror, or reflector, to correct for initial energy differences (Fig. 3.3). The *m/z* value is related to the time it takes an ion to reach the detector; the small ions have a higher velocity and are recorded on a detector before the larger ones. The ions are detected by a channel electron multiplier (Mann *et al*., 2001).

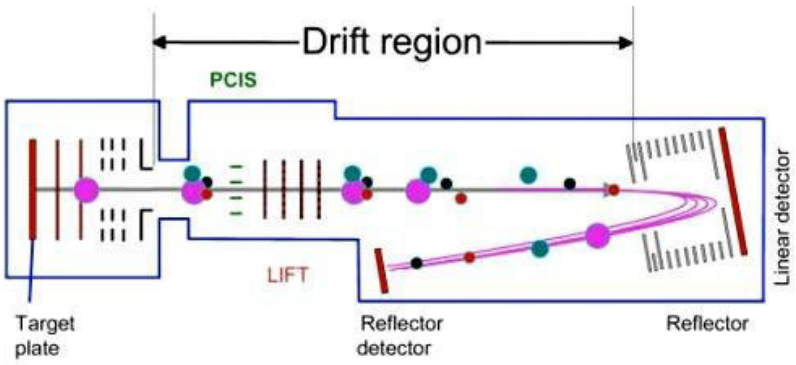

Fig. 3.3 The principle of MALDI-TOF MS. Ions are desorbed and ionized from the target plate and accelerate into the analyzer by an electric field of known strength. Here, the ions are separated according to their velocity that is strictly related to their m/z values. As MALDI source generates mono-charged ions, the m/z measured for each ion from the detector represents the mass value of a certain ion.

Mass data were obtained by accumulating several spectra from laser shots with an accelerating voltage of 20,000 V. All MALDI mass spectra were externally calibrated using a standard peptide mixture containing des-Arg-Bradykinin (*m/z* 904.4681), angiotensin I (*m/z* 1296.6853), 1-17 (*m/z* 2093.0867) and 18-39 (*m/z* 2465.1989) adrenocorticotropic hormon fragments. The MS spectra were also internally calibrated with two tryptic autolytic peptides (*m/z* 842.5100 and 2807.3145). The spectra were processed by MoverZ software (Proteometrics). A monoisotopic mass list from each MALDI-TOF spectrum was obtained after exclusion of contaminant mass values, corresponding to those expected from porcine trypsin and human keratins, automatically achieved by the PeakErazor program (http://www.protein.sdu.dk/gpmaw/Help/PeakErazor/peakerazor.html).
Peptide mass fingerprints were used to search for protein candidates in SwissProt *Mus musculus* database (v. 2011_01, 524420 sequences, 185205850 residues), using MASCOT search engine (www.matrixscience.com) according to the following parameters: cleavage on Arg/Lys, up to two missed cleavage permission and a maximum error of 50 ppm. Carbamidomethylation of cysteine as fixed modification, oxidation of methionine and NH_2-terminal protein acetylation as variable modification were also considered.

3.6.e LC-MS/MS analyses

Profiling of enriched fractions from plasma membrane, of 14-3-3ε interactomes and of the redoxome enriched by biotin-switch were performed on an LTQ-Orbitrap XL Discovery instrument (Thermo Fisher Scientific), a hybrid mass spectrometer in which two mass analyzers (a Linear Trapping Quadrupole and an Orbitrap cell) are built in tandem. Particularly, as suggested by the name, Orbitrap is an ion trapping

cell in which moving ions are trapped in an electrostatic field. However, unlike classic ion trap, the electrostatic attraction towards the central electrode is compensated by the centrifugal force arisen from the initial tangential velocity of ions. This electrostatic field experienced by ions inside the orbitrap forces them to move in complex spiral patterns strictly dependent on their mass value, like a satellite on orbit. The axial component of these oscillations is independent of initial energy, angles and positions, and can be detected as an image current on the two halves of an electrode encapsulating the orbitrap (Fig 3.4). A Fourier transform is employed to obtain oscillation frequencies for ions with different masses, resulting in an accurate reading of their *m/z* (Scigelova & Makarov, 2006).
Such measurements achieve very high resolution (30,000) surpassing, by an order of magnitude, the resolution presently obtainable with orthogonal time-of-flight analyzers. Accordingly, by Orbitrap analyzer mass measurements at an extreme mass accuracy (less than 2 ppm) are possible. For these features, the orbitrap analyzer represents the election instrument for that proteomics applications in which low abundant proteins could be identified also from only one detectable peptide.

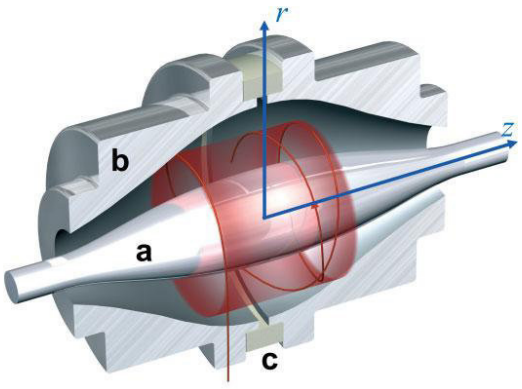

Fig. 3.4 A cut-away model of the orbitrap mass analyzer. Ions are moving in spirals around a central electrode (a). An outer electrode (b) is split in half by an insulating ceramic ring (c). An image current induced by moving ions is detected via a differential amplifier between the two halves of the outer orbitrap electrode. The *m/z* if different ions in the orbitrap can be determined from respective frequencies of oscillation after a Fourier transform (from Scigelova & Makarov, 2006).

The LTQ-Orbitrap XL Discovery mass spectrometer was connected online with HPLC system (Ultimate 3000, Thermo Fisher Scientific) via a nanoelectrospray ion source (Thermo Fisher Scientific).
The peptide mixture were desalted and concentrated using StageTip (Empore™ SPE Disks, C_{18}, Sigma; Rappsilber *et al.*, 2007); then, the mixture was autosampled onto 75 µm x 10 cm, 8 µm inside-diameter, column packed in-house with 5 µm C_{18} reversed-phase beads (Michrom Bioresources) and eluted with a gradient from 5%

to 80% of 0.1% formic acid in acetonitrile for 110 min. The MS data were acquired by the Orbitrap analyser in Full Scan mode over 300-2000 *m/z* range. Tandem mass spectra were acquired selecting parent ions into the Linear Trapping Quadrupole on the basis of Orbitrap measurements in a data-dependent scan mode (the most 5 intense ions per orbitrap cycle), with a dynamic exclusion of ions already fragmentated. All these activities, particular critical to detecting and structural characterizing low abundant peptide ions, were automatically performance by the Xcalibur software (Thermo Fisher Scientific).

3.6.f Mass spectra analysis

Mass spectrometric data acquired by the LTQ-Orbitrap XL Discovery mass spectrometer were qualitative and quantitative analyzed off-line through the free available MaxQuant software (Cox *et al*., 2009). The MS and MSMS spectra were searched against *Mus musculus* database from UniprotKB. A maximum of two missed cleavages were allowed. The required False Discovery Rate (FDR) was set to 0.01 at protein and peptide level. To increase statistical power the researches were achieved against a reverse decoy database.

Carbamidomethylation of cysteine as fixed modification and oxidation of methionine as variable modification were also considered for the analysis of 14-3-3ε interactors and for the analysis of proteins enriched in plasma membrane fraction. For the analysis of redoxome captured by the biotin-switching bait, the following variable modifications were used: oxidation of methionine and cysteine, mercaptoethanol modification of cysteine, deamidation of asparagine and glutamine.

3.7 Validation of proteomic identification by immunodetection

An equal amount of proteins for each sample (18 μg per lane) was separated by SDS-PAGE in a Tris-Glycine buffer system on 0.75-mm-thick 12%polyacrylamide gels. Electrical transfer onto a nitrocellulose membrane was carried out with a wet electroblotting apparatus (BioRad) at 85 V for 90 min at 4°C using a buffer containing 25 mM Tris, 20mM glycine, and 20% methanol. The membrane was stained with 0.2% Ponceau Red in 0.3% TCA to check for successful of transfer. Then the membrane was treated with 5% ECL blocking agent (GE Healthcare Biosciences) in 0.1% Tween-20, 10 mM Tris-HCl, 150 mM NaCl, 1 mM $CaCl_2$, and 1 mM $MgCl_2$, pH 7.4 (T-TBS), for 1 h and then incubated with primary antibody overnight at 4°C. Subsequently, the membrane was washed three times in T-TBS, and bound antibodies were detected using appropriate horseradish peroxidase-conjugated secondary antibodies, followed by an ECL Plus Western blotting Detection System (GE Healthcare Biosciences). ECL was detected using a Kodak Image Station 440cf (Eastman Kodak) and quantified using ImageJ analysis

software (http://rsbweb.nih.gov/ij/). Analysis was performed in triplicate from the two independent biological replicates. In each analyzed sample, target protein was relatively quantified by normalization to the corresponding GADPH level. Statistical analysis was performed applying T-student test; differences in protein expression with p-value of <0.05 were considered statistically significant.

Antibody were purchased from the following sources: anti-14-3-3 (rabbit polyclonal antibody, sc-629, 1:500; Santa Cruz Biotechnology); anti-14-3-3ε (rabbit polyclonal antibody, sc-1020, 1:500; Santa Cruz Biotechnology); anti-glyceraldehyde-3-phosphate dehydrogenase (anti-GAPDH, mouse monoclonal antibody, sc-32233, 1:500; Santa Cruz Biotechnology) used as the primary antibody to confirm equal protein loading in each lane; anti rabbit IgG-HRP (goat antibody, sc-2350, 1:2000; Santa Cruz Biotechnology) and anti-mouse IgG-HRP (goat antibody, sc-2500, 1:2000;Santa Cruz Biotechnology).

CHAPTER 4

RESULTS

The investigation on the role of microglia during sustained neuroinflammation induced by amyloidogenic peptides was achieved using as cell model BV2 cultures. This immortalized murine cell line (Blasi *et al*., 1990) shares functional properties with primary microglia (Henn *et al*., 2009; Stansley *et al*., 2012); accordingly, it is frequently used as a suitable cellular model in the field of neurodegeneration research. BV2 cells were challenged with the synthetic form of the $A\beta_{25-35}$ peptide, a shorter version of the full-length $A\beta_{1-42}$ peptide containing the neurotoxic domain, identified *in vivo* in the amyloid material accumulating in brains of patient with Alzheimer's disease (Kaminsky *et al*., 2010). This $A\beta_{25-35}$ has been proven to induce toxicological effects and oxidative burst on neuronal cells, overlapping those elicited by with $A\beta_{1-42}$ (Varadarajan *et al*., 2001). Unlike the native full-length peptide, $A\beta_{25-35}$ could be solubilised in aqueous buffers and easily manipulated; this ensures physiological-like conditions in culture media and high experimental reproducibility.

In our experimental setup, BV2 were treated with 50 μM $A\beta_{25-35}$, a concentration higher than that used in other studies, ranging between 0.1-10 μM, in order to mimic the environmental conditions that could lead to a sustained pro-inflammatory microglia phenotype (Sondag *et al*., 2009; Schilling & Eder, 2011; Pan *et al*., 2011; Orellana *et al*., 2011; Dhawan *et al*., 2012). Moreover, in order to discriminate between the effects specifically ascribed to amyloid material and those due to a nonspecific perturbation, BV2 cells were treated in parallel experiments with the same amount of a synthetic peptide, made up from the reverse sequence of the Ab_{25-35} peptide, named Ab_{35-25} or reverse peptide and known to miss the pro-inflammatory property (Ito *et al*., 2005).

4.1 Characterization of amyloid-induced BV2 activation at cellular level

Assays for viability of BV2 cells showed a marked proliferation upon the amyloidogenic treatment (Fig. 4.1 A) and an exocytotic response to specific drugs (*cf*. 3.3.a; Fig. 4.1 B; Liu & Schubert, 1997; Kreutzmann *et al*., 2010).

Since one of the main microglial activities is the early secretion of soluble pro-inflammatory factors, with the aim to validate our cellular model we first ascertained the specific ability of $A\beta_{25-35}$ peptide to induce in BV2 cells a specific inflammatory response. An increase in TNF-α transcription after 3 h of stimulation with $A\beta_{25-35}$

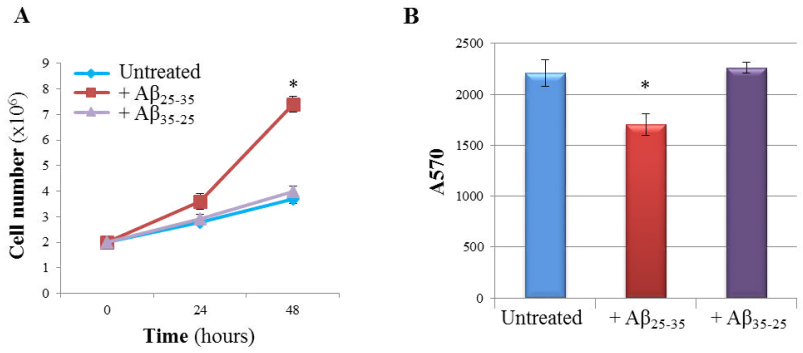

Fig. 4.1 (A) $A\beta_{25\text{-}35}$ induces cell proliferation. After treatment for 24 and 48h with 50 µM $A\beta_{25\text{–}35}$ or $A\beta_{35\text{-}25}$, the number of BV2 cells was determined by cell counts, using trypan blue staining. (B) $A\beta_{25\text{-}35}$ alters exocytotic function. BV2 cells were treated for 24 h with 50 µM $A\beta_{25\text{-}35}$ or $A\beta_{35\text{-}25}$ and then MTT reduction was performed. The absorbance of formazan solution was measured at 570 nm. T-test was used for statistical analysis; *indicates a significance of $p<0.001$.

proved that this peptide was able to rapidly trigger an inflammatory response in microglial cells (Fig. 4.2 A). Furthermore, this pro-inflammatory commitment is long lasting, as IL-1β protein remained over-expressed up to 48 h after stimulation (Fig. 4.2 B). The absence of cytokines release in the cells exposed to $A\beta_{35\text{-}25}$ peptide confirmed that only the amyloidogenic peptide was able to specifically trigger a pro-inflammatory phenotype in microglia.

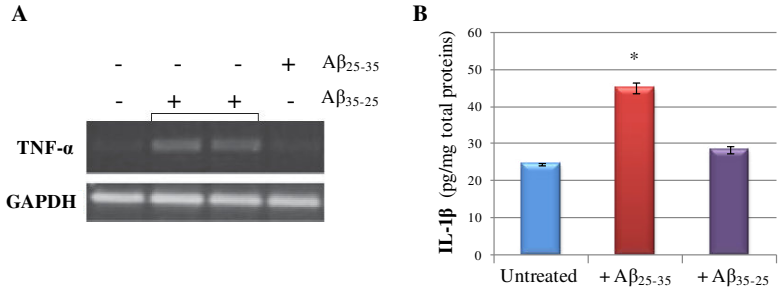

Fig. 4.2. Induction of transcription of TNF-α (A) in BV2 cells treated for 3 h with 50 µM $A\beta_{25\text{–}35}$ or $A\beta_{35\text{-}25}$. The TNF-α mRNA was detected by RT-PCR; the mRNA for GAPDH was used as reference. (B) The protein amount of IL-1β was measured by ELISA. T-test was used for statistical analysis; *indicates a significance of $p<0.001$.

4.2 Proteomics analysis of the cytosolic and organelle compartments

An unbiased proteomics approach was used to highlight the molecular scenario of late events in neuroinflammation. With this aim, we chose a stimulation time of 24 h to allow a transcriptional remodeling of the BV2 proteome.

Proteomic analyses of resting and stimulated cells were performed on diverse cellular fractions in order to simplify protein mixtures and consequently improve the chances of protein identification (Di Francesco *et al.,* 2012). We exploited two fractions of each cell lysate, respectively enriched with cytosolic or with microsomal fraction and proteins from the lumen of organelles, missing the nuclear components. Each sample was then analyzed by bi-dimensional gel electrophoresis (2-DE) comparing three analytical replicates from two independent biological replicates of each BV2 state ($A\beta_{25\text{-}35}$-, $A\beta_{35\text{-}25}$-treated and control cells).

In control BV2 cells, approximately 230 and 130 protein spots were detected by Coomassie staining among all replicates of all cell fractions, respectively (Fig. 4.3). Qualitative and quantitative changes between 2-DE maps were then achieved by comparison of protein spot densities from all replica by a specialized software. Spots that showed a ≥2-fold change in intensity, or that were uniquely present in all 2-DE maps of treated cell fractions were excised (labeled spots in Fig. 4.3), and proteins were identified by MALDI-TOF peptide mass fingerprint (PMF; Table 4.1).

Quantitative changes observed in the densitometric comparison between 2-DE gel spots of $A\beta_{25\text{-}35}$-activated cells *versus* $A\beta_{35\text{–}25}$-treated cells confirmed that the two diverse peptides (same composition but reverse sequences) induce different activation programs, with the respective molecular scenario actually distinctive, each being representative of two different response pathways.

Six proteins were proved to be specifically down-regulated by an approximately 2-fold factor in $A\beta_{25\text{-}35}$-treated cells in respect to the resting cell sample. Particularly, Hsp 90α/β, galectin 3, and L-lactate dehydrogenase A chain were down-regulated in the cytosolic fraction, whereas TOM 70, peroxiredoxins 3 and 4 were decreasing proteins in the membrane/organelle fraction. According to their annotated biochemical function, this inventory encompasses a molecular chaperon (Hsp 90), one metabolic enzyme (L-lactate dehydrogenase), two redox proteins (peroxiredoxins 3 and 4), one component of a mitochondrial membrane translocon (TOM70), and a lectin (galectin 3). Two of them had been previously associated with Alzheimer's disease: Hsp 90 seems to enhance the clearance of $A\beta_{1\text{-}42}$ (Takata *et al*., 2003) and the TOM complex has been already demonstrated to be involved in mitochondrial Aβ import (Hansson Petersen *et al*., 2008).

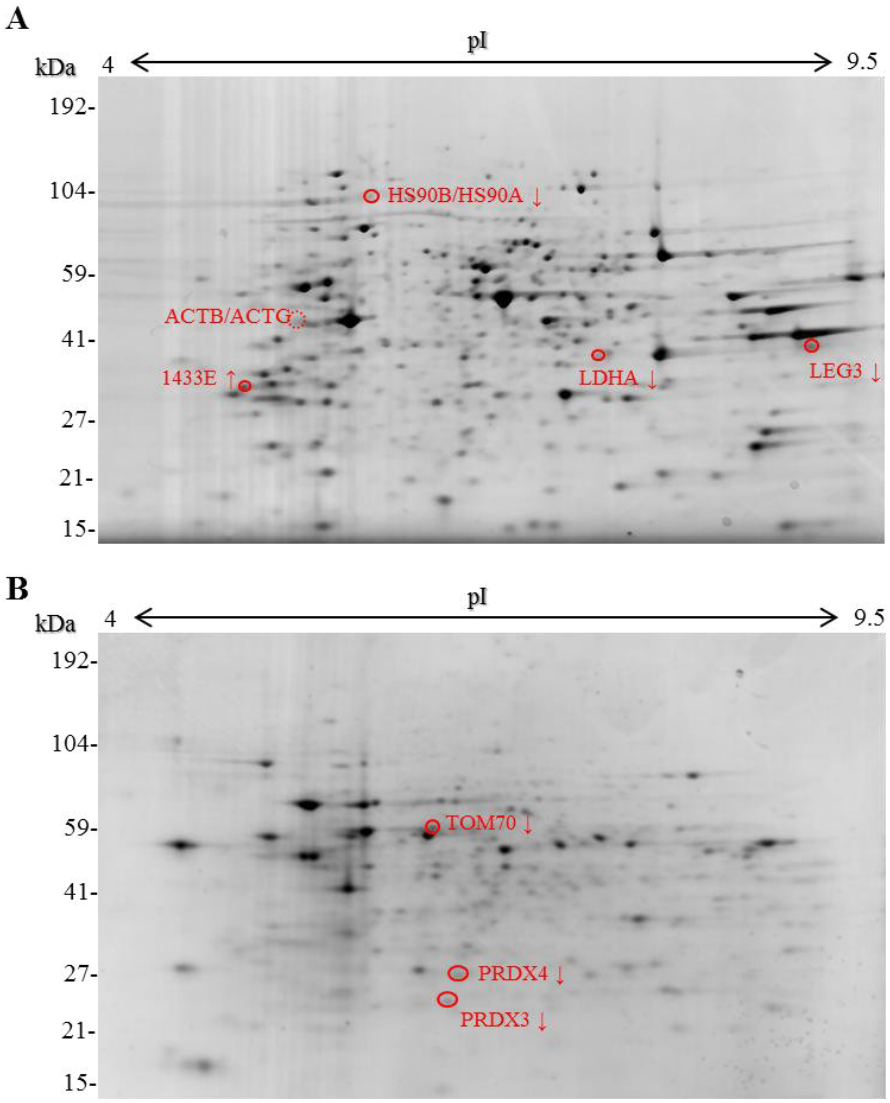

Fig. 4.3 Effects of $A\beta_{25-35}$ and $A\beta_{35-25}$ on 2-DE protein profiles of BV2. BV2 proteome was pre-fractionated according to the Qproteome Cell Compartment Kit (Qiagen) into cytosolic proteins and microsomal/organelles proteins. Protein mixtures were separated using a linear pH 3–10 gradient strip for the isoelectrofocusing and a 12% polyacrylamide gel for the second dimension. Representative 2-DE map of the resting BV2 cytosolic proteome (A) and microsomal/organelles proteome (B) are reported. Red circles refer to spots that showed ≥ 2-fold changes in intensity or that were uniquely expressed in $A\beta_{25-35}$-treated BV2 cells. Their MALDI-TOF identifications are also reported, according to Table 4.1.

Table 4.1 Summary of regulated proteins in cytosol and microsome/organelles

Entry name[a]	Protein name[b]	Quantitative change[c] (±SEM)			2-DE parameters				MOWSE Score	Sequence coverage (%)/matched peptides
					Theoretical		Measured			
		$A\beta_{25-35}$ versus untreated cells	$A\beta_{35-25}$ versus untreated cells	$A\beta_{25-35}$ versus $A\beta_{35-25}$	MW (kDa)	p*I*	MW (kDa)	p*I*		
ACTB_MOUSE[d] ACTG_MOUSE	Actin, acidic variant of isoforms β and γ	▲[e]	Not present	▲[e]	42.1	5.3	42	5.2[e]	124	46/15
CALR_MOUSE	Calreticulin	1±0.05	▼0.47±0.07	▲2.1±0.2	48.1	4.3	53	4.5	60	32/6
CH60_MOUSE	60 kDa Hsp, Hsp 60, mitochondrial	▼0.2±0.05	▼0.46±0.2	▼0.32±0.1	61.1	5.3	59	6.2	139	29/15
ENPL_MOUSE	Endoplasmin	1.4±0.2	▼0.24±0.1	▲5.8±0.8	92.7	4.7	92	5.1	207	35/27
FRIL1_MOUSE[d] FRIL2_MOUSE	Ferritin light chain, isoforms 1 and 2	1±0.3	▼0.46±0.1	▼0.32±0.1	20.8 20.9	5.6 6.4	19	5.7	133 77	57/1140/9
GLYC_MOUSE	Serine hydroxymethyltransferase, cytosolic isoform	0.71±0.2	▼0.43±0.1	1.6±0.1	52.5	6.5	51	6.8	99	20/20
GPDM_MOUSE	Glycerol-3-phosphate dehydrogenase, mitochondrial	1±0.4	▼0.43±0.04	▲2.3±0.1	80.9	6.2	74	6.4	55	16/10
HSP7C_MOUSE	Heat shock cognate 71 kDa protein	0.93±0.1	▼0.47±0.05	▲2±0.1	71.1	5.4	72	5.7	169	47/22
HS90A_MOUSE[d] HS90B_MOUSE	Hsp 90, isoforms α and β	▼0.38±0.1	0.70±0.2	0.6±0.1	84.7 83.3	4.9	95	5.8	80 86	20/12 21/12
LDHA_MOUSE	L-Lactate dehydrogenase A chain	▼0.48±0.07	1.0±0.1	▼0.48±0.08	36.8	7.6	37	7.4	92	34/12
LEG3_MOUSE	Galectin 3	▼0.38±0.06	0.8±0.1	0.5±0.1	27.6	8.5	38	9.0	85	40/10
PRDX4_MOUSE	Peroxiredoxin 4	▼0.34±0.08	0.7±0.1	▼0.43±0.04	26.4	6.6	26	6.4	112	37/9
PRDX3_MOUSE	Peroxiredoxin 3 (thioredoxin-dependent peroxide reductase, mitochondrial)	▼0.36±0.1	0.9±0.1	▼0.39±0.1	21.5	5.7	23	6.3	74	26/7
QCR1_MOUSE	Cytochrome *b*–*c*1 complex subunit 1, mitochondrial	1.0±0.1	▼0.45±0.06	▲2.2±0.2	52.7	5.7	49	5.7	143	34/12
SERA_MOUSE	D-3-phosphoglycerate dehydrogenase	0.9±0.12	▼0.48±0.07	▲2.5±0.4	56.5	6.1	64	6.6	197	36/19
TOM70_MOUSE	Mitochondrial import receptor subunit TOM70	▼0.2±0.1	0.8±0.1	▼0.3±0.1	67.4	7	58	6.4	85	18/12
1433E_MOUSE	14-3-3 Protein, ε isoform	▲2.3±0.2	0.8±0.1	▲2.0±0.3	29.3	4.6	31	4.8	11	48/13

a) UniProtKB protein identifier.
b) Proteins were identified by MALDI-TOF-MS. Identifications were accepted when the probability-based MOWSE protein score was significant according to MASCOT.
c) Up (▲) and down (▼) regulation were determined by comparison of the 2-DE Coomassie spot densities from two biological replicates (cell lysate fractions) and three technical replicates (n=5) following treatment with amyloid peptide ($A\beta_{25-35}$) and its reverse peptide ($A\beta_{35-25}$). Quantitative data were achieved by PDQuest software, compared with control. Only two-fold increase/decrease was accepted. Ratio of the spot densities is reported.
d) Protein isoforms differentially identified in the same spot through distinctive peptides.
e) Referred to the actin species present only in 2-DE map of $A\beta_{25-35}$-treated cells (Fig. 3.4). This actin species shows an experimental p*I* more acidic than the experimental p*I* of actin isoforms found in all three samples.

Notably, only two components of the entire BV2 proteome were up-regulated. The first was a more acidic species of the cytosolic actin, found in $A\beta_{25-35}$-stimulated BV2 2-DE profile, but not in those of control and of reverse peptide-treated cells (Fig. 4.4).

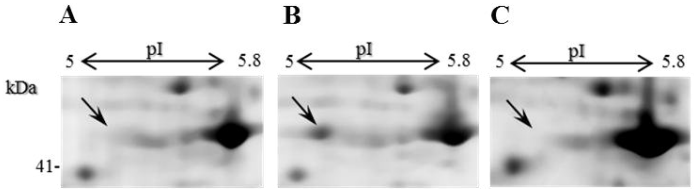

Fig. 4.4 Representative 2DE maps of the cytosolic fraction of control (A), $A\beta_{25-35}$ (B) and $A\beta_{35-25}$ (C) treated BV2 cells, zoomed in to focus on an acidic isoform of actin (arrow), found uniquely expressed in $A\beta_{25-35}$ samples.

The second protein was the epsilon isoform of the protein 14-3-3, a family of conserved regulatory molecules expressed in all eukaryotic cells. This latter proteome signature was also validated by western blot analysis (*p*-value of 0.025 *versus* control; Fig. 4.5 A). According to this validation, we planned to further decoding the 14-3-3ε role in microglia activation.

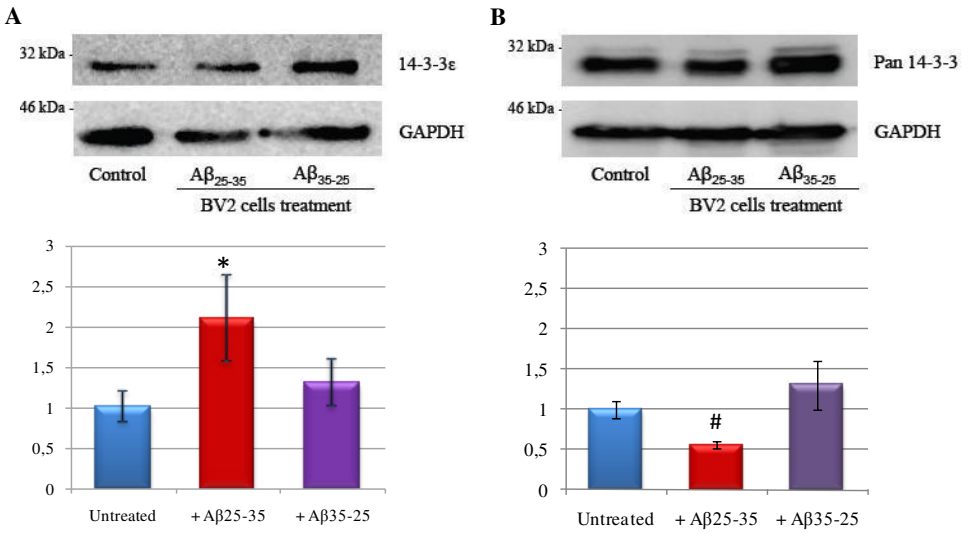

Fig. 4.5 Effects of $A\beta_{25-35}$ and $A\beta_{35-25}$ on the expression of 14-3-3 proteins. Immunodetection of the 14-3-3ε protein (A) and of the entire 14-3-3 family (B) in the cytosolic fraction of lysates from untreated BV2 cells (control) and cells treated for 24 h with 50 μM $A\beta_{25-35}$ or $A\beta_{35-25}$, respectively. Quantification were performed normalizing the optical density to the 14-3-3ε band in each sample versus the corresponding GADPH optical density. Results are represented as a mean (±SD) of n=5 replicates. Statistical analysis was performed by Student' T-test. * p-value of 0.05 versus control; # p-value of 0.002 versus control.

4.3 Defining the protein-protein interaction network of the epsilon 14-3-3-pathway in microglia toxic activation

The 14-3-3 proteins belong to a complex family that participate into the cell proteome in a wide range of cellular processes through the binding with unrelated proteins. Several distinct mechanisms of the 14-3-3 protein function were described, including conformational modulation of the bound protein, masking of its sequence-specific or structural features, and scaffolding that facilitates interaction between bound proteins (Obsil & Obsilova, 2011).

With the aim to in depth characterize the specific involvement of 14-3-3 family components in the neuroinflammatory response to amyloid, level of the epsilon isoform was compared with the global expression of the entire family in the cytosolic fraction of lysates from BV2 cells, untreated and treated with $Ab_{25–35}$ or $Ab_{35–25}$ respectively. Whereas a decrease in the global expression of the 14-3-3 proteins was immunodetected, the epsilon isoform fraction presents a dramatically and specific increase (Fig. 4.5 B).

Aimed to corroborate the validity of these findings, more recently we concentrated efforts on a comparative characterization of the BV2 proteome specifically interacting with a tagged form the 14-3-3ε protein, conveniently expressed in cells by transient transfection. For disclosing differential expression patterns also at the level of minor components, we benefit of an advanced proteomic setup. In this platform, accuracy in measuring relative protein abundances of a quantitative mass spectrometry-dependent analysis (Stable Isotope Labeling with Aminoacids in Cell culture, SILAC; Ong & Mann, 2006) is coupled with the identification power of shot-gun proteomics (Wu & MacCoss, 2002) where proteins are identified on poorly resolved mixtures, with the evident advantage to minimize component loss. Specifically, the SILAC approach measures differential protein expression through the ratio between unlabeled (from untreated cells) and stable isotope labeled (from treated cells) ion signals of protein peptides. Upon the biological treatment, labeled (amyloid treated cell lysate) and unlabeled (resting cell lysate) samples are then mixed, upstream of the proteomic sample preparation. The proteomic characterization of these high complex peptide mixtures strictly requires nano-liquid chromatography (nano-LC) hyphenated with highest resolution and fast mass spectrometry, such as that incorporated an “orbitrap” analyzer (Makarov, 2000; Hu *et al*., 2005).

According with this setup, proteins co-immunoprecipitated with 14-3-3ε were first resolved on SDS-PAGE gradient gel to reduce mixture complexity, and the entire gel lane was cut in 11 slices each treated according to shot-gun proteomics. We identified by LC-MS/MS analysis 196 proteins immunoprecipitated with tagged 14-

3-3ε. Among these proteins, several previously reported 14-3-3ε binding partners were present, *e.g.* 14-3-3θ, 14-3-3ζ /δ (Liang *et al.*, 2009; Chaudhri *et al.*, 2003), 14-3-3β/α, 14-3-3η, 14-3-3γ (Chaudhri *et al.*, 2003), ribosomal proteins S3 and P0, elongation factor 1-γ, elongation factor 1-α, tubulin β-2, poly(rC)-binding protein 1, Hsp 90 (Liang *et al.*, 2009; Zuo *et al.*, 2010), tropomyosin 3, glyceraldehyde-3-phosphate dehydrogenase, cofilin-1, calmodulin (Liang *et al.*, 2009) and vimentin (Satoh *et al.*, 2004).

Relative quantification of the identified proteins were then obtained comparing the heavy and light mass signals for each peptide identified by the LC-MS/MS, using a specialized open source software (MaxQuant). Quantitative data, collectable only from signals of protein peptides containing arginine residues on the basis of the experimental design we used, were expressed as H/L ratio (*i.e.* the ratio between signals of peptides labeled with a stable isotope enriched arginine residue, 10 amu heavier than peptide signals from untreated cells). Untill today, we carried out a single biological replica. According to this preliminary experiment, we found six proteins that were present only in the 14-3-3ε interactome following $A\beta_{25-35}$ treatment (Table 4.2). Among these proteins there were gene products already annotated in protein data bases as involved in negative regulation of protein transport (lysophospholipase-like protein 1), meiosis (meiotic nuclear division protein 1 homolog), protein ubiquitination (protein Herc1), arginine metabolism (arginase-2) and protein import into mitochondrial matrix (mitochondrial translocator assembly and maintenance protein 41 homolog). Moreover, we found eight interacting proteins involved in the 14-3-3ε network only in resting BV2 cells. These proteins are annotated in protein data bases as involved in signal transduction (desmoglein 1-β, protein phosphatase 1J, vomeronasal 1 receptor C23), exocytosis (exocyst complex component 3-like protein 4), cell cycle regulation (katanin p80 WD40-containing subunit B1), protein metabolism (insulin-degrading enzyme), establishment of cell polarity (serologically defined colon cancer antigen 8 homolog) and actin cytoskeleton organization (nebulin-related-anchoring protein). Finally, 15 proteins showed a $\geq$ 2-fold change in their H/L ratio. Among the 5 proteins showing an higher level of association with the 14-3-3ε node were proteome components known to be involved both in remodeling of cytoskeleton (vimentin and annexin A2) and of other cellular structure (rootletin and protein SERAC1), and in DNA repair and maintenance (zinc finger Ran-binding domain-containing protein 3). Conversely, the ten proteins displaying a decreased level of association are known to be involved in the immune response of microglia (lysozyme C-1 and peroxiredoxin-2), signaling pathway (peroxiredoxin-2, junction plakoglobin, sialoadhesin and adam 22), protein metabolism (ribosomal protein S20), lipid metabolism (patatin-like phospholipase domain-containing protein 2),

regulation of actin polymerization (actin-related protein 2/3 complex subunit 5), cell cycle regulation (enhancer of rudimentary homolog), regulation of gene expression (cryptochrome-1).

Table 4.2 - Summary of proteomics identifications of 14-3-3ε interacting proteins displaying a differential detection in activated microglia.

Protein ID [a]	Protein names	Ratio H/L [b]	# peptides [e]	PEP [f]
Q3UFF7	Lysophospholipase-like protein 1	Aβ-activated [c]	1	0.0016002
Q8K396	Meiotic nuclear division protein 1 homolog	Aβ-activated [c]	1	0.029635
E9PZP8	Protein Herc1	Aβ-activated [c]	1	0.037794
Q9D4Z5	Protein Prame	Aβ-activated [c]	1	0.047453
O08691	Arginase-2, mitochondrial	Aβ-activated [c]	1	0.047677
Q3TUH1	Mitochondrial translocator assembly and maintenance protein 41 homolog	Aβ-activated [c]	2	0.048394
P20152	Vimentin	2.47	7	7.182E-223
Q6NZP1	Zinc finger Ran-binding domain-containing protein 3	3.15	1	0.0091068
P07356	Annexin A2	4.20	1	5.947E-170
Q8CJ40	Rootletin	4.69	1	0.0010916
Q3U213	Protein SERAC1	17.63	3	0.027651
Q149T7	Protein phosphatase 1J	Resting [d]	1	0.0028657
Q6DIA2	Exocyst complex component 3-like protein 4	Resting [d]	1	0.005014
Q9JHR7	Insulin-degrading enzyme	Resting [d]	1	0.0077617
Q7TSF1	Desmoglein-1	Resting [d]	1	0.011064
Q8R2D1	Protein Vmn1r22	Resting [d]	1	0.017472
Q80XB4	Nebulin-related-anchoring protein	Resting [d]	1	0.021332
Q8BG40	Katanin p80 WD40-containing subunit B1	Resting [d]	1	0.031362
Q80UF4	Serologically defined colon cancer antigen 8 homolog	Resting [d]	1	0.045869
P97784	Cryptochrome-1	0.04	1	0.0056852
P17897	Lysozyme C-1	0.18	1	1.1705E-62
Q9CPW4	Actin-related protein 2/3 complex subunit 5	0.21	3	2.7825E-09
Q9R1V6	Adam 22	0.45	1	0.0068393
Q8BJ56	Patatin-like phospholipase domain-containing protein 2	0.45	4	2.2939E-27
Q62230	Sialoadhesin	0.46	2	1.289E-08
Q02257	Junction plakoglobin	0.46	5	4.1954E-14
Q61171	Peroxiredoxin-2	0.46	4	2.775E-11
P60867	40S ribosomal protein S20	0.50	2	4.0612E-11
P84089	Enhancer of rudimentary homolog	0.50	3	4.2683E-21

a) UniProtKB protein identifier.
b) SILAC H/L ratio determined by Maxquant software on the basis of mass spectrum analysis; a ratio higher than 1 means an enhanced association, while a ratio lower than 1 means a reduced association.
c) Protein associated only in the activated BV2 sample.
d) Protein associated only in the resting BV2 sample.
e) Number of peptides identified by MaxQuant search engine.
f) Posterior error probability that is the probability of a false hit, calculated by MaxQuant.

4.4 Quantitative proteomic analysis of plasma membrane proteins during neuroinflammation

Plasma membrane plays a fundamental role in microglial cells; its protein composition is not only involved in the stimulus recognition, but it is also essential in turning on activated cell populations. In analogy with the experimental setup conducted for the characterization of the 14-3-3ε network, we approached a comparative analysis of the BV2 plasma membrane by means of SILAC. The membrane pellets from resting and activated BV2 were 1:1 pooled and a fraction enriched in plasma membrane was isolated, according to its differential partition into a serialized two-phase system (Schindler *et al*., 2007).

Proteins from this fraction were then partially resolved by SDS-PAGE on a gradient gel (Fig. 4.6). Peptide mixtures obtained upon cutting the entire lane in 11 slides were analyzed in triplicate by nanoLC-MS/MS, and 998 proteins were there identified at least in two replica.

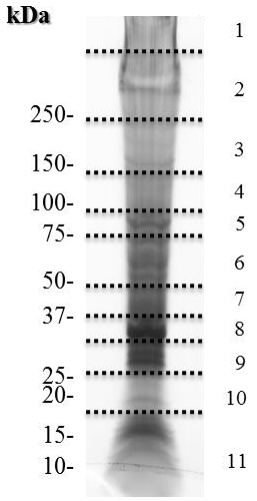

Fig. 4.6 Plasma membrane proteins enriched by two-phase partition. The selected protein fractions from untreated and $A\beta_{25-35}$-treated BV2 cells were mixed in 1:1 proportion as described in the text. Proteins were resolved on a SDS-PAGE 4-20% gradient gel. After colloidal Coomassie staining, the gel was cut in 11 slice according to the dotted lines reported; the number of each slice is reported on the right. Molecular weight marker are also reported on the left.

Relative quantification of 139 proteins, encompassed in this list and annotated in the gene ontology (GO) database as located in plasma membrane, was then performed by SILAC signals, *i.e.* comparing the MS signals of each couple of detected peptide ions encompassing "light" and "heavy" arginine residues, and expressed as H/L ratio (Tab. 4.3). We found only four plasma membrane proteins with a ≥ 2 fold change in membrane abundance between resting and activated BV2. In particular, Hsp 60 (a marker of the cellular response to cell adhesion, according to its role in protein folding), syntenin-1 (a component of the signal transduction machinery) and syntaxin-binding protein 3 (already annotated as involved in exocytosis) were proved to increase its abundance abundance in the plasma membrane of activated

cells. Only the presence of integrin β-6 (known to be involved in cell adhesion) showed to be less present at the plasma membrane level upon neuroinflammation.

Table - 4.3 Summary of proteomics identification of plasma membrane associated proteins displaying a differential detection in activated microglia

Protein ID [a]	Protein names	Ratio H/L [b] (±SEM)	# peptides [c]	PEP [d]
Q9Z0T9	Integrin beta-6	0.2 ± 0.09	1	4.69E-13
P63038	60 kDa heat shock protein, mitochondrial	2.3 ± 0.09	9	0.000024
O08992	Syntenin-1	2.5 ± 0.01	6	1.23E-292
Q60770	Syntaxin-binding protein 3	6.4 ± 0.74	4	2.34E-09

a) UniProtKB protein identifier.
b) SILAC H/L ratio determined by Maxquant software on the basis of mass spectrum analysis; a ratio higher than 1 means an up-regulation higher than 2-fold, while a ratio lower than 1 means a downregulation.
c) Number of peptides identified by MaxQuant search engine.
d) Posterior error probability that is the probability of a false hit, calculated by MaxQuant.

4.5 Oxidative stress induced by $A\beta_{25–35}$ in BV2 cells

The relatively small differences depicted in the proteome profiles of $A\beta_{25-35}$-treated cells seems to suggest that, alternatively to the change of transcriptional levels, faster regulatory mechanisms are critical in pushing microglia into the neuroinflammatory state. For this reason, we very recently came to turn our proteomic approach in investigating protein post-translational modifications that specifically marked the microglia commitment by beta amyloid. Since microglial cells are the major source of ROS in injured brain and the production of these oxidants is crucial for both pro-inflammatory activity and survival, first we looked for an unbalanced redox state and for its possible effects on the microglia proteome in the later events of neuroinflammation.

As mark of the microglia redox state, we first measured the intracellular glutathione concentrations at early (2 h) and late (24 h) times from the $A\beta_{25-35}$ treatment. The amount of total glutathione (GSx) showed a decrease already at 2 h after stimulation (Fig. 4.7 A). This decline is ascribable principally to the drop of reduced glutathione (GSH), the predominant cellular species (Fig. 4.7 B). The oxidized glutathione (GSSG), that usually represents only 1-1.5% of cellular GSx, conversely displayed an increased level both after 2 h and 24 h of treatment (Fig. 4.7 C). These augmented levels of GSSG caused a lowering of GSH/GSSG in the amyloid-treated samples with respect to the control one (Fig. 4.7 D).

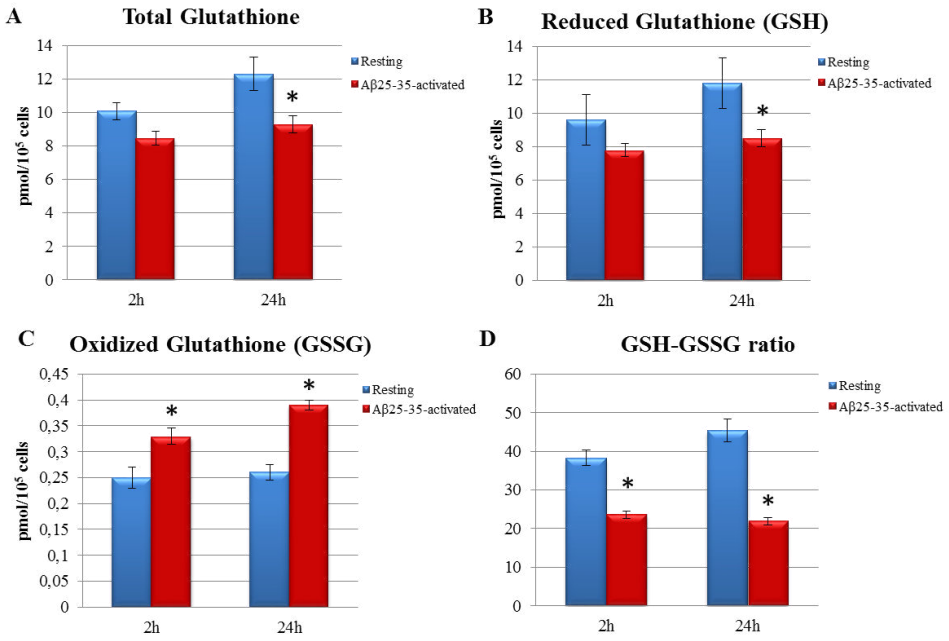

Fig. 4.7 $A\beta_{25-35}$ induced changes in cellular glutathione content and ratio. GSH (B) and GSSG (C) were separated by HPLC and amperometrically measured after 2 h and 24 h from the stimulation. Total glutathione (A) and GSH/GSSG ratio (D) were calculated from the previous measures. Histograms represent the mean (± SD) of n=3 replicates. T-student was used for statistical analysis. * $p \leq 0.05$.

These results proved that $A\beta_{25-35}$ peptide does induce a change in the redox balance of microglial cells; moreover, a doubling of carbonyl groups on proteins after 72 h of treatment with $A\beta_{25-35}$ strongly suggests that the microglia could indeed sustain a long term oxidative stress, but with a significant effect on the proteostasis mantainence (Fig. 4.8).

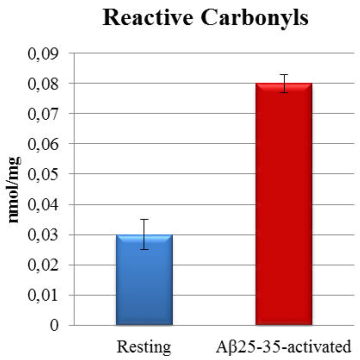

Fig. 4.8 $A\beta_{25-35}$ induced long term oxidative effect on BV2 proteins. Protein carbonyls were measured after 72 h form stimulation with $A\beta_{25-35}$ by colorimetric assay using 2,4-dinitrophenylhydrazine (DNPH). Histograms represent the mean (± SD) of n=3 replicates. T-student was used for statistical analysis. * $p \leq 0.05$.

4.6 Redox shotgun proteomics for the identification of reversibly oxidized proteins

Cysteine residues in proteins represent one of the major proteome sensitive target of the intracellular oxidative stress. In particular, the level of reversible oxidative modification are nowadays investigated as a crucial step for global regulation of cellular activities (Dalle-Donne *et al*., 2008; Ghezzi, 2013).

Once we determined an altered redox potential inside the activated microglia population, we became interested in looking for possible BV2 proteome components whose biochemical function are modulated by amyloid activation through a reversible modification on cysteine residues. For this purpose, we investigated the proteome of $A\beta_{25–35}$-treated BV2 cells using the highly sensitive shotgun strategy, recommended for detecting also low-abundance components. Due to the instable nature of reversible redox modified cysteines, we employed an approach to specifically enrich proteins encompassing reversible modified cysteines as stable derivatives upstream of the proteomic analysis ("biotin switch", *cf.* 3.5.d). With the aim to overcome the experimental variability arisen from both the high dynamic range expected in the intracellular level of each cysteine modification and from the higher number of proteome manipulations to be carried out, protein identifications and quantitative data were globally achieved without any labeling through the comparison between peak intensities of all proteolitic peptides identified from the untreated and $A\beta_{25-35}$-treated cells by MS/MS. A total of twelve analyses were performed on two technical replicates for each of the three biological replicates for treated and untreated samples .

From a total of 1022 peptides containing redox modified cysteines identified at least in one of these twelve samples, only 308 peptides were taken into account since they were identified in all three independent biological replicates. The summary of all these peptides is reported in Appendix I.

Among these peptides, 122 peptides were specifically enriched from amyloid treated cells, 90 from the resting BV2, and 96 were found in both the two samples. Particularly among this latter group, in sample isolated from amyloid treated cells with respect to resting ones 6 peptides showed a significant (by at least a 2-fold factor) increase in abundance, and 18 peptides were found significantly less abundant (Fig. 4.9 and Table I in Appendix I).

Turning on to proteins identified through these peptides, since some of the captured cysteines belong to the same protein the total number of redox-ome components specifically identified was 80 in lysates from amyloid treated cells, 64 in the samples from the resting cells, and 81 in both samples. Notably, among this latter group 15 proteins were differentially modified at the same cysteine residue between the

treated sample and the untreated one, and in 13 proteins the oxidized cysteine occupied a different position in the sequence in the sample isolated from amyloid-treated cells with respect to the control ones (Table I in Appendix I). These latter findings seem to highlight a highly specific switching code for regulation of proteome activities in response to the redox burst.

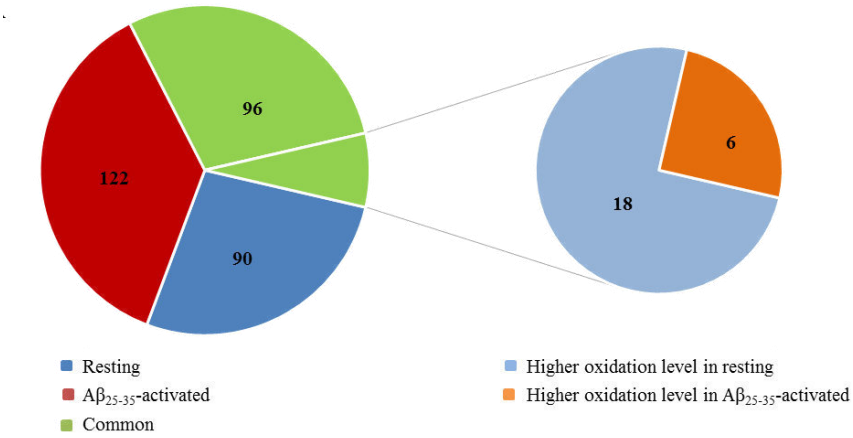

Fig. 4.9 Pie chart of peptides identified as redox reversible modified by biotin-switch enrichment and LC-MS/MS analysis.

In order to globally highlight the biological processes susceptible to this oxidative control of cell activities, we submitted to the DAVID (Database for Annotation, Visualization an Integrated Discovery) tool the database entry names of the 172 proteins for which redox-modified peptides were specifically isolated, distinguished them in two lists according to the cell condition in which the higher level of redox modification was observed. Twelve major biological processes emerged from this analysis (Fig. 4.10). In the $A\beta_{25–35}$-treated BV2, the most affected class was represented by proteins involved in proteostasis maintenance (*e.g.* ribosomal proteins, elongation factors, and chaperones and mRNA processing). Moreover stress response, cytoskeleton remodeling (named protein complex assembly) and purine metabolism were proven as further emerging processis according bioinformatics. In particular, in the purine metabolism Rac1 and Rac2 (ras-related C3 botulinum toxin substrate 1 and 2) proteins, known to be involved in the activation of NADPH oxidase complex, are included.

Beside proteins annotated into the main microglia processes affect by amyloid, we also found two proteins whose function was reported as regulated by cellular redox potential, *i.e.* the glyceraldehyde 3-phosphate dehydrogenase, a well-known moonlighting protein, that could relocate in the nucleus and act as a regulator of

gene expression (Brune & Lapetina, 1996), and the chloride intracellular channel 1 (CLIC1), a metamorphic protein existing in a cytosolic and an integral to plasma membrane form (Tulk *et al*., 2002).

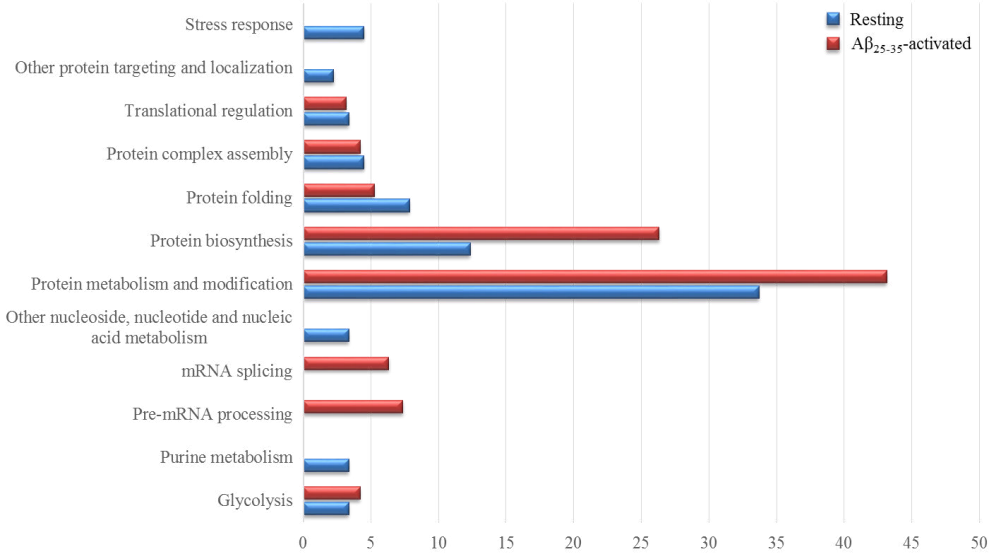

Fig. 4.10 Major processes regulated by differential oxidation. Biological processes enrichment analysis was performed inspecting PANTHER database through DAVID online tool.

CHAPTER 5
DISCUSSION & CONCLUSIONS

The comprehension of the molecular basis that lead microglia to assume sustained neuroinflammatory phenotypes during neurodegenerative processes could be inferred through the analysis of changes in protein expression levels and the analysis of dynamic post-translational modification (PTM) of proteins during a chronic stimulation with Aβ peptides.

With this aim, during the PhD fellowship I focused my research activity on characterizing with the unbiased tool of proteomics, the protein landscape ofa cellular model of the Alzheimer's disease (Stansley *et al*., 2012).The immortalized BV2 cell line,an established substitute for primary microglia, has been used to capture information on the events triggering a long-term neuroinflammations.

A picture of the neuroinflammatory process as global as possible was achieved collecting molecular details on different sub-proteomes (*i.e.* soluble and plasma membrane proteins, and cysteine redox reversible PTMs). For this purpose, classical proteomics approach and advanced quantitative strategies were applied.

Comparison of proteomic maps on cytosolic and organelle proteins (*cf.* 3.6.a) showed only seven proteins involved in the signature of the amyloidogenic peptide-activated microglia. Most of the identified proteins showed a decrease in their expression level, suggesting a slight decrease in the global levels of expression, and thus evocating alteration on mechanisms of proteostasis.

Despite this event, we were able to identify two proteins whose expression increased in stimulated BV2, that therefore might be candidates as suitable biomarkers of the microglia commitment toward neuroinflammation.

Of these proteins, the former is an acidic variant of the cytosolic actin ascribable to a PTM lowering its pI, *i.e.* phosphorylation or nitration. The first trait of microglial activation is the change in the cytoskeleton architecture, which ultimately leads to the loss of the membranous processes and to the acquisition of amoeboid features, including migration and phagocyte properties (Bernhart *et al*., 2010). Accordingly, the presence of this actin species in activated BV2 may suggest its role in processes related to cytoskeleton remodeling, as the morphological change during the transition from resting to the activated cells (Plantier *et al*., 1998; Abd-El-Basset *et al*., 2004). Furthermore, actin re-organization may be a pre-requisite for endocytosis and macropinocytosis, events involved in the extracellular removal of Aβ in microglial cells (Mandrekar *et al*., 2009). Finally, when microglia act as a

phagocyte, different states of actin cytoskeleton can enhance assembly and activity of NADPH oxidase, a multicomponent enzyme complex that, upon activation, produces the highly reactive free radical superoxide (Rassmussen *et al*., 2010).
The latter marker of microglia activation we found, was the epsilon isoform of 14-3-3 proteins. This isoform is a member of the 14-3-3 protein family involved in multiple cell processes, as proliferation, differentiation, transformation, and apoptosis (Aitken, 2006; Morrison, 2009). The 14-3-3 proteins are expressed in all cell types and tissues, and are coded by seven different genes in mammals. They are constitutively associated to form homo/heterodimers and can bind various structurally and functionally unrelated proteins thanks to their highly conserved peculiar folding (Obsil & Obsilova; Fig. 5.1 A).The only common feature shared by 14-3-3 interacting proteins is a non-stringent binding motif containing mainly phosphorylated serine residues(Fig. 5.1 B). Since their interactors are both kinases and their substrates, 14-3-3 proteins play a relevant role in the regulation of signal transduction, cell cycle and intracellular trafficking.

A

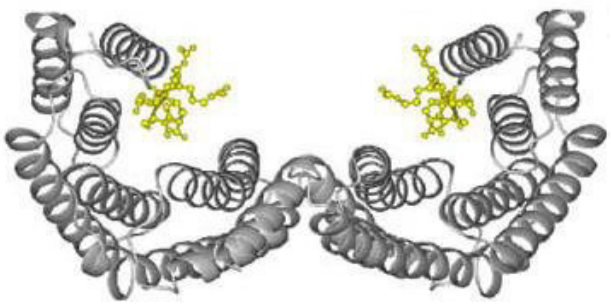

B

- R – S – X – **S** – X – P -	Mode I
- R – X – Y/F – K – **S** – X – P -	Mode II

Fig. 5.1 (A) Side view of the **c**rystal structures of human 14-3-3ε protein bound to a phosphopeptide (in yellow; from Gardino *et al*., 2006). (B) The protein sequences of the main14-3-3 binding motifs (*i.e.* mode I or mode II), where X is any type of residue and the phosphorylated serine is highlighted.

The importance of the 14-3-3 protein family in the neuronal compartment and their participation in neurodegenerative disease is today an established issue (Berg *et al*., 2003). In cerebrospinal fluid (CSF), 14-3-3 proteins have long been associated with the establishment of neurodegenerative diseases including AD (Jayaratnam *et al*.,

2008), and to date their presence in cerebrospinal fluid is able to assist in the diagnosis of Creutzfeldt–Jakob disease (Zerr *et al*., 2000). In the glia compartment, isoforms gamma and zeta were correlated to the immune response and to the secretion of pro-inflammatory cytokines in the models of Parkinson's disease (Reynolds *et al*., 2009), and an altered level of isoforms epsilon, gamma, and zeta were found in the hippocampus of AD patients (Di Domenico *et al*., 2009). Furthermore, in astrocytes, which together with microglia represent the reactive cells of nervous system, the 14-3-3 epsilon seems to play a role in the reorganization of intermediate filaments network, and its overexpression is a marker of activation following the demyelination process (Satoh *et al*., 2004). This isoform is also present at high level specifically in several brain regions of patients with AD (Berg *et al*., 2003; Layfield *et al*., 1996), although its role in AD pathogenesis is still unclear. Despite an increasing general concern on this protein family, very limited data are today available for the presence and the functional role of 14-3-3 in microglia cells.

To identify 14-3-3ε-mediated signaling pathways involved in the specific microglia response to amyloid, we selectively isolated complexes associated to this protein. The proteomics approach we applied (*cf.* 4.3), allowed us to prove that amyloid does induce a significant re-organization in the 14-3-3ε network, turning on or off signaling pathways (Table 4.2). Since all the partners detected by co-immunoprecipitation with 14-3-3ε were absent in the 2DE-maps, the approach we used successfully succeeded in highlighting minor component of the activated microglia scenario. Thanks to the quantitative implementation we employed in co-immunopecipitation of 14-3-3ε, we successfully gain another level of information on the proteomic landscape followed microglia activation. The difference in abundance of some partners detected in the 14-3-3ε interactomes could be ascribed to i) difference in their expression level; ii) increase their affinity due to possible conformational transition, triggered by post-translational modification or by an allosteric effector; iii) their release in the activated microglia from cellular compartments or complexes belonging to other signaling networks, that caused their sequestration in the resting cells. These results, even if preliminary, represent the first description of signaling complexes inside the activated microglia. Further studies will be necessary to validate the 14-3-3ε interacting partners, also at post-translational level, in order to understand how they could influence the pro-inflammatory activity of microglia.

Both these reported studies describe the expression proteome at the cytosolic level. However the first cellular site where amyloid and microglia encounter is the plasma membrane. A comparative profiling of complexes that dynamically associate with plasma membrane is demanding to complete the overview of modulation that occur

at the proteomic level in amyloid-activated microglia. Profiling of the plasma membrane proteins is still a challenge, since usually mitochondrial and endoplasmatic membrane proteins are overwhelming. With the aim to selectively enrich the membrane protein fractions in plasma membrane proteins, we approached a protocol based on a two-phase partition of cell membranes able to discriminate different lipid compositions (Schindler *et al.*, 2007), slightly modified to encompass in these profiles also proteins that associate with membrane complexes (*cf.* 3.5.c). Among various efficient protocols recently employed (Stella *et al.*, 2012), we have selected the method used by Schindler and colleagues for the promising results obtained in plasma membrane proteins enrichment.

Noteworthy, 139 proteins identified in the profile are already proved to be integral or associate plasma membrane proteins, according to Gene Onthology database annotation (http://www.geneontology.org/).

Among these 139 proteins, only three of them become enriched on plasma membrane after Aβ stimulation, and hence could mark the activated pro-inflammatory microglia, namely syntaxin-binding protein 3, Hsp 60 and syntenin-1. Syntaxin-binding protein 3 is involved in the exocytosis mediated by SNARE complex and has been proved to be expressed not only in neurons but also in other glial cells, including microglia (Paco *et al*., 2009); furthermore, this protein, together with syntaxin 4, regulates cytokines secretion in macrophages activated by LPS (Pagan *et al*., 2003). Hsp 60, known for its chaperone activity, seems to be involved in the immune response when exposed on external side of plasma membrane, particularly in antigen presenting cells (Belles *et al*., 1999), as proved in T lymphocytes activation (Osterloh *et al*., 2004). Syntenin-1 is an adaptor protein mainly involved in the re-organization of cytoskeleton; indeed, it is involved in cell motility through the activation of signaling pathways governed by MAPK and NFkB (Boukerche *et al*. 2008), in T lymphocytes cell polarization and migratory response (Sala-Valdès *et al*. 2012) and receptor trafficking (Zimmermann *et al*., 2005).

The relatively small differences depicted in the proteome profiles of $A\beta_{25-35}$-treated cells seem to suggest that, alternatively to the change of transcriptional levels, faster regulatory mechanisms are critical in pushing microglia into the neuroinflammatory state. For this reason, we, very recently, came to turn our proteomic approach in investigating PTM that specifically marked the microglia commitment by beta amyloid. Since microglia cells are the major source of ROS in injured brain and the production of these oxidants is crucial for both pro-inflammatory activity and survival, we looked for the intracellular redox state.

The GSH/GSSG ratio, a good measure of redox state, was proven to decrease to a lower value in amyloid-stimulated microglia with respect to the resting cells, but it remained constant for an expanded time range (upon 48 h), suggesting that microglia

is able to sustain the oxidative injury elicited by the amyloid challenge stabilizing a chronic lower redox state. This peculiar feature of microglia, makes them a reliable model to investigate the redox protein modification as a switch for lighting their functional role in neuroinflammation.

We started to analyze the microglia redox-ome, namely the entire set of proteome components whose cysteinyl residues are covalently modified and that could play a pivotal role in the dynamic regulation of protein function(Chiappetta *et al*., 2010). Recent evidences suggest a relevant regulatory role in cell signaling for a set of reversible redox modifications(*e.g.* S-nitrosylation, S-glutathionylation, disulfide bond and sulfenic acid formation). Among them, S-glutathionylation is looked at with particular expectation since its intracellular level depend on an enzymatic controlled activity. Glutathionylation and de-glutathionylationare catalyzed by a specific class of enzymes, named glutaredoxins (Lillig & Berndt, 2012). Although a clear consensus for the molecular recognition between glutaredoxin and its substrates is not yet be determined, specificity could be achieved by structural requirement as the accessibility of the cysteine (Malvezzi *et al*., 2012). Beyond glutathionylation, also for nitrosylation the involvement of specific enzymes has been tentatively suggested (Janssen-Heininger *et al*., 2008).

The transient trait of reversible redox modifications and their chemical instability both contribute to make their targeted capture a difficult task in proteomics (Fratelli *et al*., 2002; Newman *et al*., 2007; de Luca *et al*., 2011). In a preliminary setup of experiments, we tried to specifically resolve the S-glutathionated proteome on 2DE maps by immunodetection, but with a very low degree of reproducibility. On the contrary the biotin-switch method we approached ensured us the required level of reproducibility and allowed us to map modified cysteines on the structure of identified proteins (Table I in Appendix I), although it should be make clear that this procedure is not specific for S-glutathionylation (McDonagh *et al*., 2009). Particularly, this intrinsic feature of the biotin-switch enrichment in respect to other methods highlighted that a redox modification may impact on the same protein in the resting and activated microglia, but involving different cysteines in its sequence. Once this redox-ome will be immuno-resolved for S-glutationylation, those cysteines differentially modified will represent a sort of molecular barcode for extrapolating consensus sequences and for looking for enzymatic activities acting in activated microglia.

Redox modified cysteines we found, were in proteins involved in different biological processes, the proteostasis being the major affected process, as already inferred by results of expression proteome above discussed. It is important to underline that in amyloid activated microglia, where a chronic oxidative stress is

setup, a significant number of cysteine residues, proven to be redox modified in resting cells, was missed. If these events depend on a further modification leading to an irreversible oxidation state (*e.g.* sulphonylation), or on an enzymatic driven reduction, is still to be assessed. In the former case, the event will be stochastic and with a poor regulative significance; in the latter, a regulation of the signaling pathway leading to microglia activation could be hypothesized.

Among the proteins specifically redox modified in the activated microglial cells, three proteins aroused our interest for their correlation with microglial neurotoxic activity. Two of these are small GTPases, belonging to the Rho GTPase family, that in their active form can bind different protein effectors related to secretory pathways (Humeau *et al*., 2002), phagocytosis (Yamauchi *et al*., 2004) and apoptosis (Embade *et al*., 2000), namely Ras-related C3 botulinum toxin substrate 1 (Rac1) and Ras-related C3 botulinum toxin substrate 2 (Rac2). Rac1 and Rac2 represent, together with p40phox, p47phox and p67phox, the cytosolic regulatory subunit of the NADPH oxidase complex (Fig. 5.2; Babior, 1999). In the resting microglial status, inactive GDP-bound Rac1/2 are sequestered in the cytosol by Rho GDP-dissociation inhibitor (RhoGDI). After microglial activation, Rac1/2 is activated through GTP-binding, dissociates from RhoGDI and can translocate on plasma membrane where contributes to NADPH oxidase activation (Wilkinson & Landreth, 2006). Hence, the redox reversible modification we determined for these two proteins allowed us to suggest that the modified isoform of these proteins could be involved in the extracellular ROS production and the neurotoxic activity of microglia during chronic amyloid injury.

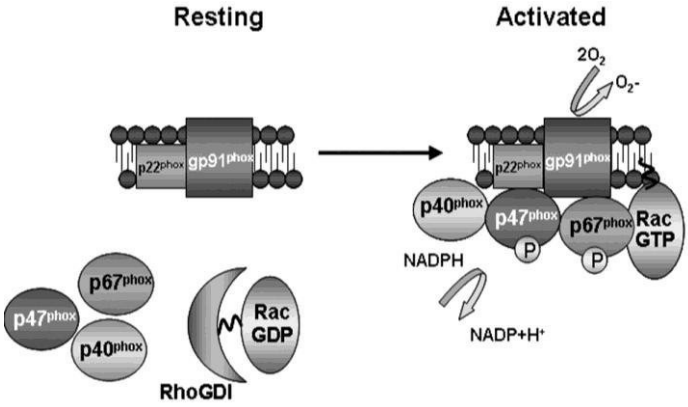

Fig. 5.2 Activation of the phagocytic NADPH oxidase complex. Stimulation of the phagocyte induces the parallel activation of oxidase components within the cytoplasm. This activation causes the conversion of Rac into an active GTP-bound form and the phosphorylation of p47phox and p67phox. Upon activation, these subunits translocate to the membrane where they interact with p22phox and gp91phox to initiate reactive oxygen production (from Wilkinson & Landreth, 2006).

Another relevant proteins identified in the redox-ome is the chloride intracellular channel 1 (CLIC1), a member of the CLICs family of highly conserved chloride channel proteins. Six different isoforms have been identified in vertebrates (CLIC1-6), homologous to those identified in invertebrates (Littler *et al*., 2010) and in plants (Elter *et al*., 2007). Despite this evolutionary conservation, their precise function remains elusive. Nevertheless, these proteins are involved in many physiological processes such as cell division (Valenzuela *et al*., 2000; Berryman & Goldenring, 2003), cell cycle and apoptosis (Shiio *et al*., 2006), cell differentiation (Suh *et al*., 2007), and also in pathophysiological processes such as pulmonary hypotension (Laudi *et al*., 2007), neurodegenerative diseases (Novarino *et al*., 2004) and different type of cancer (Suh & Yuspa, 2005). These proteins are named "metamorphic" as they exist under two different species: a soluble and an integral membrane forms (Valenzuela *et al*., 1997; Tulk *et al*., 2002). A recent study on CLIC1 reported that the incubation with hydrogen peroxide leads to the formation of an intramolecular disulfide bridge between Cys24 and Cys59, responsible for a non-covalent dimerization of the protein. This dimeric unit is able to form an ion channel in an artificial lipid bilayer, structurally similar to the native membrane (Littler *et al*., 2004). The N-terminal region encompassing Cys24 to Val46 has been proposed as the domain that upon oxidation drives the insertion of the protein into the lipid bilayer, through a conformational transition (Fig. 5.3; Littler *et al*., 2004; Goodchild *et al*., 2009). Once into the plasma membrane, CLIC1 can oligomerize forming an ion channel for the influx of chloride ions altering the membrane ionic conductance. Treatment of microglial cells with amyloid induces its localization on plasma membrane, and CLIC1 silencing alter both the release of TNF-α and NO production (Novarino *et al*., 2004). Moreover, blockade of CLIC1 stimulates amyloid phagocytosis in mononuclear phagocytes (Paradisi *et al*., 2008). Recently, it has been proposed that CLIC1 could modulate macrophagic activity through the modulation of phagosomal acidification (Jiang *et al*., 2012).

In our analysis, we do not find as redox modified neither Cys24 norCys59, involved in the stabilization of CLIC1 dimer; this is probably due to the reduction of the disulfide bridge between them during the insertion in the lipid bilayer, as proposed by Goodchild and colleagues (2010). Conversely, Cys191 was demonstrated to be specifically redox modified upon amyloid stimulation. In the proposed structural model of the plasma membrane inserted CLIC1, this cysteine is located in the cytosolic C-terminal region of the protein (Fig. 5.3 B; Goodchild *et al*., 2010). Therefore, this specific cysteine could be involved in regulation and structural stabilization of the CLIC1 isoform anchored to the plasma membrane.

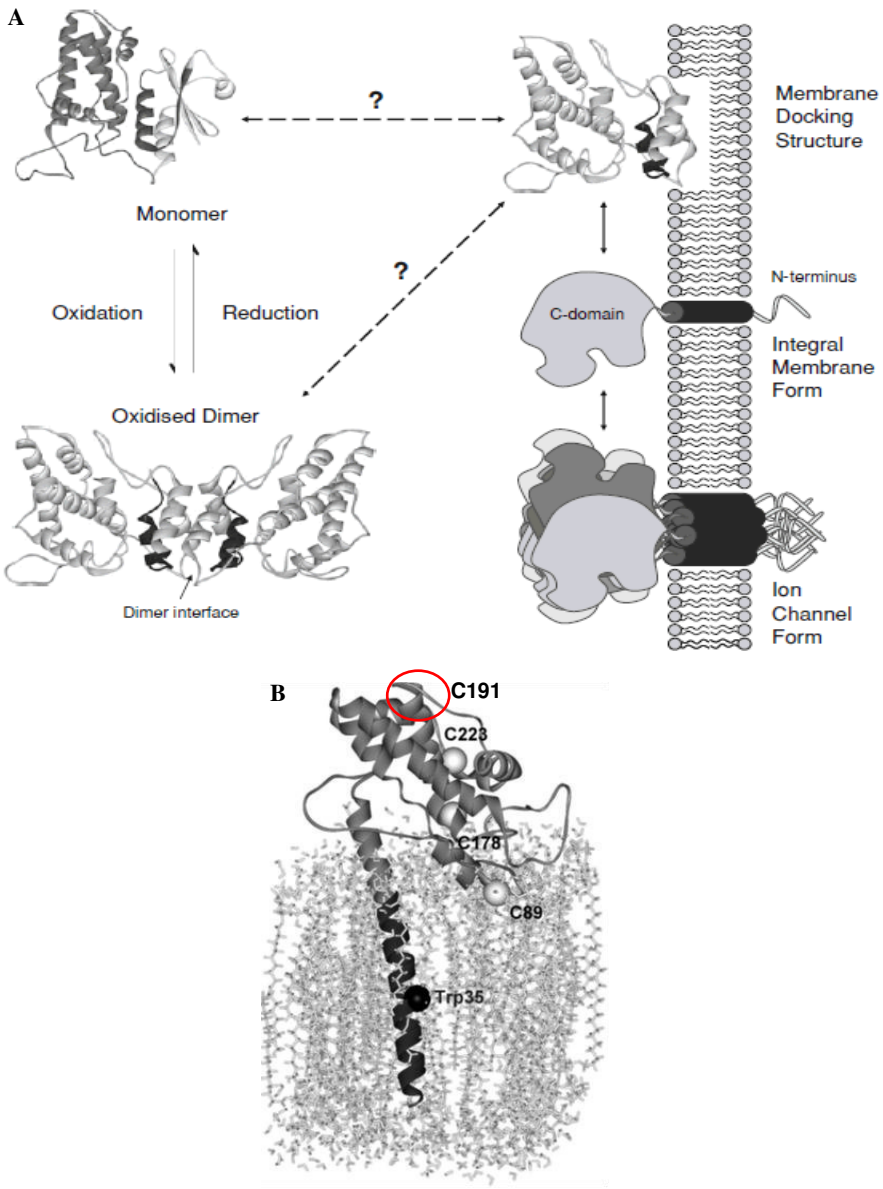

Fig. 5.3 Current proposed model of CLIC1 membrane insertion (A). Upon oxidation, the soluble CLIC1 monomer undergoes a reversible structural transition to an all α-helical, non-covalent dimer in solution. It has been proposed that in the presence of the membrane, the hydrophobic surface that forms the dimer-interface may dock to the bilayer as an initial step in the process of membrane insertion. The second stage in the process of membrane insertion involves insertion of the N-terminus across the lipid bilayer. Here, different CLIC1 subunits can converge to form an active ion channel (from Goodchild *et al*., 2009). (B) Model of the CLIC1membrane form (adapted from Goodchild *et al*., 2010).

In conclusion, our overall data provide a preliminary but comprehensive picture of microglia proteome involved in amyloid activation, and prepare the ground for further exploration of single pathways highlighted by this study.
Particularly, the integrated view we provide, suggests that:

a) in later events of neuroinflammations, post-translational regulation rather than transcriptional one play a leading role in microglialneuroinflammatory activity;
b) cytoskeleton remodeling could play an important role in shaping not only cell morphology but also the microarchitecture of membrane complex
c) an increased intracellular traffic (exocytosis) accompanies and sustains activated microglia;
d) redox dependent modifications seem to affect neurotoxic function of microglia, *e.g.*by the modulation of NADH oxidase through Rac1/2 activation turnover, and by the alteration of ionic conductance of the membrane though the stabilization of CLIC1 into the plasma membrane.

CHAPTER 6

REFERENCES

Abd-El-Basset, E.M., Prashanth, J., Ananth Lakshmi, K.V. (2004) "Up-regulation of cytoskeletal proteins in activated microglia." *Med. Princ. Pract*., 13: 325-333.

Aguzzi, A., Barres, B.A., and Bennett, M.L. (2013) "Microglia: scapegoat, saboteur, or something else?" *Science*, 339: 156-161.

Aitken, A. (2006) "14-3-3 Proteins: A historic overview." *Semin. Cancer Biol*., 16: 162–172.

Akiyama, H., Arai, T., Kondo, H., Tanno, E., Haga, C., and Ikeda, K. (2000) "Cell mediators of inflammation in the Alzheimer disease brain." *Alzheimer Dis. Assoc. Disord.*, 14:S47-S53.

Babior, B.M. (1999) "NADPH oxidase: an update." *Blood*, 93: 1464-1476.

Bayés, A., and Grant, S.G. (2009) "Neuroproteomics: understanding the molecular organization and complexity of the brain." *Nat. Rev. Neurosci*., 10: 635-646.

Belles, C., Kuhl, A., Nosheny, R., and Carding, S.R. (1999) "Plasma membrane expression of heat shock protein 60 in vivo in response to infection." *Infect. Immun*., 67: 4191-4200.

Berg, D., Holzmann, C., and Riess, O. (2003) "14-3-3 Proteins in the nervous system." *Nat. Rev. Neurosci*., 4: 752-762.

Bernhart, E., Kollroser, M., Rechberger, G., Reicher, H., Heinemann, A., Schratl, P., Hallström, S., Wintersperger, A., Nusshold, C., DeVaney, T., Zorn-Pauly, K., Malli, R., Graier, W., Malle, E., and Sattler, W. (2010) "Lysophosphatidic acid receptor activation affects the C13NJ microglia cell line proteome leading to alterations in glycolysis, motility, and cytoskeletal architecture." *Proteomics*, 10: 141-158.

Berryman, M.A., and Goldenring, J.R. (2003) "CLIC4 is enriched at cell-cell junctions and colocalizes with AKAP350 at the centrosome and midbody of cultured mammalian cells." *Cell. Motil. Cytoskeleton*, 56: 159-172.

Beauvillain, C., Donnou, S., Jarry, U., Scotet, M., Gascan, H., Delneste, Y., Guermonprez, P., Jeannin, P., and Couez, D. (2008) "Neonatal and adult microglia cross-present exogenous antigens." *Glia*, 56:69-77.

Blasi, E., Barluzzi, R., Bocchini, V., Mazzolla, R., and Bistoni, F. (1990) "Immortalization of murine microglial cells by a v-raf/v-myc carrying retrovirus." *J. Neuroimmunol.*, 27: 229-237.

Blennow, K., de Leon, M.J., and Zetterberg, H. (2006) "Alzheimer's disease." *Lancet*, 368:387-403.

Block, M.L., Zecca, L., and Hong, J.S. (2007) "Microglia-mediated neurotoxicity: uncovering the molecular mechanisms." *Nat. Rev. Neurosci*., 8:57-69.

Boche, D., Cunningham, C., Docagne, F., Scott, H., and Perry, V.H. (2006) "TGFbeta1 regulates the inflammatory response during chronic neurodegeneration." *Neurobiol. Dis*., 22:638-650.

Boukerche, H., Su, Z.Z., Prévot, C., Sarkar, D., and Fisher, P.B. (2008) "mda-9/Syntenin promotes metastasis in human melanoma cells by activating c-Src." *Proc. Natl. Acad. Sci. USA*, 105: 15914-15919.

Boyd-Kimball, D., Sultana, R., Poon, H.F., Lynn, B.C., Casamenti, F., Pepeu, G., Klein, J.B., and Butterfield, D.A. (2005) "Proteomic identification of proteins specifically oxidized by intracerebral injection of amyloid beta-peptide (1-42) into rat brain: implications for Alzheimer's disease." *Neuroscience*, 132:313-324.

Brüne, B., and Lapetina, E.G. (1996) "Nitric oxide-induced covalent modification of glycolytic enzyme glyceraldehyde-3-phosphate dehydrogenase." *Methods Enzymol*., 269: 400-407.

Butterfield, D.A., Castegna, A., Lauderback, C.M., and Drake, J. (2002) "Evidence that amyloid beta-peptide-induced lipid peroxidation and its sequelae in Alzheimer's disease brain contribute to neuronal death." *Neurobiol. Aging*, 23:655-664.

Cardona, A.E., Pioro, E.P., Sasse, M.E., Kostenko, V., Cardona, S.M., Dijkstra, I.M., Huang, D., Kidd, G., Dombrowski, S., Dutta, R., Lee, J.C., Cook, D.N., Jung, S., Lira, S.A., Littman, D.R., andRansohoff R.M. (2006) "Control of microglial neurotoxicity by the fractalkine receptor." *Nat. Neurosci*., 9:917-924.

Castegna, A., Thongboonkerd, V., Klein, J.B., Lynn, B., Markesbery, W.R., and Butterfield, D.A. (2003) "Proteomic identification of nitrated proteins in Alzheimer's disease brain." *J. Neurochem*., 85:1394-1401.

Chaudhri, M., Scarabel, M., and Aitken, A. (2003) "Mammalian and yeast 14-3-3 isoforms form distinct patterns of dimers in vivo." *Biochem. Biophys. Res. Commun*., 300: 679-685.

Chiappetta, G., Ndiaye, S., Igbaria, A., Kumar, C., Vinh, J., and Toledano, M.B. (2010) "Proteome screens for Cys residues oxidation: the redoxome." *Methods Enzymol.*, 473: 199-216.

Chun, W., and Johnson, G.V. (2007) "The role of tau phosphorylation and cleavage in neuronal cell death." *Front. Biosci*., 12:733-756.

Cox, J., Matic, I., Hilger, M., Nagaraj, N., Selbach, M., Olsen, J.V., and Mann, M. (2009) "A practical guide to the MaxQuant computational platform for SILAC-based quantitative proteomics." *Nat. Protoc.*, 4: 698-705.

Craft, J.M., Watterson, D.M., Frautschy, S.A., and Van Eldik, L.J. (2004) "Aminopyridazines inhibit beta-amyloid-induced glial activation and neuronal damage in vivo." *Neurobiol. Aging*, 25:1283-1292.

D'Andrea, M.R.,Cole, G.M., andArd, M.D. (2004) "The microglial phagocytic role with specific plaque types in the Alzheimer disease brain." *Neurobiol. Aging*, 25:675-683.

Dalle-Donne, I., Milzani, A., Gagliano, N., Colombo, R., Giustarini, D., and Rossi, R. (2008) "Molecular mechanisms and potential clinical significance of S-glutathionylation." *Antioxid. Redox Signal*., 10: 445-473.

Dalle-Donne, I., Rossi, R., Colombo, G., Giustarini, D., and Milzani, A. (2009) "Protein S-glutathionylation: a regulatory device from bacteria to humans." *Trends Biochem. Sci*., 34:85-96.

Davies, M.J. (2005) "The oxidative environment and protein damage." *Biochim. Biophys. Acta*., 1703:93-109.

de Luca, A., Moroni, N., Serafino, A., Primavera, A., Pastore, A., Pedersen, J.Z., Petruzzelli, R., Farrace, M.G., Pierimarchi, P., Moroni, G., Federici, G., Sinibaldi Vallebona, P., and Lo Bello, M. (2011) "Treatment of doxorubicin-resistant MCF7/Dx cells with nitric oxide causes histone glutathionylation and reversal of drug resistance." *Biochem. J*., 440: 175-183.

Dhawan, G., Floden, A.M., and Combs, C.K. (2012) "Amyloid-β oligomers stimulate microglia through a tyrosine kinase dependent mechanism." *Neurobiol. Aging*, 33: 2247-2261.

Di Domenico, F., Owen, J.B., Sultana, R., Sowell, R.A., Perluigi, M., Cini, C., Cai, J., Pierce, W.M., and Butterfield, D.A. (2010) "The wheat germ agglutinin-fractionated proteome of subjects with Alzheimer's disease and mild cognitive impairment hippocampus and inferior parietal lobule: Implications for disease pathogenesis and progression." *J. Neurosci. Res*., 88: 3566-3577.

Di Francesco, L., Correani, V., Fabrizi, C., Fumagalli, L., Mazzanti, M., Maras, B., and Schininà, M.E. (2012) "14-3-3ε marks the amyloid-stimulated microglia long-term activation." *Proteomics*, 12: 124-134.

Eikelenboom, P., Veerhuis, R., Familian, A., Hoozemans, J.J., van Gool, W.A., andRozemuller, A.J. (2008) "Neuroinflammation in plaque and vascular beta-amyloid disorders: clinical and therapeutic implications." *Neurodegener. Dis*., 5: 190-193

El Khoury, J., and Luster, A.D. (2008) "Mechanisms of microglia accumulation in Alzheimer's disease: therapeutic implications." *Trends Pharmacol. Sci*., 29:626-632.

Elter, A., Hartel, A., Sieben, C., Hertel, B., Fischer-Schliebs, E., Lüttge, U., Moroni, A., and Thiel, G. (2007) "A plant homolog of animal chloride intracellular channels

(CLICs) generates an ion conductance in heterologous systems." *J. Biol. Chem*., 282: 8786-8792.

Embade, N., Valerón, P.F., Aznar, S., López-Collazo, E., and Lacal, J.C. (2000) "Apoptosis induced by Rac GTPase correlates with induction of FasL and ceramides production." *Mol. Biol. Cell*, 11: 4347-4358.

Esch, F.S., Keim, P.S., Beattie, E.C., Blacher, R.W., Culwell, A.R., Oltersdorf, T., McClure, D., and Ward. P.J. (1990) "Cleavage of amyloid beta peptide during constitutive processing of its precursor." *Science*, 248:1122-1124.

Farfara, D., Lifshitz, V., andFrenkel, D. (2008) "Neuroprotective and neurotoxic properties of glial cells in the pathogenesis of Alzheimer's disease." *J. Cell Mol. Med*.,12:762-780.

Färber, K., andKettenmann, H. (2005) "Physiology of microglial cells." *Brain Res. Brain Res. Rev*., 48:133-143.

Fratelli, M., Demol, H., Puype, M., Casagrande, S., Eberini, I., Salmona, M., Bonetto, V., Mengozzi, M., Duffieux, F., Miclet, E., Bachi, A., Vandekerckhove, J., Gianazza, E., and Ghezzi, P. (2002) "Identification by redox proteomics of glutathionylated proteins in oxidatively stressed human T lymphocytes." *Proc. Natl. Acad. Sci. USA*, 99: 3505-3510.

Frautschy, S.A., Yang, F., Irrizarry, M., Hyman, B., Saido, T.C., Hsiao, K., and Cole, G.M. (1998) "Microglial response to amyloid plaques in APPsw transgenic mice." *Am. J. Pathol*., 152:307-317.

Gao, H.M., and Hong, J.S. (2008) "Why neurodegenerative diseases are progressive: uncontrolled inflammation drives disease progression." *Trends Immunol*., 29:357-365.

Gardino, A.K., Smerdon, S.J., and Yaffe, M.B. (2006) "Structural determinants of 14-3-3 binding specificities and regulation of subcellular localization of 14-3-3-ligand complexes: a comparison of the X-ray crystal structures of all human 14-3-3 isoforms." *Semin. Cancer Biol*., 16: 173-182.

Ghezzi, P. (2013) "Protein glutathionylation in health and disease." *Biochim. Biophys. Acta*, 1830: 3165-3172.

Glanzer, J.G., Enose, Y., Wang, T., Kadiu, I., Gong, N., Rozek, W., Liu, J., Schlautman, J.D., Ciborowski, P.S., Thomas, M.P., and Gendelman, H.E. (2007) "Genomic and proteomic microglial profiling: pathways for neuroprotective inflammatory responses following nerve fragment clearance and activation." *J. Neurochem*., 102: 627-645.

Goedert, M., and Spillantini, M.G. (2006) "A century of Alzheimer's disease." *Science*, 314: 777-781.

Goodchild, S.C., Howell, M.W., Cordina, N.M., Littler, D.R., Breit, S.N., Curmi, P.M., and Brown L.J. (2009) "Oxidation promotes insertion of the CLIC1 chloride intracellular channel into the membrane." *Eur. Biophys. J*., 39: 129-138.

Goodchild, S.C., Howell, M.W., Littler, D.R., Mandyam, R.A., Sale, K.L., Mazzanti, M., Breit, S.N., Curmi, P.M., and Brown, L.J. (2010) "Metamorphic response of the CLIC1 chloride intracellular ion channel protein upon membrane interaction." *Biochemistry*, 49: 5278-5289.

Haass, C., andSelkoe, D.J. (2007) "Soluble protein oligomers in neurodegeneration: lessons from the Alzheimer's amyloid beta-peptide." *Nat. Rev. Mol. Cell. Biol*., 8:101-112.

Hanisch, U.K., andKettenmann, H. (2007) "Microglia: active sensor and versatile effector cells in the normal and pathologic brain." *Nat. Neurosci*., 10:1387-1394.

Hansen, M.B., Nielsen, S.E., and Berg, K., (1989) "Re-examination and further development of a precise and rapid dye method for measuring cell growth/cell kill." *J. Immunol. Methods*, 119: 203-210.

Hansson Petersen, C.A., Alikhani, N., Behbahani, H., Wiehager, B., Pavlov, P.F., Alafuzoff, I., Leinonen, V., Ito, A., Winblad, B., Glaser, E., and Ankarcrona, M. (2008) "The amyloid beta-peptide is imported into mitochondria via the TOM import machinery and localized to mitochondrial cristae." *Proc. Natl. Acad. Sci. USA*, 105: 13145-13150.

Hardy, J.A., and Higgins, G.A. (1992) "Alzheimer's disease: the amyloid cascade hypothesis." *Science*, 256:184-185.

Hardy, J., andSelkoe, D.J. (2002) "The amyloid hypothesis of Alzheimer's disease: progress and problems on the road to therapeutics." *Science*, 297: 353-356.

Harry, G.J., and Kraft, A.D. (2008) "Neuroinflammation and microglia: considerations and approaches for neurotoxicity assessment." *Expert Opin. Drug Metab. Toxicol*., 4:1265-1277.

Heneka, M.T., andO'Banion, M.K. (Inflammatory processes in Alzheimer's disease." *J. Neuroimmunol*., 184:69-91.

Henn, A., Lund, S., Hedtjärn, M., Schrattenholz, A., Pörzgen, P., and Leist, M. (2009) "The suitability of BV2 cells as alternative model system for primary microglia cultures or for animal experiments examining brain inflammation." *ALTEX*, 26: 83-94.

Hensley, K., Maidt, M.L., Yu, Z., Sang, H., Markesbery, W.R., and Floyd, R.A. (1998) "Electrochemical analysis of protein nitrotyrosine and dityrosine in the Alzheimer brain indicates region-specific accumulation." *J. Neurosci*., 18:8126-8132.

Hickman, S.E., Allison, E.K., and El Khoury, J. (2008) "Microglial dysfunction and defective beta-amyloid clearance pathways in aging Alzheimer's disease mice." *J. Neurosci*., 28:8354-8360.

Hoek, R.M., Ruuls, S.R., Murphy, C.A., Wright, G.J., Goddard, R., Zurawski, S.M., Blom, B., Homola, M.E., Streit, W.J., Brown, M.H., Barclay, A.N., and Sedgwick, J.D. (2000) "Down-regulation of the macrophage lineage through interaction with OX2 (CD200)." *Science*, 290:1768-1771.

Hu, Q., Noll, R.J., Li, H., Makarov, A., Hardman, M., and Graham Cooks, R. (2005) "The Orbitrap: a new mass spectrometer." *J. Mass Spectrom*., 40: 430-443.

Humeau, Y., Popoff, M.R., Kojima, H., Doussau, F., and Poulain, B. (2002) "Rac GTPase plays an essential role in exocytosis by controlling the fusion competence of release sites." *J. Neurosci*., 22: 7968-7981.

Ito, S., Sawada, M., Haneda, M., Fujii, S., Oh-Hashi, K., Kiuchi, K., Takahashi, M., and Isobe, K. (2005) "Amyloid-b peptides induce cell proliferation and macrophage colonystimulating factor expression via the PI3-kinase/Akt pathway in cultured Ra2 microglial cells." *FEBS Lett*., 579: 1995-2000.

Janssen-Heininger, Y.M., Mossman, B.T., Heintz, N.H., Forman, H.J., Kalyanaraman, B., Finkel, T., Stamler, J.S., Rhee, S.G., and van der Vliet, A. (2008) "Redox-based regulation of signal transduction: principles, pitfalls, and promises." *Free Radic. Biol. Med*., 45: 1-17.

Jayaratnam, S., Khoo, A. K., and Basic, D., (2008) "Rapidly progressive Alzheimer's disease and elevated 14-3-3 proteins in cerebrospinal fluid." *Age Ageing*, 37: 467-469.

Jiang, L., Salao, K., Li, H., Rybicka, J.M., Yates, R.M., Luo, X.W., Shi, X.X., Kuffner, T., Tsai, V.W., Husaini, Y., Wu, L., Brown, D.A., Grewal, T., Brown, L.J., Curmi, P.M., and Breit, S.N. (2012) "Intracellular chloride channel protein CLIC1 regulates macrophage function through modulation of phagosomal acidification." *J. Cell. Sci.*, 125: 5479-5488.

Kaminsky, Y.G., Marlatt, M.W., Smith, M.A., and Kosenko, E.A. (2010) "Subcellular and metabolic examination of amyloid-beta peptides in Alzheimer disease pathogenesis: evidence for Abeta(25-35)." *Exp. Neurol.*, 221: 26-37.

Kim, S.U., and de Vellis, J. (2005) "Microglia in health and disease." *J. Neurosci. Res*., 81:302-313.

Kreutzberg G.W. (1996) "Microglia: a sensor for pathological events in the CNS." *Trends Neurosci*., 19:312-318.

Kreutzmann, P., Wolf, G., and Kupsch, K. (2010) "Minocycline recovers MTT-formazan exocytosis impaired by amyloid beta peptide." *Cell. Mol. Neurobiol*., 30: 979-984.

Lansbury, P.T., andLashuel, H.A. (2006) "A century-old debate on protein aggregation and neurodegeneration enters the clinic." *Nature*, 443:774-779.

Larson, M.E., andLesné, S.E. (2012) "Soluble Aβ oligomer production and toxicity." *J. Neurochem*., 120 Suppl 1:125-139.

Laudi, S., Steudel, W., Jonscher, K., Schöning, W., Schniedewind, B., Kaisers, U., Christians, U., and Trump, S. (2007) "Comparison of lung proteome profiles in two rodent models of pulmonary arterial hypertension." *Proteomics*, 7: 2469-2478.

Lawson, L.J., Perry, V.H., Dri, P., and Gordon, S. (1990) "Heterogeneity in the distribution and morphology of microglia in the normal adult mouse brain." *Neuroscience*, 39:151-170.

Layfield, R., Fergusson, J., Aitken, A., Lowe, J., Landon, M., and Mayer, R.J. (1996) "Neurofibrillary tangles of Alzheimer's disease brains contain 14-3-3 proteins." *Neurosci. Lett*., 209: 57-60.

Liang, S., Yu, Y., Yang, P., Gu, S., Xue, Y., and Chen, X. (2009) "Analysis of the protein complex associated with 14-3-3 epsilon by a deuterated-leucine labeling quantitative proteomics strategy." *J. Chromatogr. B Analyt. Technol. Biomed. Life Sci.*, 877: 627-634.

Lillig, C.H., and Berndt, C. (2012) "Glutaredoxins in thiol/disulfide exchange." *Antioxid. Redox Signal*., 18: 1654-1665.

Littler, D.R., Harrop, S.J., Fairlie, W.D., Brown, L.J., Pankhurst, G.J., Pankhurst, S., DeMaere, M.Z., Campbell, T.J., Bauskin, A.R., Tonini, R., Mazzanti, M., Breit, S.N., and Curmi, P.M. (2004) "The intracellular chloride ion channel protein CLIC1 undergoes a redox-controlled structural transition." *J. Biol. Chem*., 279: 9298-9305.

Littler, D.R., Harrop, S.J., Goodchild, S.C., Phang, J.M., Mynott, A.V., Jiang, L., Valenzuela, S.M., Mazzanti, M., Brown, L.J., Breit, S.N., and Curmi, P.M. (2010) "The enigma of the CLIC proteins: Ion channels, redox proteins, enzymes, scaffolding proteins?" *FEBS Lett*., 584: 2093-2101.

Liu, Y., and Schubert, D. (1997) "Cytotoxic amyloid peptides inhibit cellular 3-(4,5-dimethylthiazol-2-yl)-2,5-diphenyltetrazolium bromide (MTT) reduction by enhancing MTT formazan exocytosis." *J. Neurochem*., 69: 2285-2293.

Liu, B., and Hong, J.S.(2003)"Role of microglia in inflammation-mediated neurodegenerative diseases: mechanisms and strategies for therapeutic intervention."*J. Pharmacol. Exp. Ther*.,304: 1-7.

Lucin, K.M., and Wyss-Coray, T. (2009) "Immune activation in brain aging and neurodegeneration: too much or too little?" *Neuron*,64:110-122.

Makarov, A. (2000) "Electrostatic axially harmonic orbital trapping: a high-performance technique of mass analysis." *Anal. Chem*., 72: 1156-1162.

Mahley, R.W., Weisgraber, K.H., and Huang, Y. (2006) "Apolipoprotein E4: a causative factor and therapeutic target in neuropathology, including Alzheimer's disease." *Proc. Natl. Acad. Sci. U S A*, 103:5644-5651.

Maler, J.M., Klafki, H.W., Paul, S., Spitzer, P., Groemer, T.W., Henkel, A.W., Esselmann, H., Lewczuk, P., Kornhuber, J., and Wiltfang, J. (2007) "Urea-based two-dimensional electrophoresis of beta-amyloid peptides in human plasma: evidence for novel Abeta species."*Proteomics*, 7:3815-3820.

Malvezzi, A., Higa, P.M., T-do Amaral, A., Silva, G.M., Gozzo, F.C., Ferro, E.S., Castro, L.M., de Rezende, L., Monteiro, G., and Demasi, M. (2012) "The cysteine-rich protein thimet oligopeptidase as a model of the structural requirements for S-glutathiolation and oxidative oligomerization." *PLoS One*, 7: e39408.

Mandrekar, S., Jiang, Q., Lee, C.Y., Koenigsknecht-Talboo, J., Holtzman, D.M., and Landreth, G.E. (2009) "Microglia mediate the clearance of soluble Abeta through fluid phase macropinocytosis." *J. Neurosci*., 29: 4252-4262.

Mann, M., Hendrickson, R.C., and Pandey, A. (2001) "Analysis of proteins and proteomes by mass spectrometry." *Annu. Rev. Biochem.*, 70: 437-473.

Mantovani, A., Sica, A., Sozzani, S., Allavena, P., Vecchi, A., and Locati, M. (2004) "The chemokine system in diverse forms of macrophage activation and polarization." *Trends Immunol*.,25:677-786.

Markesbery, W.R. (1997) "Oxidative stress hypothesis in Alzheimer's disease." *Free Radic. Biol. Med*., 23:134-147.

McDonagh, B., Ogueta, S., Lasarte, G., Padilla, C.A., and Bárcena, J.A. (2009) "Shotgun redox proteomics identifies specifically modified cysteines in key metabolic enzymes under oxidative stress in Saccharomyces cerevisiae." *J. Proteomics*, 72: 677-689.

McGeer, P.L., andMcGeer, E.G. (2011) "History of innate immunity in neurodegenerative disorders." *Front. Pharmacol*.,2:77.

Mieyal, J.J., Gallogly, M.M., Qanungo, S., Sabens, E.A., and Shelton, M.D. (2008) "Molecular mechanisms and clinical implications of reversible protein S-glutathionylation." *Antioxid. Redox Signal*., 10:1941-1988.

Morrison, D. K. (2009) "The 14-3-3 proteins: integrators of diverse signaling cues that impact cell fate and cancer development." *Trends Cell Biol*., 19: 16-23.

Newman, S.F., Sultana, R., Perluigi, M., Coccia, R., Cai, J., Pierce, W.M., Klein, J.B., Turner, D.M., and Butterfield, D.A. (2007) "An increase in S-glutathionylated proteins in the Alzheimer's disease inferior parietal lobule, a proteomics approach." *J. Neurosci. Res.*, 85: 1506-1514.

Nimmerjahn, A., Kirchhoff, F., and Helmchen, F. (2005) "Resting microglial cells are highly dynamic surveillants of brain parenchyma in vivo." *Science*, 308:1314-1318.

Novarino, G., Fabrizi, C., Tonini, R., Denti, M.A., Malchiodi-Albedi, F., Lauro, G.M., Sacchetti, B., Paradisi, S., Ferroni, A., Curmi, P.M., Breit, S.N., and Mazzanti, M. (2004) "Involvement of the intracellular ion channel CLIC1 in microglia-mediated beta-amyloid-induced neurotoxicity." *J. Neurosci*., 24: 5322-5330.

Obsil, T., and Obsilova, V. (2011) "Structural basis of 14-3-3 protein functions." *Semin. Cell Dev. Biol*., 22: 663-672.

O'Keefe, G.M., Nguyen, V.T., and Benveniste, E.N. (2002) "Regulation and function of class II major histocompatibility complex, CD40, and B7 expression in macrophages and microglia: Implications in neurological diseases." *J. Neurovirol*., 8:496-512.

Ong, S.E., Blagoev, B., Kratchmarova, I., Kristensen, D.B., Steen, H., Pandey, A., and Mann, M. (2002) "Stable isotope labeling by amino acids in cell culture, SILAC, as a simple and accurate approach to expression proteomics." *Mol. Cell. Proteomics*, 1: 376-386.

Orellana, J.A., Shoji, K.F., Abudara, V., Ezan, P., Amigou, E., Sáez, P.J., Jiang, J.X., Naus, C.C., Sáez, J.C., and Giaume, C. (2011) "Amyloid β-induced death in neurons involves glial and neuronal hemichannels." *J. Neurosci*., 31: 4962-4977.

Osterloh, A., Meier-Stiegen, F., Veit, A., Fleischer, B., von Bonin, A., and Breloer, M. (2004) "Lipopolysaccharide-free heat shock protein 60 activates T cells." *J. Biol. Chem*., 279: 47906-47911.

Paco, S., Margelí, M.A., Olkkonen, V.M., Imai, A., Blasi, J., Fischer-Colbrie, R., and Aguado, F. (2009) "Regulation of exocytotic protein expression and Ca2+-dependent peptide secretion in astrocytes." *J. Biol. Chem*., 279: 47906-47911.

Pagan, J.K., Wylie, F.G., Joseph, S., Widberg, C., Bryant, N.J., James, D.E., and Stow, J.L. (2003) "The t-SNARE syntaxin 4 is regulated during macrophage activation to function in membrane traffic and cytokine secretion." *Curr. Biol*., 13: 156-160.

Pan, X.D., Zhu, Y.G., Lin, N., Zhang, J., Ye, Q.Y., Huang, H.P., and Chen, X.C. (2011) "Microglial phagocytosis induced by fibrillar β-amyloid is attenuated by oligomeric β-amyloid: implications for Alzheimer's disease." *Mol. Neurodegener*., 6: 45." *J. Neurochem*., 110: 143-156.

Paradisi, S., Matteucci, A., Fabrizi, C., Denti, M.A., Abeti, R., Breit, S.N., Malchiodi-Albedi, F., and Mazzanti, M. (2008) "Blockade of chloride intracellular ion channel 1 stimulates Abeta phagocytosis." *J. Neurosci. Res*., 86: 2488-2498.

Perry, V.H., Nicoll, J.A., and Holmes, C. (2009) "Microglia in neurodegenerative disease." *Nat. Rev. Neurol*., 6:193-201.

Plantier, M., Der Terrossian, E., and Represa, A. (1998) "Beta-actin immunoreactivity in rat microglial cells: developmental pattern and participation in microglial reaction after kainate injury." *Neurosci. Lett*., 247: 49-52.

Praticò, D.,and Sung, S. (2004)"Lipid peroxidation and oxidative imbalance: early functional events in Alzheimer's disease."*J. Alzheimer Dis*., 6:171-175.

Praticò, D. (2008)"Oxidative stress hypothesis in Alzheimer's disease: a reappraisal."*Trends Pharmacol. Sci*., 29:609-615.

Qin, L., Liu, Y., Wang, T., Wei, S.J., Block, M.L., Wilson, B., Liu, B., and Hong, J.S. (2004) "NADPH oxidase mediates lipopolysaccharide-induced neurotoxicity and proinflammatory gene expression in activated microglia." *J. Biol. Chem*., 279:1415-1421.

Ransohoff, R.M., and Perry, V.H. (2009) "Microglial physiology: unique stimuli, specialized responses." *Annu. Rev. Immunol*., 27:119-145.

Ransohoff, R.M., and Cardona, A.E. (2010) "The myeloid cells of the central nervous system parenchyma." *Nature*, 468:253-262.

Rappsilber, J., Mann, M., and Ishihama, Y. (2007) "Protocol for micro-purification, enrichment, pre-fractionation and storage of peptides for proteomics using StageTips." *Nat. Protoc.*, 2: 1896-1906.

Rasmussen, I., Pedersen, L.H., Byg, L., Suzuki, K., Sumimoto, H., and Vilhardt, F. (2010) "Effects of F/G-actin ratio and actin turn-over rate on NADPH oxidase activity in microglia." *BMC Immunol*., 11: 44.

Reynolds, A. D., Stone, D. K., Mosley, R. L., and Gendelman, H. E. (2009) "Proteomic studies of nitrated alpha-synuclein microglia regulation by CD4+ CD25+ T cells." *J. Proteome Res*., 8: 3497-3511.

Rhee, S.G., Bae, Y.S., Lee, S.R., and Kwon, J. (2000) "Hydrogen peroxide: a key messenger that modulates protein phosphorylation through cysteine oxidation." *Sci. STKE*, 2000:pe1.

Sala-Valdés, M., Gordón-Alonso, M., Tejera, E., Ibáñez, A., Cabrero, J.R., Ursa, A., Mittelbrunn, M., Lozano, F., Sánchez-Madrid, F., and Yáñez-Mó, M. (2012) Association of syntenin-1 with M-RIP polarizes Rac-1 activation during chemotaxis and immune interactions." *J. Cell. Sci*., 125: 1235-1246.

Satoh, J., Yamamura, T., and Arima, K. (2004) "The 14-3-3 protein epsilon isoform expressed in reactive astrocytes in demyelinating lesions of multiple sclerosis binds to vimentin and glial fibrillary acidic protein in cultured human astrocytes." *Am. J. Pathol*., 165: 577-592.

Scigelova, M., and Makarov, A. (2006) "Orbitrap mass analyzer--overview and applications in proteomics." *Proteomics*, Suppl., 2: 16-21.

Schindler, J., Lewandrowski, U., Sickmann, A., and Friauf, E. (2008) "Aqueous polymer two-phase systems for the proteomic analysis of plasma membranes from minute brain samples." *J. Proteome Res.*, 7: 432-442.

Schilling, T., and Eder, C. (2011) "Amyloid-β-induced reactive oxygen species production and priming are differentially regulated by ion channels in microglia." *J. Cell. Physiol.*, 226: 3295-3302.

Selkoe, D.J. (1997) "Alzheimer's disease: genotypes, phenotypes, and treatments." *Science*, 275:630-631.

Serrano-Pozo, A., Mielke, M.L., Gómez-Isla, T., Betensky, R.A., Growdon, J.H., Frosch, M.P., and Hyman, B.T. (2011) "Reactive glia not only associates with plaques but also parallels tangles in Alzheimer's disease." *Am. J. Pathol*., 179:1373-1384.

Shiio, Y., Suh, K.S., Lee, H., Yuspa, S.H., Eisenman, R.N., and Aebersold, R. (2006) "Quantitative proteomic analysis of myc-induced apoptosis: a direct role for Myc induction of the mitochondrial chloride ion channel, mtCLIC/CLIC4." *J. Biol. Chem*., 281: 2750-2756.

Sierra, A., Abiega, O., Shahraz, A., and Neumann, H. (2013) "Janus-faced microglia: beneficial and detrimental consequences of microglial phagocytosis." *Front. Cell Neurosci*., 7:6.

Sondag, C.M., Dhawan, G., and Combs, C.K. (2009) "Beta amyloid oligomers and fibrils stimulate differential activation of primary microglia." *J. Neuroinflammation*, 6: 1.

Stansley, B., Post, J., and Hensley, K. "A comparative review of cell culture systems for the study of microglial biology in Alzheimer's disease." *J. Neuroinflammation*, 9: 115.

Stella, R., Cifani, P., Peggion, C., Hansson, K., Lazzari, C., Bendz, M., Levander, F., Sorgato, M.C., Bertoli, A., and James, P. (2012) "Relative quantification of membrane proteins in wild-type and prion protein (PrP)-knockout cerebellar granule neurons." *J. Proteome Res*., 11: 523-536.

Steen, H., and Mann, M. (2004) "The ABC's (and XYZ's) of peptide sequencing." *Nat. Rev. Mol. Cell. Biol.*, 5: 699-711.

Strle, K., Zhou, J.H., Broussard, S.R., Venters, H.D., Johnson, R.W., Freund, G.G., Dantzer, R., and Kelley, K.W. (2002) "IL-10 promotes survival of microglia without activating Akt." *J. Neuroimmunol*., 122:9-19.

Sugama, S., Takenouchi, T., Kitani, H., Fujita, M., and Hashimoto, M. (2009) "Microglial activation is inhibited by corticosterone in dopaminergic neurodegeneration." *J. Neuroimmunol*., 208:104-114.

Suh, K.S., and Yuspa, S.H. (2005) "Intracellular chloride channels: critical mediators of cell viability and potential targets for cancer therapy." *Curr. Pharm. Des*., 11: 2753-2764.

Suh, K.S., Mutoh, M., Mutoh, T., Li L, Ryscavage, A., Crutchley, J.M., Dumont, R.A., Cheng, C., and Yuspa, S.H. (2007) "CLIC4 mediates and is required for Ca_2^+-induced keratinocyte differentiation." *J. Cell. Sci*., 120: 2631-2640.

Takata, K., Kitamura, Y., Tsuchiya, D., Kawasaki, T., Taniguchi, T., and Shimohama, S. (2003) "Heat shock protein-90-induced microglial clearance of exogenous amyloid-beta1-42 in rat hippocampus in vivo." *Neurosci. Lett*., 344: 87-90.

Town, T., Nikolic, V., and Tan, J. (2005) "The microglial "activation" continuum: from innate to adaptive responses." *J. Neuroinflammation*, 2:24.

Trapp, B.D., Wujek, J.R., Criste, G.A., Jalabi, W., Yin, X., Kidd, G.J., Stohlman, S., and Ransohoff, R. (2007) "Evidence for synaptic stripping by cortical microglia." *Glia*, 55:360-368.

Tulk, B.M., Kapadia, S., and Edwards, J.C. (2002) "CLIC1 inserts from the aqueous phase into phospholipid membranes, where it functions as an anion channel." *Am. J. Physiol. Cell Physiol.*, 282: C1103-C1112.

Underhill D.M., and Goodridge, H.S. (2012) "Information processing during phagocytosis." *Nat. Rev. Immunol*., 12:492-502.

Uylings, H.B., and de Brabander, J.M. (2002) "Neuronal changes in normal human aging and Alzheimer's disease." Brain Cogn., 49:268-276.

Valenzuela, S.M., Martin, D.K., Por, S.B., Robbins, J.M., Warton, K., Bootcov, M.R., Schofield, P.R., Campbell T.J., and Breit, S.N. (1997) "Molecular cloning and expression of a chloride ion channel of cell nuclei." *J. Biol. Chem*., 272: 12575-12582.

Valenzuela, S.M., Mazzanti, M., Tonini, R., Qiu, M.R., Warton, K., Musgrove, E.A., Campbell, T.J., and Breit S.N. (2000) "The nuclear chloride ion channel NCC27 is involved in regulation of the cell cycle." *J. Physiol*., 529: 541-552.

Varadarajan, S., Kanski, J., Aksenova, M., Lauderback, C., and Butterfield, D.A. (2001) "Different mechanisms of oxidative stress and neurotoxicity for Alzheimer's A beta(1-42) and A beta(25-35)." *J. Am. Chem. Soc.*, 123: 5625-5631.

vonBernhardi, R., andEugenín, J. (2012) "Alzheimer's disease: redox dysregulation as a common denominator for diverse pathogenic mechanisms." *Antioxid. Redox Signal*., 16:974-1031.

Wilkinson, B.L., and Landreth, G.E. (2006) "The microglial NADPH oxidase complex as a source of oxidative stress in Alzheimer's disease." *J. Neuroinflammation*, 3: 30.

Wu, C.C., and MacCoss, M.J. (2002) "Shotgun proteomics: tools for the analysis of complex biological systems." *Curr. Opin. Mol. Ther.*, 4: 242-250.

Yamauchi, A., Kim, C., Li, S., Marchal, C.C., Towe, J., Atkinson, S.J., and Dinauer, M.C. (2004) "Rac2-deficient murine macrophages have selective defects in superoxide production and phagocytosis of opsonized particles." *J. Immunol.*, 173: 5971-5979.

Zimmermann, P., Zhang, Z., Degeest, G., Mortier, E., Leenaerts, I., Coomans, C., Schulz, J., N'Kuli, F., Courtoy, P.J., and David, G. (2005) "Syndecan recycling [corrected] is controlled by syntenin-PIP2 interaction and Arf6." *Dev. Cell*, 9: 377-388.

Zerr, I., Pocchiari, M., Collins, S., Brandel, J.P., de Pedro Cuesta, J., Knight, R.S., Bernheimer, H., Cardone, F., Delasnerie-Lauprêtre, N., Cuadrado Corrales, N., Ladogana, A., Bodemer, M., Fletcher, A., Awan, T., Ruiz Bremón, A., Budka, H., Laplanche, J.L., Will, R.G., and Poser, S. (2000) "Analysis of EEG and CSF 14-3-3 proteins as aids to the diagnosis of Creutzfeldt-Jakob disease." *Neurology*, 55: 811-815.

Zhou, Y.,Wang, Y., Kovacs, M., Jin, J., and Zhang, J. (2005)"Microglial activation induced by neurodegeneration: a proteomic analysis." Mol. Cell. *Proteomics*, 4:1471-1479.

Zuo, S., Xue, Y., Tang, S., Yao, J., Du, R., Yang, P., and Chen, X. (2010) "14-3-3 epsilon dynamically interacts with key components of mitogen-activated protein kinase signal module for selective modulation of the TNF-alpha-induced time course-dependent NF-kappaB activity." *J. Proteom*

ACKNOWLEDGMENTS

I would like to thank Prof. M.Eugenia Schininà for her critical supervision and her contribution to my thesis.

Special thanks to Prof. Bruno Maras, Prof. Giuseppina Mignogna, Dr. Alessandra Giorgi and Dr. Laura Di Francesco for their continual encouragement and active support given to me during my PhD.

I would also like to thank Prof. Cinzia Fabrizi and Dr. Alberto Macone for their precious and fundamental collaboration to this project.

Furthermore, I would like to thank the Coordinator of my Ph.D. Course, Prof. Francesco Malatesta, all Professors of the Department of Biochemichal Sciences, and all my collegues for their valuable contribution to my scientific education during the Ph.D. course.

APPENDIX I

Table I - Differentially redox modified proteins identified by "biotin-switch" approach

Protein ID [a]	Protein name	Reversible oxidized Cys detected [b]	Reversible oxidation annotated [c]
P14869	60S acidic ribosomal protein P0	Cys226	S-nitrosylation[18]
P27659	60S ribosomal protein L3	Cys253	/
Q9D8E6	60S ribosomal protein L4	Cys96, Cys125* Cys208	S-nitrosylation[18]
P47962	60S ribosomal protein L5	Cys76	S-nitrosylation[8]
P14148	60S ribosomal protein L7	Cys208	/
P62918	60S ribosomal protein L8	Cys114, Cys115	/
P35979	60S ribosomal protein L12	Cys141, Cys162	S-nitrosylation[9]
P62717	60S ribosomal protein L18a	Cys109	/
P62830	60S ribosomal protein L23	Cys125	S-nitrosylation[15]
P14115	60S ribosomal protein L27a	Cys70	S-nitrosylation[9]
P62889	60S ribosomal protein L30	Cys52, Cys92	/
P62911	60S ribosomal protein L32	Cys91	/
P47964	60S ribosomal protein L36	Cys48	/
P83882	60S ribosomal protein L36a	Cys72, Cys77	/
P14206	40S ribosomal protein SA	Cys163	S-nitrosylation [1] S-glutathionylation[2]
P25444	40S ribosomal protein S2	Cys229	S-nitrosylation[9]
P62908	40S ribosomal protein S3	Cys97	S-nitrosylation[8]
P97351	40S ribosomal protein S3a	Cys139	S-nitrosylation[9]
P62702	40S ribosomal protein S4, X isoform	Cys41*	S-nitrosylation[9]
P62754	40S ribosomal protein S6	Cys12 Cys100*	S-nitrosylation[9]
P62242	40S ribosomal protein S8	Cys72, Cys100, Cys174	S-nitrosylation[9]
P62281	40S ribosomal protein S11	Cys116	/
Q6ZWZ6	40S ribosomal protein S12	Cys92	S-glutathionylation[3]
P63276	40S ribosomal protein S17	Cys35	/
Q9CQR2	40S ribosomal protein S21	Cys56	S-nitrosylation[18]
P62267	40S ribosomal protein S23	Cys90	/
Q6ZWU9	40S ribosomal protein S27	Cys59	S-nitrosylation[18]
Q5XJF6	Ribosomal protein	Cys66	/
P10605	Cathepsin B	Cys93	Disulfide bond #
P06797	Cathepsin L1	Cys269	Disulfide bond #
P18242	Cathepsin D	Cys284	Disulfide bond #
O70370	Cathepsin S	Cys178	Disulfide bond #
Q9WUU7	Cathepsin Z	Cys156, Cys299	Disulfide bond #
P35700	Peroxiredoxin-1	Cys52* (active site), Cys71 Cys83	S-nitrosylation[6], S-glutathionylation[2] Sulfenic acid #
O08709	Peroxiredoxin-6	Cys47 (active site)	S-nitrosylation[4], S-glutathionylation [3] Sulfenic acid #
Q9WV32	Actin-related protein 2/3 complex subunit 1B;1A	Cys162	/

Q99JY9	Actin-related protein 3	Cys235	/
Q9QZB7	Actin-related protein 10	Cys291	/
P13020	Gelsolin (actin depolimerizing factor)	Cys329	S-nitrosylation[6]
Q61233	Plastin-2	Cys42, Cys164, Cys336, Cys460, Cys618	S-nitrosylation[19]
P18760	Cofilin-1	Cys39* Cys139*	S-nitrosylation[4] S-glutathionylation[3]
P20152	Vimentin	Cys328	S-nitrosylation[8] S-glutathionylation[3]
P68369	Tubulin alpha-1A	Cys347	S-nitrosylation[1]
P68372	Tubulin beta-4B chain,4A chain	Cys12, Cys303	S-nitrosylation[1] S-glutathionylation[2]
Q60605	Myosin light polypeptide 6	Cys32	S-nitrosylation[19] S-glutathionylation[3]
P11983	T-complex protein 1 subunit alpha	Cys76	S-nitrosylation S-glutathionylation
P80318	T-complex protein 1 subunit gamma	Cys173, Cys213, Cys455	S-nitrosylation[8] S-glutathionylation[3]
P80316	T-complex protein 1 subunit epsilon	Cys302, Cys407	S-glutathionylation[3]
P42932	T-complex protein 1 subunit theta	Cys136	S-nitrosylation[10] S-glutathionylation[3]
P80313	T-complex protein 1 subunit eta	Cys29*, Cys511	S-glutathionylation[3]
P80317	T-complex protein 1 subunit zeta	Cys406*	S-nitrosylation[8] S-glutathionylation[3]
P26041	Moesin	Cys117	/
O89053	Coronin-1A	Cys285	/
Q3TLP8	Ras-related C3 botulinum toxin substrate 1	Cys105	/
Q05144	Ras-related C3 botulinum toxin substrate 2	Cys105, Cys157, Cys178	/
B2RXS4	Plexin-B2	Cys557	Disulfide bond #
Q80TM9	Nischarin	Cys884	/
P14211	Calreticulin	Cys105	S-nitrosylation[7] Disulfide bond #
P27773	Protein disulfide-isomerase A3	Cys244	S-nitrosylation[8] S-glutathionylation[2]
P63017	Heat shock cognate 71 kDa protein	Cys603	S-nitrosylation[6] S-glutathionylation[2]
P07901	Heat shock protein HSP 90-alpha	Cys530	S-nitrosylation #
P11499	Heat shock protein HSP 90-beta	Cys521	S-nitrosylation[18] S-glutathionylation[2]
P99029	Peroxiredoxin-5, mitochondrial	Cys200*	S-nitrosylation[8] S-glutathionylation[21] Disulfide bond #
Q9CQN1	Heat shock protein 75 kDa, mitochondrial	Cys135	S-nitrosylation[6]
P08249	Malate dehydrogenase, mitochondrial	Cys88, Cys93, Cys212,	S-nitrosylation [13] S-glutathionylation[5]

		Cys275, Cys285	
P05202	Aspartate aminotransferase, mitochondrial	Cys295	/
P47738	Aldehyde dehydrogenase, mitochondrial	Cys388	S-nitrosylation[13] S-glutathionylation[12]
P56391	Cytochrome c oxidase subunit 6B1	Cys65	S-glutathionylation[3] Disulfide bond #
Q9DCX2	ATP synthase subunit d, mitochondrial	Cys101	S-nitrosylation[4]
O08749	Dihydrolipoyl dehydrogenase, mitochondrial	Cys477, Cys484	S-nitrosylation[1]
Q8BFR5	Elongation factor Tu	Cys122	S-nitrosylation[8]
O88569	Heterogeneous nuclear ribonucleoproteins A2/B1	Cys50	S-nitrosylation[1]
P14152	Malate dehydrogenase, cytoplasmic	Cys137	S-nitrosylation[6]
P05064	Fructose-bisphosphate aldolase A	Cys290	S-nitrosylation[1] S-glutathionylation[2]
P06745	Glucose-6-phosphate isomerase	Cys404	S-nitrosylation[1]
P16858	Glyceraldehyde-3-phosphate dehydrogenase	Cys150, Cys154 Cys245*	S-nitrosylation[15]
P17182	Alpha-enolase	Cys337, Cys357*, Cys389*	S-nitrosylation[19] S-glutathionylation[2]
P17751	Triosephosphate isomerase	Cys268	S-nitrosylation[6] S-glutathionylation[3]
P21956	Lactadherin	Cys463	Disulfide bond #
P30681	High mobility group protein B2	Cys106	/
P50580	Proliferation-associated protein 2G4	Cys149	/
P60335	Poly(rC)-binding protein	Cys54	S-nitrosylation[15]
P60843	Eukaryotic initiation factor 4A-I	Cys66	S-nitrosylation[10]
P63158	High mobility group protein B1	Cys106	S-glutathionylation[16]
P63242	Eukaryotic translation initiation factor 5A-1,5A-2	Cys73	S-nitrosylation[4] S-glutathionylation[2]
P97429	Annexin A4	Cys108, Cys198	S-nitrosylation[8]
Q01768	Nucleoside diphosphate kinase B	Cys260	S-nitrosylation [6] S-glutathionylation[17]
Q01853	Transitional endoplasmic reticulum ATPase	Cys105	S-nitrosylation[18]
Q05816	Fatty acid-binding protein, epidermal	Cys67, Cys87	S-nitrosylation[7] S-glutathionylation[3]
Q3U9N4	Granulins	Cys98, Cys99, Cys183	/
Q60930	Voltage-dependent anion-selective channel protein 2	Cys77	/
Q61598	Rab GDP dissociation inhibitor beta	Cys302	S-nitrosylation[18]
Q6PDM2	Serine/arginine-rich splicing factor 1	Cys148	S-glutathionylation[3]
Q7TPV4	Myb-binding protein 1A	Cys676	/

Q8BG05	Heterogeneous nuclear ribonucleoprotein A3	Cys64	S-nitrosylation[8]
Q8BP47	Asparagine--tRNA ligase, cytoplasmic	Cys522	/
Q8BTS0	Probable ATP-dependent RNA helicase	Cys170	/
Q8C2Q7	Heterogeneous nuclear ribonucleoprotein H	Cys22, Cys267	S-nitrosylation[8]
Q8K114	Integrator complex subunit 9	Cys492	/
Q8VEK6	Inhibitor of growth protein 3	Cys384, Cys393	/
Q99K48	Non-POU domain-containing octamer-binding protein	Cys147	/
Q9D0I9	Arginine--tRNA ligase, cytoplasmic	Cys86	/
Q9DCD0	6-phosphogluconate dehydrogenase, decarboxylating	Cys402	/
Q9JIK5	Nucleolar RNA helicase 2	Cys754	/
Q9QUI0	Transforming protein RhoA	Cys16, Cys159	/
P61079	Ubiquitin-conjugating enzyme E2 D3/E2 D2	Cys85, Cys107	S-nitrosylation[18] S-glutathionylation[3]
P26516	26S proteasome non-ATPase regulatory subunit 7	Cys116	S-nitrosylation[18]
Q9R1P4	Proteasome subunit alpha type-1	Cys85	/
Q9R1P0	Proteasome subunit alpha type-4	Cys74	/
Q9Z0J0	Epididymal secretory protein E1	Cys93, Cys99, Cys140	Disulfide bond #
Q9Z1Q5	Chloride intracellular channel protein 1	Cys191	S-nitrosylation[4] Disulfide bond #
Q9Z2X1	Heterogeneous nuclear ribonucleoprotein F	Cys290	/
P17918	Proliferating cell nuclear antigen	Cys135, Cys162	S-nitrosylation[1]
P51881	ADP/ATP translocase 2	Cys160, Cys257	S-nitrosylation[15]
P61979	Heterogeneous nuclear ribonucleoprotein K	Cys132, Cys145 Cys185	S-nitrosylation[8]
P68040	Guanine nucleotide-binding protein subunit beta-2-like 1	Cys138, Cys153, Cys182 Cys240*, Cys249 Cys286	S-nitrosylation[1]
Q60932	Voltage-dependent anion-selective channel protein 1	Cys140, Cys245	S-nitrosylation[13]
Q61753	D-3-phosphoglycerate dehydrogenase	Cys48, Cys281 Cys369*	S-nitrosylation[6]
O09131	Glutathione S-transferase omega-1	Cys237	S-nitrosylation[4] S-glutathionylation[20]
O55143	Sarcoplasmic/endoplasmic reticulum calcium ATPase 2	Cys1007	/
P10126	Elongation factor 1-alpha 1	Cys411	S-nitrosylation[8] S-glutathionylation[3]
O70251	Elongation factor 1-beta	Cys161	S-nitrosylation[1]

P57776	Elongation factor 1-delta	Cys217	/
P58252	Elongation factor 2	Cys41, Cys466* Cys591, Cys693 Cys751*	S-nitrosylation[1] S-glutathionylation[14]
O88587	Catechol O-methyltransferase	Cys200	S-nitrosylation[9] S-glutathionylation[20]
P08030	Adenine phosphoribosyltransferase	Cys140	S-nitrosylation [4]
P08752	Guanine nucleotide-binding protein G(i) subunit alpha-2	Cys112	S-nitrosylation[11]
P08905	Lysozyme C-2	Cys95	Disulfide bond #
P11835	Integrin beta-2	Cys247	S-nitrosylation[8] Disulfide bond #
P19096	Fatty acid synthase	Cys274, Cys893	S-nitrosylation[9]
P34884	Macrophage migration inhibitory factor	Cys57	/
P50247	Adenosylhomocysteinase	Cys266	S-nitrosylation[9]
P51660	Peroxisomal multifunctional enzyme type 2	Cys175	S-glutathionylation[21]
P51906	Excitatory amino acid transporter 3	Cys158	/
P52480	Pyruvate kinase isozymes M1/M4	Cys152	S-nitrosylation[6] S-glutathionylation[2]
P61982	14-3-3 protein gamma	Cys97	S-glutathionylation
P68254	14-3-3 protein theta	Cys94	/
P62814	V-type proton ATPase subunit B, brain isoform	Cys162, Cys258	/
P84228	Histone H3.2	Cys111	/
P84244	Histone H3.3	Cys111	/
Q07076	Annexin A7	Cys260	S-nitrosylation[8] S-glutathionylation[20]
Q3TCU5	Tapasin	Cys318	Disulfide bond #
Q3TW96	UDP-N-acetylhexosamine pyrophosphorylase-like protein 1	Cys271	/
Q61035	Histidine--tRNA ligase, cytoplasmic	Cys455	/
Q61543	Golgi apparatus protein 1	Cys1067	/
Q6P4T2	Small nuclear ribonucleoprotein 200 (U5)	Cys133	/
Q6P9L4	Ubiquitin carboxyl-terminal hydrolase 49	Cys259 (active site)	/
Q8BGQ7	Alanine--tRNA ligase, cytoplasmic	Cys723, Cys947	/
Q8BKC5	Importin-5	Cys1078	/
Q8C605	6-phosphofructokinase	Cys122, Cys342	S-nitrosylation[6]
Q8CGC7	Bifunctional glutamate/proline--tRNA ligase	Cys381, Cys856, Cys1309	/
Q8K124	Pleckstrin homology domain-containing family O member 2	Cys444	/

Q8R081	Heterogeneous nuclear ribonucleoprotein L	Cys401	S-nitrosylation[8]
Q8R313	Exocyst complex component 6	Cys657	/
Q8VEK3	Heterogeneous nuclear ribonucleoprotein U	Cys473, Cys624	/
Q91VI7	Ribonuclease inhibitor	Cys129, Cys137, Cys357 Cys404	/
Q91WM3	U3 small nucleolar RNA-interacting protein 2	Cys416	/
Q921F2	TAR DNA-binding protein 43	Cys39	/
Q99JR1	Sideroflexin-1; Sideroflexin-3	Cys190	/
Q9CQ89	Protein CutA	Cys94	/
Q9CQC6	Basic leucine zipper and W2 domain-containing protein 1	Cys35	/
Q9CWJ9	Bifunctional purine biosynthesis protein PURH	Cys287	/
Q9CZN7	Serine hydroxymethyltransferase	Cys119	/
Q9D8U8	Sorting nexin-5	Cys397	/
Q9DBG5	Perilipin-3	Cys345	/
Q9DCL9	Multifunctional protein ADE2	Cys63	S-nitrosylation[19]
Q9JHJ3	Lysosomal protein NCU-G1	Cys214	/
Q9R0P3	S-formylglutathione hydrolase	Cys56	S-nitrosylation[1]
E9PVA8	Protein Gcn1l1- translational activator	Cys756*	/
Q3U132	Thymocyte-expressed positive selection-associated protein 1	Cys216*	/
Q61599	Rho GDP-dissociation inhibitor 2	Cys75*	/
Q76MZ3	Serine/threonine-protein phosphatase 2A	Cys390*	S-nitrosylation[18] S-glutathionylation[22]

a) UniProtKB protein identifier.
b) Specific redox modified cysteines, and their position in the protein sequences, identified in our experiments; in red are reported cysteines modified only after $A\beta_{25-35}$ stimulation, while in blue those modified only in the resting microglia.
c) Revesrible redox modification previously reported in literature or in database for the listed proteins.
* peptides containing cysteine with a statistical significant ($p \leq 0.05$) and by at least a 2-fold factor change in abundance after stimulation.
# annotation as in UniprotKB database.

References

1 Komatsubara, A.T., Asano, T., Tsumoto, H., Shimizu, K., Nishiuchi, T., Yoshizumi, M., and Ozawa, K. (2012) "Proteomic analysis of S-nitrosylation induced by 1-methyl-4-phenylpyridinium (MPP+)." *Proteome Sci*., 10: 74.

2 Lind, C., Gerdes, R., Hamnell, Y., Schuppe-Koistinen, I., von Löwenhielm, H.B., Holmgren, A., and Cotgreave, I.A. (2002) "Identification of S-glutathionylated cellular proteins during oxidative stress and constitutive metabolism by affinity purification and proteomic analysis." *Arch. Biochem. Biophys*., 406: 229-240.

3 Fratelli, M., Demol, H., Puype, M., Casagrande, S., Eberini, I., Salmona, M., Bonetto, V., Mengozzi, M., Duffieux, F., Miclet, E., Bachi, A., Vandekerckhove, J., Gianazza, E., and Ghezzi, P. (2002) "Identification by redox proteomics of glutathionylated proteins in oxidatively stressed human T lymphocytes." *Proc. Natl. Acad. Sci. U S A*, 99: 3505-3510.

4 Zhang, H.H., Feng, L., Livnat, I., Hoh, J.K., Shim, J.Y., Liao, W.X., and Chen, D.B. (2010) "Estradiol-17beta stimulates specific receptor and endogenous nitric oxide-dependent dynamic endothelial protein S-nitrosylation: analysis of endothelial nitrosyl-proteome." *Endocrinology*, 151: 3874-3887.

5 Mieyal, J.J., Gallogly, M.M., Qanungo, S., Sabens, E.A., and Shelton, M.D. (2008) "Molecular mechanisms and clinical implications of reversible protein S-glutathionylation." *Antioxid. Redox Signal*., 10: 1941-1988.

6 Lefièvre, L., Chen, Y., Conner, S.J., Scott, J.L., Publicover, S.J., Ford, W.C., and Barratt, C.L. (2007) "Human spermatozoa contain multiple targets for protein S-nitrosylation: an alternative mechanism of the modulation of sperm function by nitric oxide?" *Proteomics*, 7: 3066-3084.

7 Dall'Agnol, M., Bernstein, C., Bernstein, H., Garewal, H., and Payne, C.M. (2006) "Identification of S-nitrosylated proteins after chronic exposure of colon epithelial cells to deoxycholate." Proteomics, 6: 1654-1662.

8 Lam, Y.W., Yuan, Y., Isaac, J., Babu, C.V., Meller, J., and Ho, S.M. (2010) "Comprehensive identification and modified-site mapping of S-nitrosylated targets in prostate epithelial cells." *PLoS One*, 5: e9075.

9 Doulias, P.T., Greene, J.L., Greco, T.M., Tenopoulou, M., Seeholzer, S.H., Dunbrack, R.L., and Ischiropoulos, H. (2010) "Structural profiling of endogenous S-nitrosocysteine residues reveals unique features that accommodate diverse mechanisms for protein S-nitrosylation." *Proc. Natl. Acad. Sci. U S A*, 107: 16958-16963.

10 Tello, D., Tarín, C., Ahicart, P., Bretón-Romero, R., Lamas, S., and Martínez-Ruiz, A. (2009) "A "fluorescence switch" technique increases the sensitivity of proteomic detection and identification of S-nitrosylated proteins." *Proteomics*, 9:5359-5370.

11 Kuncewicz, T., Sheta, E.A., Goldknopf, I.L., and Kone, B.C. (2003) "Proteomic analysis of S-nitrosylated proteins in mesangial cells." *Mol. Cell. Proteomics*, 2: 156-163.

12 Tsou, P.S., Addanki, V., Haas, J.A., Page, N.A., and Fung, H.L. (2009) "Role of glutaredoxin-mediated protein S-glutathionylation in cellular nitroglycerin tolerance." *J. Pharmacol. Exp. Ther*., 329: 649-656.

13 Moon, K.H., Hood, B.L., Kim, B.J., Hardwick, J.P., Conrads, T.P., Veenstra, T.D., and Song, B.J. (2006) "Inactivation of oxidized and S-nitrosylated mitochondrial proteins in alcoholic fatty liver of rats." *Hepatology*, 44: 1218-1230.

14 Townsend, D.M., Findlay, V.J., Fazilev, F., Ogle, M., Fraser, J., Saavedra, J.E., Ji, X., Keefer, L.K., and Tew, K.D. (2005) "A glutathione S-transferase pi-activated prodrug causes kinase activation concurrent with S-glutathionylation of proteins." *Mol. Pharmacol*., 69: 501-508.

15 Wu, C., Liu, T., Chen, W., Oka, S., Fu, C., Jain, M.R., Parrott, A.M., Baykal, A.T., Sadoshima, J., and Li, H. (2010) "Redox regulatory mechanism of transnitrosylation by thioredoxin." *Mol. Cell. Proteomics*, 9: 2262-2275.

16 Hoppe, G., Talcott, K.E., Bhattacharya, S.K., Crabb, J.W., and Sears, J.E. (2006) "Molecular basis for the redox control of nuclear transport of the structural chromatin protein Hmgb1." *Exp. Cell Res*., 312: 3526-3538.

17 Lee, E., Jeong, J., Kim, S.E., Song, E.J., Kang, S.W., and Lee, K.J. (2009) "Multiple Functions of Nm23-H1 Are Regulated by Oxido-Reduction System." *PLoS One*, 4: e7949.

18 Liu, M., Hou, J., Huang, L., Huang, X., Heibeck, T.H., Zhao, R., Pasa-Tolic, L., Smith, R.D., Li, Y., Fu, K., Zhang, Z., Hinrichs, S.H., and Ding, S.J. (2010) "Site-Specific Proteomics Approach for Study Protein S-Nitrosylation." *Anal. Chem*., 82: 7160-7168.

19 Benhar, M., Thompson, J.W., Moseley, M.A., and Stamler, J.S. (2010) "Identification of S-nitrosylated targets of thioredoxin using a quantitative proteomics approach." *Biochemistry*, 49: 6963-6969.

20 Chiang, B.Y., Chou, C.C., Hsieh, F.T., Gao, S., Lin, J.C., Lin, S.H., Chen, T.C., Khoo, K.H., and Lin, C.H. (2012) "In Vivo Tagging and Characterization of S-Glutathionylated Proteins by a Chemoenzymatic Method" *Angew. Chem. Int. Ed. Engl*., 51: 5871-5875.

21 Fratelli, M., Demol, H., Puype, M., Casagrande, S., Villa, P., Eberini, I., Vandekerckhove, J., Gianazza, E., and Ghezzi, P. (2003) "Identification of proteins undergoing glutathionylation in oxidatively stressed hepatocytes and hepatoma cells" *Proteomics*, 3: 1154-1161.

22 Rao, R.K., and Clayton, L.W. (2002) "Regulation of protein phosphatase 2A by hydrogen peroxide and glutathionylation" *Biochem. Biophys. Res. Commun.*, 293: 610-616.

23 Townsend, D.M., Findlay, V.J., Fazilev, F., Ogle, M., Fraser, J., Saavedra, J.E., Ji, X., Keefer, L.K., and Tew, K.D. (2006) "A Glutathione S-Transferase -Activated Prodrug Causes Kinase Activation Concurrent with S-Glutathionylation of Proteins" *Mol. Pharmacol*., 69: 501-508.

APPENDIX II

SCIENTIFIC PUBBLICATIONS DURING THE Ph.D COURSE (2010-2013)

124 DOI 10.1002/pmic.201100113 *Proteomics* 2012, *12*, 124–134

RESEARCH ARTICLE

14-3-3ε marks the amyloid-stimulated microglia long-term activation*

Laura Di Francesco[1]**, *Virginia Correani*[1]**, *Cinzia Fabrizi*[2]**, *Lorenzo Fumagalli*[2], *Michele Mazzanti*[3], *Bruno Maras*[1] *and M. Eugenia Schininà*[1]

[1] Dipartimento di Scienze Biochimiche, Sapienza, University of Rome, Rome, Italy
[2] Dipartimento di Scienze Anatomiche, Istologiche, Medico-Legali e dell'Apparato Locomotore, Sapienza, University of Rome, Rome, Italy
[3] Dipartimento di Scienze Biomolecolari e Biotecnologie, University of Milan, Milan, Italy

Microglia-mediated inflammation in the central nervous system is a hallmark of the pathogenesis of several neurodegenerative diseases including Alzheimer's disease. Microglial cells activation follows the deposition of amyloid β fibrils and it is generally considered a triggering factor in the early steps of the onset of Alzheimer's disease. Although the initial engagement of microglia seems to play a neuroprotective role, many lines of evidence indicate that a persistent activation with the production of proinflammatory molecules contributes to dismantle neuronal activity and to induce neuronal loss occurring in neurodegenerative diseases. To date, limited proteomic data are available on activated microglial cells in response to extracellular amyloidogenic peptides. In this study, murine microglial cells have been employed to investigate the effects of amyloid β peptides in triggering microglial activation. The response was monitored at the proteome level through a two-dimensional gel electrophoresis-based approach. Results show only a limited number of differentially expressed proteins, among these a more acidic species of the cytosolic actin, and the 14-3-3ε protein, found significantly upregulated in Aβ-activated cells. 14-3-3ε belongs to a regulatory protein family involved in important cellular processes, including those leading to neurodegenerative diseases, and thus its increased expression suggests a role of this protein in tuning microglia activation.

Received: March 1, 2011
Revised: October 5, 2011
Accepted: October 10, 2011

Keywords:
14-3-3ε / Actin / Alzheimer's disease / Amyloid β peptides / Biomedicine / Microglia

1 Introduction

Alzheimer's disease (AD) is an age-related neurodegenerative disorder associated with extensive neuronal loss in selected brain regions, progressive formation of neurofibrillary tangles, and accumulation of extracellular amyloid plaques (for comprehensive reviews, see [1, 2]). This amyloid material is mainly composed of peptides produced by proteolytic cleavage of the larger membrane-bound amyloid precursor protein (APP) [3]. These amyloid β peptides (Aβ), mainly $A\beta_{1-40}$ and $A\beta_{1-42}$ [4], are insoluble and spontaneously prone to aggregate, and have long been thought to be responsible of neurodegeneration observed in AD [5, 6]. Microglial cells are macrophagic cells within the central nervous system (CNS) playing a pivotal role in the brain homeostasis maintenance, the detection of invading pathogens, and tissue repair in neuronal compartment. They are

Correspondence: Professor M. Eugenia Schininà, Dipartimento di Scienze Biochimiche, Sapienza, University of Rome, Piazzale Aldo Moro, 5, 00185 Roma, Italy
E-mail: eugenia.schinina@uniroma1.it
Fax: +39-06-4440062

Abbreviations: Aβ, amyloid β peptides; **AD,** Alzheimer's disease; **IAM,** iodoacetamide; **MTT,** 3-(4,5-dimethylthiazol-2-yl)-2,5-diphenyltetrazolium bromide

*This article is dedicated to Professor Francesco Bossa on the occasion of his 70th birthday.
**These authors have contributed equally to this study.

cells able to quickly react to perturbing agents within the brain [7]. Many reports demonstrate that in response to inflammatory stimuli, microglia become morphologically and functionally activated and produce a variety of proinflammatory factors, including neurotoxic reactive oxygen species (e.g. superoxide and nitric oxide), eicosanoids, and cytokines (e.g. tumor necrosis factor-α, interleukins 1α, 1β, and 6). Microglia is today considered an emerging actor in neurodegenerative disorders [8]. In transgenic mouse models of AD, microglia are observed to accumulate within the core of amyloid plaques [9], where they are able to phagocyte β-amyloid deposits [10]. Several data have shown that Aβ may act on microglia as inflammatory stimuli to elicit a cellular-mediated response, leading to the release of immunomodulators [11, 12]. Only few of these factors are thought to contribute to tissue repair and to promote neuronal survival, thanks to their neuroprotective activities (e.g. transforming growth factor β) [13]. The majority is believed to induce or exacerbate neurodegeneration by causing neuronal apoptosis through mechanisms not yet fully understood [14]. Thus, clarifying the molecular events leading to microglia activation may be critical in highlighting pathways involved in inflammation-mediated nervous system disorders, such as neuronal degeneration in AD.

For few years, genomics and proteomics have been used to conduct a limited number of studies on microglia activation [15, 16]. When these studies have been carried out using primary microglia cultured from pathological nervous tissues, molecular profiles were able to describe the microglial phenotype at the end point of the pathological activation, but failed to define the genomic or proteomic changes involved in the first steps of the complex pathway leading to the stable activation.

In this article, we investigated the early onset of long-term activation using BV2 cells derived from raf/myc-immortalized murine neonatal microglia, which are the most frequently used substitutes for primary microglia [17, 18]. We challenged BV2 cells with $A\beta_{25-35}$, a toxic $A\beta_{1-42}$ fragment [19] and analyzed the differential phenotype between resting and activated microglia by proteomics.

Results show a limited change in the protein pattern and indicate the protein 14-3-3ε as the most intriguing candidate to mark the long-term molecular response of microglial cells in neurodegenerative diseases.

2 Materials and methods

2.1 Chemicals and materials

Acrylamide, *N,N*-methylene *bis*-acrylamide, ammonium sulfate and persulfate, ammonium bicarbonate, Tris-HCl, bromophenol blue, β-mercaptoethanol, glycerol, urea, thiourea, CHAPS, amidosulfobetaine-14 (ASB-14), sodium chloride, and CHCA matrix were purchased from Sigma-Aldrich. Chemicals purchased from Bio-Rad are SDS, Tris, Glycine, TEMED, iodoacetamide (IAM), Coomassie Brilliant Blue G250, DTT, carrier ampholytes, IPG strips, Tween-20, mineral oil, precasted gels (Criterion XT Bis-Tris gel), and nitrocellulose membrane. Ethanol, magnesium chloride, methyl alcohol, and ACN were purchased from Carlo Erba. Calcium chloride was purchased from Merck (Germany). Phosphoric acid and TFA were purchased from Fluka. Trypsin was purchased from Promega. All aqueous solutions were prepared with ultrapure water (18.2 MΩ/cm) from Milli-Q water purification system (Millipore).

2.2 BV2 cell cultures

The murine microglial cell line BV2, generated by infecting primary mouse microglial cultures with a v-raf/v-myc oncogene carrying retrovirus [17], was grown in DMEM (Invitrogen) supplemented with penicillin, streptomycin, and 10% FCS (Sigma); cultures were maintained at 37°C in 5% CO_2/95% humidified air atmosphere. Synthetic $A\beta_{25-35}$ (GSNKGAIIGLM) and reverse $A\beta_{35-25}$ (MLGIIAGKNSG) were purchased from Sigma-Aldrich. Peptides were dissolved in sterile, distilled water at a concentration of 1 mM and incubated for 72 h at 37°C to allow aggregation. Two replicates for each of resting, $A\beta_{25-35}$ and $A\beta_{35-25}$-treated BV2 cells were carried out. For this purpose, BV2 cells were cultured in 100-mm tissue culture dish at a density of 6×10^6 cells/dish, washed with serum-free media, and treated for 24 h with 50 μM amyloid peptides. BV2 cells were trypsinized after 24 and 48 h of treatment and the viable cell number was determined by trypan-blue exclusion and cell counting with a hemocytometer.

2.3 Cell viability

Cell viability was measured by 3-(4,5-dimethylthiazol-2-yl)-2,5-diphenyltetrazolium bromide (MTT) reduction essentially as described previously [20]. Following 24-h treatment with 50 μM $A\beta_{25-35}$ or $A\beta_{35-25}$, 10 μL of MTT solution (5 mg/mL) was added to each well and the incubation was continued for 3 h. Lysis buffer was prepared by dissolving 40% w/v SDS in deionized water; after adding an equal volume of DMF and the pH was adjusted to 4.7. After 3-h incubation with MTT, 100 μL of the lysis buffer was added to each well and the absorbance read at 570 nm on a Microplate Reader.

2.4 Tumor necrosis factor mRNA

After the 4-h treatment with either 50 μM $A\beta_{25-35}$ or $A\beta_{35-25}$, total RNA was purified by 2×10^6 BV2 cells by a single extraction with Trizol (Invitrogen) and reverse transcribed by oligo$(dT)_{15-18}$ primers and MML-V reverse transcriptase

(Invitrogen). The cDNA was amplified by *Taq* DNA polymerase in a thermal cycle (PerkinElmer Life Sciences) in the presence of primers for tumor necrosis factor (TNF-α) (5′-primer, GAGCACTGAAAGCATGATCCG; 3′-primer, GCAGGTCTACTTTGGGATCATT). Conditions for TNF-α amplifications were as follows: 30 s at 94°C, 30 s at 64°C, and 30 s at 72°C. Ten microliter of each PCR product was electrophoresed on 1% agarose gel and then visualized by ethidium bromide staining. The mRNA for GAPDH was used as reference.

2.5 Protein extraction and quantification

Both replicates for $A\beta_{25-35}$, $A\beta_{35-25}$ treated and control BV2 cells underwent a subcellular fractionation by Qproteome Cell Compartment Kit (Qiagen). According to the protocol used, fractions enriched with cytosolic or with membrane proteins and proteins from the lumen of organelles except the nuclear components (named hereafter organelle proteins), respectively, were obtained from each lysate.

2.6 Two-dimensional electrophoresis separation

Protein mixtures from each cellular fraction were analyzed by two-dimensional electrophoresis (2-DE). An equivalent protein amount (180 μg) from each of the cytosolic and organelle samples was desalted by precipitation with cold ethanol. The cytosolic pellet was resuspended with rehydration buffer (5 M urea, 2 M thiourea, 50 mM DTT, 2% w/v CHAPS, 0.2% v/v ampholytes, pH 3–10) and loaded on linear pH 3–10 IPG strips. The pellet obtained from the organelle fraction was resuspended in the same rehydration buffer, as above, added with 2% w/v of ASB-14 and loaded on 11-cm immobilized linear pH 3–10 IPG strips. After passive rehydration for 12 h at a temperature of 20°C, IEF was performed as follows: (i) 250 V for 15 min; (ii) 250–8000 V in 2.5 h; (iii) 8000 V for 4 h. Strips were reducted/alkylated soaking them in a DTT-buffered solution (6 M urea, 2% SDS, 50 mM Tris, pH 8.8, 20% glycerol, 130 mM DTT) followed by a IAM treatment (6 M urea, 2% SDS, 50 mM Tris, pH 8.8, 20% glycerol, 135 mM IAM) and then loaded on 1-mm thick precasted 4–12% SDS-PAGE gels and fixed with warm low-melting agarose. Second-dimension electrophoreses were performed applying a ramping voltage (from 100 to 200 V). The 2-D gels were stained with by colloidal Coomassie. For each cellular fraction, three replicates were carried out.

2.7 Image analyses

2-DE gels were digitized using GS-710 Densitometer (BioRad). The images were analyzed for the detection and quantification of protein spots using PDQuest software version 8.0 (BioRad) according to the manufacturer's procedures. Where gel and spot quality strongly influenced the matching capabilities of the software used for protein quantization, the replicate gels were critically reviewed for their reproducibility. Subsequently, analysis sets were set up to check the proteins expressed in control and treated sample in a differentially manner. Proteins identified in the majority of the replica and present in a twofold differential amount in the majority of the treated samples compared with control samples were analyzed by MALDI-TOF-MS.

2.8 In-gel digestion, MS analysis, and database search

Selected spots were manually excised from gels and submitted to in-gel digestion using sequencing grade trypsin. Briefly, the selected spots were excised from gel, washed with a solution of 50 mM ammonium bicarbonate containing 50% ACN, dehydrated with 100% ACN, and speed-vac dried. The dried gel pieces were then rehydrated by adding about 10 μL of 25 mM ammonium bicarbonate containing 11 ng/μL of trypsin and incubated on ice. After 30 min, more trypsin buffer was added, if necessary. Gel pieces were then incubated for 16 h at 37°C. An aliquot of 1 μL from each peptide mixture was mixed with the same volume of a solution of CHCA matrix (5 mg/mL in 70% ACN, containing 0.1% TFA) and the mixture was analyzed on MALDI-TOF (Model Voyager-DE STR, Applied Biosystems, Foster, CA) in reflectron mode as described previously [21]. Mass data were collected in the mass range of 800–5000 Da and processed using data analyzer software MoverZ (Proteometrics), according to the default parameters. All mass spectra were externally calibrated using a standard peptide mixture containing *des*-Arg-bradykinin ($m/z = 904.4681$), angiotensin I ($m/z = 1296.6853$), 1–17 ($m/z = 2093.0867$), and 18–39 ($m/z = 2465.1989$) adrenocorticotropic hormone fragments. Two tryptic autolytic peptides were also used for the internal calibration ($m/z = 842.5100$ and 2807.3145). Identification by peptide mass fingerprint (PMF) was performed using the MASCOT search engine version 2.2 (http://www.matrixscience.com) against the Swiss-Prot *Mus musculus* database (version 2011_01, 524 420 sequences, 185 205 850 residues), after the exclusion of contaminant mass values, as keratine masses and trypsin autodigestion products, using the software PeakErasor (http://www.protein.sdu.dk/gpmaw/Help/PeakErazor/peakerazor.html). Matching parameters generally selected in the search program were maximum error of 50 ppm, up to two missed trypsin cleavages, carbamidomethyl cysteine as fixed modification, oxidation of methionine, and NH_2-terminal protein acetylation as variable modification. Identifications were validated when the probability-based MOWSE protein score was significant according to MASCOT.

2.9 Western blot analysis

For Western blotting analysis, an equal amount of protein for each cytosolic sample (18 µg per lane) was separated by SDS-PAGE in a Tris-glycine buffer system on 0.75-mm thick 12% polyacrylamide gels. Electrical transfer onto a nitrocellulose membrane was performed using an electroblotting apparatus (BioRad) at 85 V for 90 min at 4°C in a 25-mM Tris, 20 mM glycine, and 20% methanol buffer. The membrane was stained with 0.2% Ponceau Red in 0.3% trichloroacetic acid to check for transfer success. Then, the membrane was treated with 5% ECL-blocking agent (GE Healthcare Biosciences) in T-TBS buffer (10 mM Tris-HCl, 150 mM NaCl, 1 mM $CaCl_2$, and 1 mM $MgCl_2$, pH 7.4, 0.1% Tween-20), for 1 h and then incubated with primary antibody overnight at 4°C. Subsequently, the membrane was washed three times in T-TBS, and the immunocomplexes were labeled using HRP-conjugated secondary antibodies, and then detected by an ECL Plus Western blotting Detection System (GE Healthcare Biosciences). ECL was detected using a Kodak Image Station 440cf (Eastman Kodak) and quantified using ImageJ analysis software (http://rsbweb.nih.gov/ij/). Analysis was performed in triplicate from two independent biological replicates. Antibodies were purchased from the following sources: anti-14-3-3 (rabbit polyclonal antibody, sc-629, 1:500; Santa Cruz Biotechnology); anti-14-3-3ε (rabbit polyclonal antibody, sc-1020, 1:500; Santa Cruz Biotechnology); anti-glyceraldehyde-3-phosphate dehydrogenase (anti-GAPDH, mouse monoclonal antibody, sc-32233, 1:500; Santa Cruz Biotechnology) used as the loading control anti-rabbit IgG-HRP (goat antibody, sc-2350, 1:2000; Santa Cruz Biotechnology) and anti-mouse IgG-HRP (goat antibody, sc-2500, 1:2000; Santa Cruz Biotechnology). In each analyzed sample, target protein was relatively quantified by normalization to the corresponding GADPH level. Statistical analysis was performed by applying Student's *T*-test; differences in protein expression with *p*-value of <0.05 were considered statistically significant.

3 Results

3.1 BV2 cells activation after amyloid stimulation

The proteomic profile of amyloid-activated microglia was achieved on BV2 cells, an immortalized microglial cell line [17, 18]. BV2 cells were challenged with 50 µM $A\beta_{25-35}$ peptide, the neurotoxic domain of the full-length $A\beta_{1-42}$ peptide [19]. In fact, $A\beta_{25-35}$ has been frequently used in the investigations of Aβ properties because it is a more easily manipulating substitute for the native full-length peptide. Although both $A\beta_{1-42}$ and $A\beta_{25-35}$ had been demonstrated to induce toxicological and oxidative effects on neuronal cells, Butterfield and colleagues in 2001 suggested that the $A\beta_{25-35}$ peptide could act its neurotoxicity with a mechanism only partially overlapping with the neuronal activity of the full-length peptide [19]. Moreover, a recent investigation on the presence of shorter peptides in Alzheimer's tissues describes peptide $A\beta_{25-35}$ as just a possible component of human amyloid [22]. Nevertheless, the requirement to induce highly reproducible changes in the medium of the cultured cells, mandatory for proteomic studies, led us to refuse $A\beta_{1-42}$ as elicitor in our preliminary investigation on responsiveness of microglia to neuroinflammatory injury.

Early activation of BV2 cells induced by $A\beta_{25-35}$ was established by the RT-PCR detection of the transcription of TNF-α after 4 h of treatment (Fig. 1A). This response is long lasting, according to a significant inhibition of the cellular MTT reduction detected up to 24 h in $A\beta_{25-35}$-treated cells (Fig. 1B). The reduction observed by MTT test in $A\beta_{25-35}$-treated BV2 cells is associated with an increased proliferation, as showed by cell counting (Fig. 1C). In order to discriminate between the effects specifically ascribed to amyloid material and those due to a nonspecific perturbation, BV2 cells were parallelly treated with the same amount of a synthetic peptide, made up from the reverse sequence of the $A\beta_{25-35}$ peptide (named $A\beta_{35-25}$ or reverse peptide) and known to miss the proinflammatory property [23]. The absence of TNF-α transcription in the cells exposed to $A\beta_{35-25}$ confirms that only the amyloidogenic peptide $A\beta_{25-35}$ is able to trigger a proinflammation in microglia (Fig. 1).

3.2 Changes in the microglial protein profile during $A\beta_{25-35}$ activation

The presence of biomarkers for molecular pathways accounting for the specific BV2 responsiveness to $A\beta_{25-35}$ was then investigated through the unbiased proteomic approach. We used two fractions of each cell lysate, after 24 h of treatment, respectively, enriched either with cytosolic proteins or with proteins from membrane and from the lumen of organelles, except the nuclear components. Each sample was then analyzed by 2-DE using a linear pH gradient in the first separation. 2-DE profiles from the two BV2 compartments were made up from three analytical replicates for two independent biological replicates of each BV2 state ($A\beta_{25-35}$-, $A\beta_{35-25}$-treated and control cells).

In control BV2 cells, approximately 230 and 130 protein spots were detected by colloidal Coomassie staining among all replicates of cytosolic and organelle fractions, respectively (Fig. 2); several of them have been identified by MALDI-TOF PMF (data not reported). Qualitative and quantitative changes between 2-DE maps of control and stimulated cells were then achieved by PDQuest software. Spots that showed ≥2-fold changes in intensity or were uniquely expressed in the 2-DE maps of treated cell fractions respect to resting BV2 fraction samples were excised, and proteins were identified by MALDI-TOF PMF (labeled spots in Fig. 2). These identifications are summarized in Table 1.

This approach was able to prove a downregulation by an approximately twofold factor for seven proteins in $A\beta_{25-35}$-

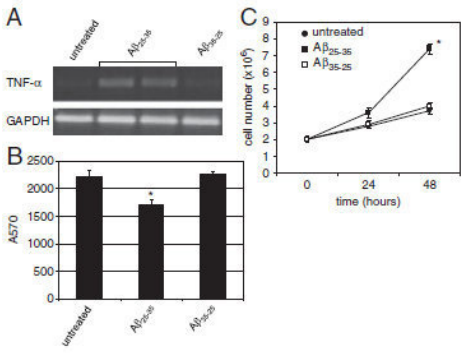

Figure 1. Effects of $A\beta_{25-35}$ and $A\beta_{35-25}$ on BV2 cells. (A) Induction of TNF-α mRNA in BV2 cells treated for 4 h with 50 μM $A\beta_{25-35}$ or $A\beta_{35-25}$; TNF-α was detected by RT-PCR. The mRNA for GAPDH was used as reference. (B) $A\beta_{25-35}$ inhibits MTT reduction; BV2 cells were treated for 24 h with 50 μM $A\beta_{25-35}$ or $A\beta_{35-25}$ and then MTT reduction was performed. (C) $A\beta_{25-35}$ induces cell proliferation; BV2 cells were treated for 24 and 48 h with 50 μM $A\beta_{25-35}$ or $A\beta_{35-25}$ and cell number was determined by trypan-blue exclusion and cell counts. ANOVA with Bonferroni-corrected *t*-test (*$p<0.001$ versus untreated cultures).

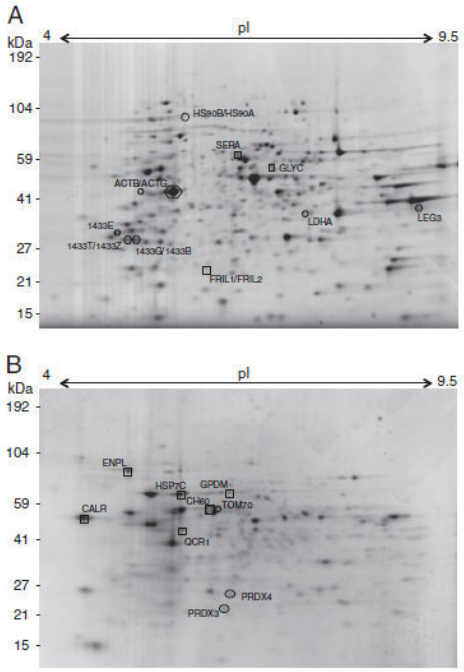

Figure 2. Effects of $A\beta_{25-35}$ and $A\beta_{35-25}$ on 2-DE protein profiles of BV2. BV2 proteome was prefractionated according to the Qproteome Cell Compartment Kit (Qiagen) into cytosolic proteins and a fraction enriched with membrane proteins and proteins from the lumen of organelles except the nuclear components. Protein mixtures were then electrophoretically separated in the linear pH range 3–10 (*X*-axis) and molecular mass (*Y*-axis, according to the migration of molecular mass markers), and visualized by staining with colloidal Coomassie. (A) Representative 2-DE map of the resting BV2 cytosolic proteome. (B) Representative 2-DE map of resting BV2 organelle proteome. Circles and squares refer to spots that showed ≥2-fold changes in intensity or that were uniquely expressed in $A\beta_{25-35}$- and $A\beta_{35-25}$-treated BV2 cells, respectively, with respect to the control cell map reported here. Their MALDI-TOF identifications are also reported, according to Table 1. Diamonds label further protein spots discussed in the text.

treated cells in respect to the resting control sample. Particularly, Hsp 90α/β, galectin 3, and L-lactate dehydrogenase A chain were observed to be downregulated in the cytosolic fraction, whereas TOM 70, peroxiredoxins 3 and 4, Hsp 60 are decreasing proteins in the membrane/organelle fraction. According to their proposed biochemical function, this inventory encompasses two molecular chaperons (Hsp 90 and Hsp 60), one metabolic enzyme (L-lactate dehydrogenase), two redox proteins (peroxiredoxins 3 and 4), one mitochondrial membrane carrier (TOM70), and a lectin (galectin 3). Only few of them have been associated with neurodegeneration: Hsp 90 seems to enhance the clearance of $A\beta_{1-42}$ [24] and TOM complex has been already demonstrated to be involved in Aβ import [25].

Notably, only two components of the entire BV2 proteome were demonstrated upregulated. The first is a more acidic species of the cytosolic actin, absent in the control and in the reverse peptide-treated BV2 2-DE maps, but present in $A\beta_{25-35}$-stimulated BV2 2-DE profile (Fig. 3). The second protein is the ε isoform of the protein 14-3-3, a family of conserved regulatory molecules expressed in all eukaryotic cells. This latter proteome signature was also validated by Western blot analysis, challenging the BV2 cytosolic fraction with the antibody specific for the ε isoform of the 14-3-3 proteins (Fig. 4A). This result confirmed the significant increase (*p*-value of 0.025 versus control) in the cytosolic copies of the 14-3-3ε that accompany microglia into the late response to the amyloidogenic peptide. Conversely, a decrease in the level of the entire protein family has been proved, screening the same lysates with an antibody able to recognize all 14-3-3 isoforms (*p*-value of 0.002 versus control; Fig. 4B). Since differential analysis of protein spots did not highlight any significant decrease in Coomassie densities for the other 14-3-3 isoforms (Fig. 2), the immunoblotting result could be justified by a mild overall downregulation of the components of this protein family.

3.3 Protein profile of microglial cells stimulated by a nonamyloidogenic peptide

To discriminate between specific and nonspecific responses of microglia to amyloidogenic peptides, we also challenged

BV2 cell culture with the $A\beta_{35-25}$ reverse peptide, known to be unable to trigger a proinflammatory response ([23]; Fig. 1). 2-DE maps from cytosolic and membrane/organelle fractions were also then obtained from these proteomes (Fig. 2 and Table 1). Only Hsp 60 was found to be downregulated in both $A\beta_{25-35}$- and $A\beta_{35-25}$-treated samples. Conversely, a diverse responsive pathway of microglia to the reverse peptide could be depicted by a downregulation of unique eight proteins (ferritin light chain 1/2, serine hydroxymethyltransferase and D-3-phosphoglycerate dehydrogenase, in the cytosolic fraction; calreticulin, endoplasmin, glycerol-3-phosphate dehydrogenase, heat shock 71 kDa protein, and cytochrome *b*–*c*1 complex subunit 1, in the membrane/organelle fraction).

3.4 Comparison between changes in proteomes from $A\beta_{25-35}$-activated cells versus $A\beta_{35-25}$-activated cells

Quantitative changes observed in the densitometric comparison between 2-DE gel spots of $A\beta_{25-35}$-activated cells versus $A\beta_{35-25}$-treated cells were also investigated. Few protein spots showed $\geq$2-fold changes in intensity (Table 1). Apart from the more acidic species of the cytosolic actin and the 14-3-3ε, the changes in expression of the other proteins do not correlate with those observed when $A\beta_{35-25}$-treated cells are compared with the resting status. In our opinion, this result rules out the use of $A\beta_{35-25}$-treated cells as a control state of a neuroinflammatory activation of microglia, at least at the proteomic level.

4 Discussion

Microglia with a morphologically activated phenotype are abundant in CNS tissues extracted from patients with chronic neurodegenerative diseases, including AD [7]. In vitro activation of cultured microglia by Aβ has been used as a model experimental system to mimic the effects of the interaction of microglia with Aβ in AD brains. The molecular signature of Aβ-activated microglial cells has been evidenced up to now by functional genomic studies [26–28], whereas no proteomic data are still available.

Hence, in the current study, we used a differential proteomic approach to investigate the phenotypic alteration induced on Aβ-stimulated microglia. Because of the limited microglia proliferation capacity, we utilized murine BV2 cells, an immortalized cell line frequently used as substitute for primary microglia. With the aim to settle experimental conditions able to produce stable replicates, we decided to start the proteomic analysis of microglia activation using $A\beta_{25-35}$, that is considered as efficient modulator of microglia [26, 29], even if revealed as just a possible component of human amyloid [22], and although the toxicological and oxidative effects on neuronal cells take place with a mechanism only partially overlapping with the neuronal activity of the full-length peptide [19].

AD is a chronic subacute degenerative disease and the effects of Aβ accumulation in the brain are suspected to require a number of years to become clinically manifest. Changes in gene expression of microglia after a time of stimulation shorter than 24 h (acute) were already reported in the previous studies [26–28, 30]. To depict a picture, proteome-based, resembling that of microglia under a chronic activation, we here focus specifically on the early phase of the long-term activation of microglia exposed to the pathological perturbation. To this purpose, we built our investigation based on the selection of an immortalized cell line, which allowed us to analyze proteomic responsiveness over a longer temporal threshold.

To discriminate between specific and nonspecific responses of BV2 cells to amyloidogenic injury, we also challenged BV2 cell cultures with the reverse peptide. Our results show that $A\beta_{25-35}$, but not its reverse peptide, was able to upregulate the mRNA expression of TNF-α after 4 h of treatment and to inhibit the cellular MTT reduction at 24 h. The inhibition in MTT reduction observed in our experiments after $A\beta_{25-35}$ treatment is associated with an increased cell proliferation with respect to the untreated control cells or to those treated with the reverse peptide. It is worth noting that amyloidogenic peptides (such as $A\beta_{1-41}$, $A\beta_{1-40}$, and $A\beta_{25-35}$) have been demonstrated to inhibit cellular MTT reduction not because they kill the cells but because they dramatically enhance the exocytosis of MTT formazan-containing vesicles [31, 32] and this can help to explain the apparent discrepancy between the inhibition of MTT reduction and the increased cell number observed in our experiments after $A\beta_{25-35}$ treatment.

Proteomic analyses of control and stimulated cells were performed on diverse cellular fractions in order to simplify protein mixtures and consequently improve the chances of protein identification.

The generally accepted approach to a comparative study would have been to compare the amyloidogenic sample to a resting cell. Therefore, to unambiguously depict the responsive molecular profile of $A\beta_{25-35}$-treated cells, proteome comparisons were then performed against untreated cells. The results, summarized in Table 1, show only seven proteins involved in the signature of the amyloidogenic peptide-activated microglia. Most of the identified proteins show a decrease in their expression level, indicating a general lowering of microglia proteostasis. This effect is also shared by the reverse peptide-treated cells. However, the high plasticity of microglia, not being yet fully clarified on a molecular level, imposed us to approach the discovery of biomarkers of neuroinflammatory response also though a direct proteome comparison between 2-DE gel patterns of extracts from $A\beta_{25-35}$-treated cells versus $A\beta_{35-25}$ nonamyloid-activated cells. Results obtained suggest that proteomes of $A\beta_{25-35}$- and $A\beta_{35-25}$-treated cells are actually distinctive, each being representative of two different response pathways

Table 1. Summary of regulated proteins in BV2 cells

Entry name[a]	Protein name[b]	Quantitative change[c] (±SEM)			2-DE parameters				MOWSE Score	Sequence coverage (%)/matched peptides
					Theoretical		Measured			
		$A\beta_{25-35}$ versus untreated cells	$A\beta_{25-25}$ versus untreated cells	$A\beta_{25-35}$ versus $A\beta_{35-25}$	MW (kDa)	p/	MW (kDa)	p/		
ACTB_MOUSE[d] ACTG_MOUSE	Actin, acidic variant of isoforms β and γ	▲[e]	Not present	▲[e]	42.1	5.3	42	5.2[e]	124	46/15
CALR_MOUSE	Calreticulin	1±0.05	▼0.47±0.07	▲2.1±0.2	48.1	4.3	53	4.5	60	32/6
CH60_MOUSE	60 kDa Hsp, Hsp 60, mitochondrial	▼0.2±0.05	▼0.46±0.2	▼0.32±0.1	61.1	5.3	59	6.2	139	29/15
ENPL_MOUSE	Endoplasmin	1.4±0.2	▼0.24±0.1	▲5.8±0.8	92.7	4.7	92	5.1	207	35/27
FRIL1_MOUSE[d] FRIL2_MOUSE	Ferritin light chain, isoforms 1 and 2	1±0.3	▼0.46±0.1	▼0.32±0.1	20.8 20.9	5.6 6.4	19	5.7	133 77	57/1140/9
GLYC_MOUSE	Serine hydroxymethyltransferase, cytosolic isoform	0.71±0.2	▼0.43±0.1	1.6±0.1	52.5	6.5	51	6.8	99	20/20
GPDM_MOUSE	Glycerol-3-phosphate dehydrogenase, mitochondrial	1±0.4	▼0.43±0.04	▲2.3±0.1	80.9	6.2	74	6.4	55	16/10
HSP7C_MOUSE	Heat shock cognate 71 kDa protein	0.93±0.1	▼0.47±0.05	▲2±0.1	71.1	5.4	72	5.7	169	47/22
HS90A_MOUSE[d] HS90B_MOUSE	Hsp 90, isoforms α and β	▼0.38±0.1	0.70±0.2	0.6±0.1	84.7 83.3	4.9	95	5.8	80 86	20/12 21/12
LDHA_MOUSE	L-Lactate dehydrogenase A chain	▼0.48±0.07	1.0±0.1	▼0.48±0.08	36.8	7.6	37	7.4	92	34/12
LEG3_MOUSE	Galectin 3	▼0.38±0.06	0.8±0.1	0.5±0.1	27.6	8.5	38	9.0	85	40/10
PRDX4_MOUSE	Peroxiredoxin 4	▼0.34±0.08	0.7±0.1	▼0.43±0.04	26.4	6.6	26	6.4	112	37/9
PRDX3_MOUSE	Peroxiredoxin 3 (thioredoxin-dependent peroxide reductase, mitochondrial)	▼0.36±0.1	0.9±0.1	▼0.39±0.1	21.5	5.7	23	6.3	74	26/7
QCR1_MOUSE	Cytochrome *b*-*c*1 complex subunit 1, mitochondrial	1.0±0.1	▼0.45±0.06	▲2.2±0.2	52.7	5.7	49	5.7	143	34/12
SERA_MOUSE	D-3-phosphoglycerate dehydrogenase	0.9±0.12	▼0.48±0.07	▲2.5±0.4	56.5	6.1	64	6.6	197	36/19
TOM70_MOUSE	Mitochondrial import receptor subunit TOM70	▼0.2±0.1	0.8±0.1	▼0.3±0.1	67.4	7	58	6.4	85	18/12
1433E_MOUSE	14-3-3 Protein, ε isoform	▲2.3±0.2	0.8±0.1	▲2.0±0.3	29.3	4.6	31	4.8	11	48/13

a) UniProtKB protein identifier.
b) Proteins were identified by MALDI-TOF-MS. Identifications were accepted when the probability-based MOWSE protein score was significant according to MASCOT.
c) Up (▲) and down (▼) regulation were determined by comparison of the 2-DE Coomassie spot densities from two biological replicates (cell lysate fractions) and three technical replicates ($n = 5$) following treatment with amyloid peptide ($A\beta_{25-35}$) and its reverse peptide ($A\beta_{35-25}$). Quantitative data were achieved by PDQuest software, compared with control. Only two-fold increase/decrease was accepted. Ratio of the spot densities is reported.
d) Protein isoforms differentially identified in the same spot through distinctive peptides.
e) Referred to the actin species present only in 2-DE map of $A\beta_{25-35}$-treated cells (Fig. 3). This actin species shows an experimental p/ more acidic than the experimental p/ of actin isoforms found in all three samples (labeled with a diamond in Fig. 2).

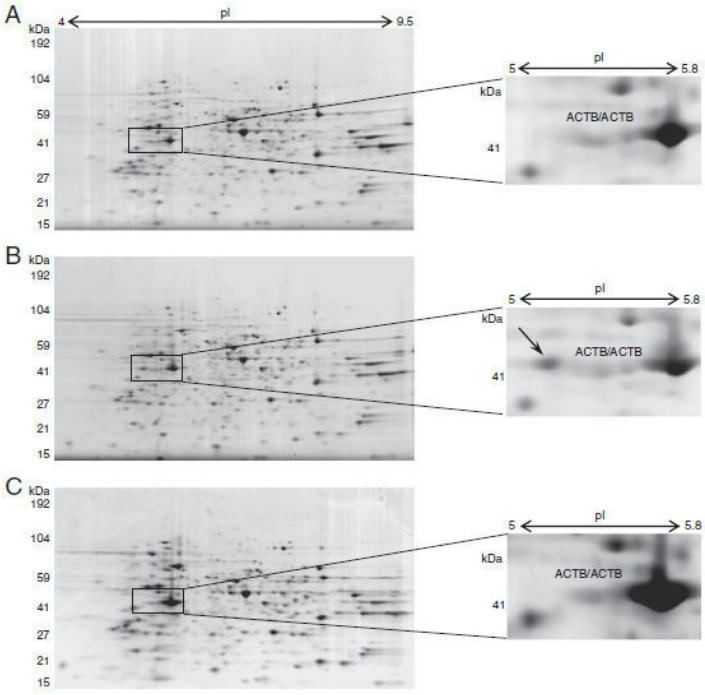

Figure 3. Effects of $A\beta_{25-35}$ and $A\beta_{35-25}$ on the abundance of an acidic isoform of actin. Representative 2DE maps of the cytosolic fraction of resting (A), $A\beta_{25-35}$ (B) and $A\beta_{35-25}$ (C) treated BV2 cells, zoomed in to focus on an acidic isoform of actin (arrow), found uniquely expressed in $A\beta_{25-35}$ samples. The pI gradient of the first dimension is given on the X-axis, and the migration of molecular mass markers for the second dimension on the Y-axis. MALDI-TOF identification of the actin isoform present in all BV2 is also reported.

(Table 1), and then in our opinion the proteome of cells treated with nonamyloidogenic peptide $A\beta_{35-25}$ could not be used as proteomic control. In the case of $A\beta_{25-35}$, it has been suggested that these peptides may aggregate in oligomeric structures, which in turn bring about molecular pores that could colonize the membrane and then alter the barrier of the lipid bilayer [33]. This is not the case of the reverse peptide, where the effect on proteomic profile may be only due to a transient disturbance of the lipid bilayer.

Proteomic studies, including the one presented here, are proving an essential tool in depicting the molecular bases of the microglia action [15, 16]. Diverse substances could induce different activation programs, and the detection of biomarkers could be useful in highlighting the molecular pathway, leading to the specific cellular response. In microglia trigged to an immune response by amyloidogenic peptide, two proteins are demonstrated to increase in 2-DE maps. One of these, a more acidic species of the cytosolic actin (Fig. 3), is detectable only in the amyloid-treated cells; this actin variant may be specifically involved in the morphological change during the transition from resting to the activated cells [34, 35]. In fact, the first trait of microglial activation is the change in the cytoskeletal architecture, which ultimately leads to the loss of the membranous processes and to the acquisition of amoeboid features [36]. Furthermore, actin reorganization may be a prerequisite for macropinocytosis, an event involved in the intracellular removal of soluble Aβ in both in vivo and in vitro microglial cells [37]. Finally, when microglia act as a phagocyte, different states of actin cytoskeleton can enhance assembly and activity of NADPH oxidase, a multicomponent enzyme complex that, upon activation, produces the highly reactive free radical superoxide [38].

The other upregulated proteome component revealed in the current differential proteomic approach is the 14-3-3ε protein. This isoform is a member of the 14-3-3 protein family involved in multiple cell processes, as proliferation, differentiation, transformation, and apoptosis [39, 40]. These proteins are expressed in all cell types and tissues, and are coded by seven different genes in mammals. They are constitutively associated to form homo/heterodimers. A wide array of regulative functions has been assigned to these proteins, ranging from protein–protein interactions and enzyme activity to subcellular localization, DNA binding, and transcriptional activity. The importance of the 14-3-3 protein family in the neuronal compartment and their participation in neurodegenerative disease is today an established issue [41]. In cerebrospinal fluid (CSF), 14-3-3

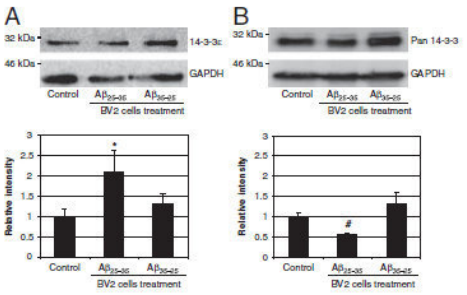

Figure 4. Effects of $A\beta_{25-35}$ and $A\beta_{35-25}$ on the expression of 14-3-3 proteins. Immunodetection of the ε isoform of the 14-3-3 protein (A) and of the entire 14-3-3 family (B) in the cytosolic fraction of lysates from untreated BV2 cells (control) and cells treated for 24 h with 50 μM $A\beta_{25-35}$ or $A\beta_{35-25}$, respectively. Quantitative data were collected from two independent cell preparations from which three Western blot replica were carried out ($n = 5$). Electrophoretic molecular markers are also shown on the left side (kDa). To quantify protein expression, optical density relative to the 14-3-3ε band in each sample is normalized to the corresponding GADPH optical density and averaged (±SD). Statistical analysis was performed by Student' *T*-test; **p*-value of 0.05 versus control; #*p*-value of 0.002 versus control.

proteins have long been associated with the establishment of neurodegenerative diseases including AD [42], and to date their presence in cerebrospinal fluid is able to assist in the diagnosis of Creutzfeldt–Jakob disease [43]. In the glia compartment, the isoforms γ and ζ were correlated to the immune response and to the secretion of proinflammatory cytokines in the models of Parkinson's disease [44], and an altered level of isoforms ε, γ, and ζ were found in the hippocampus of AD patients [45]. Furthermore, in astrocytes, which together with microglia represent the reactive cells of nervous system, the 14-3-3ε seems to play a role in the reorganization of intermediate filaments network, and its overexpression is a marker of activation following the demyelination process [46]. This isoform is also present at high level specifically in several brain regions of patients with AD [41, 47] although its role in AD pathogenesis is still unclear. Despite an increasing general concern on this protein family, very limited data are today available for the presence and the functional role of 14-3-3 in microglia cells.

In order to validate the results of the 14-3-3 activation by $A\beta_{25-35}$ peptide, BV2 cells were also challenged with the naturally occurring form $A\beta_{1-42}$. Preliminary experiments indicated that when activation occurs in BV2 cells challenged with $A\beta_{1-42}$, according to the procedure described by Nichols' group [48], a slight increase (1.5-fold) of the 14-3-3ε could be observed by Western blotting (data not shown) although these results were poorly reproducible, possibly due to the physical–chemical features of the $A\beta_{1-42}$ peptide. Nevertheless, the data generated up to now appear to prove that a similar molecular pathway is evoked by both $A\beta_{25-35}$ and $A\beta_{1-42}$ peptides.

Our data show that 14-3-3ε protein expression is significantly increased after a 24-h stimulation with $A\beta_{25-35}$, whereas the other members of the family decreased (Fig. 4). The exclusive upregulation of this isoform confirms this protein as a peculiar switch in the signaling sorting of the microglia long-term activation and paves the way to explore the recruitment pathway which tunes BV2 activation.

This work has been partly supported by a grant from the Ministero dell'Istruzione dell'Università e della Ricerca (MIUR) to M.E.S. and to B.M. (PRIN, project 20078RWJBN_004). The authors acknowledge the precious help of Alessandra Franco for technical and editorial assistance.

The authors have declared no conflict of interest.

5 References

[1] Blennow, K., de Leon, M. J., Zetterberg, H., Alzheimer's disease. *Lancet* 2006, *368*, 387–403.

[2] Goedert, M., Spillantini, M. G., A century of Alzheimer's disease. *Science* 2006, *314*, 777–781.

[3] Kang, J., Lemaire, H. G., Unterbeck, A., Salbaum, J. M. et al., The precursor of Alzheimer's disease amyloid A4 protein !resembles a cell-surface receptor. *Nature* 1987, *325*, 733–736.

[4] Maler, J. M., Klafki, H. W., Paul, S., Spitzer, P. et al., Urea-based two-dimensional electrophoresis of beta-amyloid peptides in human plasma: evidence for novel Aβ species. *Proteomics* 2007, *7*, 3815–3820.

[5] Hardy, J. A., and Higgins, G. A., Alzheimer's disease: The amyloid cascade hypothesis. *Science* 1992, *256*, 184–185.

[6] Lansbury, P. T., Lashuel, H. A., A century-old debate on protein aggregation and neurodegeneration enters the clinic. *Nature* 2006, *443*, 774–779.

[7] Ransohoff, R. M., Perry, V. H., Microglial physiology: Unique stimuli, specialized responses. *Annu. Rev. Immunol.* 2009, *27*, 119–145.

[8] Perry, V. H., Nicoll, J. A. R., Holmes, C., Microglia in neurodegenerative disease. *Nat. Rev. Neurol.* 2010, *6*, 193–201.

[9] Frautschy, S. A., Yang, F., Irrizarry, M., Hyman, B. et al., Microglial response to amyloid plaques in APPsw transgenic mice. *Am. J. Pathol.* 1998, *152*, 307–317.

[10] Sheng, J. G., Mrak, R. E., Griffin, W. S. T., Neuritic plaque evolution in Alzheimer's disease is accompanied by transition of activated microglia from primed to enlarged to phagocytic forms. *Acta Neuropathol.* 1997, *94*, 1–5.

[11] Eikelenboom, P., Veerhuis, R., Familian, A., Hoozemans, J. J. M. et al., Neuroinflammation in plaque and vascular β-amyloid disorders: clinical and therapeutic implications. *Neurodegener. Dis.* 2008, *5*, 190–193.

[12] Akiyama, H., Barger, S., Barnum, S., Bradt, B. et al., Inflammation and Alzheimer's disease. *Neurobiol. Aging* 2000, *21*, 383–421.

[13] Shibata, A., Zelivyanskaya, M., Limoges, J., Carlson, K. A. et al., Peripheral nerve induces macrophage neurotrophic activities: regulation of neuronal process outgrowth, intracellular signaling and synaptic function. *J. Neuroimmunol.* 2003, *142*, 112–129.

[14] Serrano-Pozo, A., Mielke, M. L., Gómez-Isla, T., Betensky, R. A. et al., Reactive Glia not only associates with plaques but also parallels tangles in Alzheimer's disease. *Am. J. Pathol.* 2011 *179*, 373–384.

[15] Zhou, Y., Wang, Y., Kovacs, M., Jin, J. et al., Microglial activation induced by neurodegeneration: a proteomic analysis. *Mol. Cell. Proteomics* 2005, *4*, 1471–1479.

[16] Glanzer, J. G., Enose, Y., Wang, T., Kadiu, I. et al., Genomic and proteomic microglial profiling: pathways for neuroprotective inflammatory responses following nerve fragment clearance and activation. *J. Neurochem.* 2007, *102*, 627–645.

[17] Blasi, E., Barluzzi, R., Bocchini, V., Mazzolla, R. et al., Immortalization of murine microglial cells by a v-raf/v-myc carrying retrovirus. *J. Neuroimmunol.* 1990, *27*, 229–237.

[18] Henn, A., Lund, S., Hedtjärn, M., Schrattenholz, A. et al., The suitability of BV2 cells as alternative model system for primary microglia cultures or for animal experiments examining brain inflammation. *ALTEX* 2009, *26*, 83–94.

[19] Varadarajan, S., Kanski, J., Aksenova, M., Lauderback, C., Butterfield, D. A., Different mechanisms of oxidative stress and neurotoxicity for Alzheimer's Aβ(1-42) and Aβ(25-35). *J. Am. Chem. Soc.* 2001, *123*, 5625–5631.

[20] Hansen, M. B., Nielsen, S. E., Berg, K., Re-examination and further development of a precise and rapid dye method for measuring cell growth/cell kill. *J. Immunol. Methods* 1989, *119*, 203–210.

[21] Giorgi, A., Di Francesco, L., Principe, S., Mignogna, G. et al., Proteomic profiling of PrP27-30-enriched preparations extracted from the brain of hamsters with experimental scrapie. *Proteomics* 2009, *9*, 3802–3814.

[22] Kaminsky, Y. G., Marlatt, M. W., Smith, M. A., Kosenko, E. A., Subcellular and metabolic examination of amyloid-beta peptides in Alzheimer disease pathogenesis: evidence for Abeta(25-35). *Exp. Neurol.* 2010, *221*, 26–37.

[23] Ito, S., Sawada, M., Haneda, M., Fujii, S. et al., Amyloid-β peptides induce cell proliferation and macrophage colony-stimulating factor expression via the PI3-kinase/Akt pathway in cultured Ra2 microglial cells. *FEBS Lett.* 2005, *579*, 1995–2000.

[24] Takata, K., Kitamura, Y., Tsuchiya, D., Kawasaki, T. et al., Heat shock protein-90-induced microglial clearance of exogenous amyloid-β_{1-42} in rat hippocampus in vivo. *Neurosci. Lett.* 2003, *344*, 87–90.

[25] Hansson Petersen, C. A., Alikhani, N., Behbahani, H., Wiehager, B. et al., The amyloid β-peptide is imported into mitochondria via the TOM import machinery and localized to mitochondrial cristae. *Proc. Natl. Acad. Sci. USA* 2008, *105*, 13145–13150.

[26] Walker, D. G., Lue, L. F., Beach, T. G., Gene expression profiling of amyloid beta peptide-stimulated human post-mortem brain microglia. *Neurobiol. Aging* 2001, *22*, 957–966.

[27] Gan, L., Ye, S., Chu, A., Anton, K. et al., Identification of cathepsin B as a mediator of neuronal death induced by Aβ-activated microglial cells using a functional genomics approach. *J. Biol. Chem.* 2004, *279*, 5565–5572.

[28] Walker, D. G., Link, J., Lue, L. F., Dalsing-Hernandez, J. E., Boyes, B. E., Gene expression changes by amyloid βpeptide-stimulated human postmortem brain microglia identify activation of multiple inflammatory processes. *J. Leukoc. Biol.* 2006, *79*, 596–610.

[29] Gengler, S., Gault, V. A., Harriott, P., Hölscher, C., Impairments of hippocampal synaptic plasticity induced by aggregated beta-amyloid (25-35) are dependent on stimulation-protocol and genetic background. *Exp. Brain Res.* 2007, *179*, 621–630.

[30] Garção, P., Oliveira, C. R., Agostinho, P., Comparative study of microglia activation induced by amyloid-beta and prion peptides: role in neurodegeneration. *J. Neurosci. Res.* 2006, *84*, 182–193.

[31] Liu, Y., Schubert, D., Cytotoxic amyloid peptides inhibit cellular 3-(4,5-dimethylthiazol-2-yl)-2,5-diphenyltetrazolium bromide (MTT) reduction by enhancing MTT formazan exocytosis. *J. Neurochem.* 1997, *69*, 2285–2293.

[32] Kreutzmann, P., Wolf, G., Kupsch, K., Minocycline recovers MTT-formazan exocytosis impaired by amyloid beta peptide. *Cell. Mol. Neurobiol.* 2010, *30*, 979–984.

[33] Jang, H., Zheng, J., Lal, R., Nussinov, R., New structures help the modeling of toxic amyloid βion channels. *Trends Biochem. Sci.* 2008, *33*, 91–100.

[34] Plantier, M., Der Terrossian, E., Represa, A., β-Actin immunoreactivity in rat microglial cells: developmental pattern and participation in microglial reaction after kainate injury. *Neurosci. Lett.* 1998, *247*, 49–52.

[35] Abd-El-Basset, E. M., Prashanth, J., Ananth Lakshmi, K. V. V., Up-regulation of cytoskeletal proteins in activated microglia. *Med. Princ. Pract.* 2004, *13*, 325–333.

[36] Bernhart, E., Kollroser, M., Rechberger, G., Reicher, H. et al., Lysophosphatidic acid receptor activation affects the C13NJ microglia cell line proteome leading to alterations in glycolysis, motility, and cytoskeletal architecture. *Proteomics* 2010, *10*, 141–158.

[37] Mandrekar, S., Jiang, Q., Lee, C. Y. D., Koenigsknecht-Talboo, J. et al., Microglia mediate the clearance of soluble Aβ through fluid phase macropinocytosis. *J. Neurosci.* 2009, *29*, 4252–4262.

[38] Rasmussen, I., Pedersen, L. H., Byg, L., Suzuki, K. et al., Effects of F/G-actin ratio and actin turn-over rate on NADPH oxidase activity in microglia. *Biomed. Chromatogr. Immunol.* 2010, *11*, 44.

[39] Aitken, A., 14-3-3 Proteins: A historic overview. *Semin. Cancer Biol.* 2006, *16*, 162–172.

[40] Morrison, D. K., The 14-3-3 proteins: integrators of diverse signaling cues that impact cell fate and cancer development. *Trends Cell Biol.* 2009, *19*, 16–23.

[41] Berg, D., Holzmann, C., Riess, O., 14-3-3 Proteins in the nervous system. *Nat. Rev. Neurosci.* 2003, *4*, 752–762.

[42] Jayaratnam, S., Khoo, A. K., Basic, D., Rapidly progressive Alzheimer's disease and elevated 14-3-3 proteins in cerebrospinal fluid. *Age Ageing* 2008, *37*, 467–469.

[43] Zerr, I., Pocchiari, M., Collins, S., Brandel, J. P. et al., Analysis of EEG and CSF 14-3-3 proteins as aids to the diagnosis of Creutzfeldt-Jakob disease. *Neurology* 2000, *55*, 811–815.

[44] Reynolds, A. D., Stone, D. K., Mosley, R. L., Gendelman, H. E., Proteomic studies of nitrated alpha-synuclein microglia regulation by $CD4^+CD25^+$ T cells. *J. Proteome Res.* 2009, *8*, 3497–3511.

[45] Di Domenico, F., Owen, J. B., Sultana, R., Sowell, R. A. et al., The wheat germ agglutinin-fractionated proteome of subjects with Alzheimer's disease and mild cognitive impairment hippocampus and inferior parietal lobule: implications for disease pathogenesis and progression. *J. Neurosci. Res.* 2010, *88*, 3566–3577.

[46] Satoh, J., Yamamura, T., Arima, K., The 14-3-3 protein epsilon isoform expressed in reactive astrocytes in demyelinating lesions of multiple sclerosis binds to vimentin and glial fibrillary acidic protein in cultured human astrocytes. *Am. J. Pathol.* 2004, *165*, 577–592.

[47] Layfield, R., Fergusson, J., Aitken, A., Lowe, J. et al., Neurofibrillary tangles of Alzheimer's disease brains contain 14-3-3 proteins. *Neurosci. Lett.* 1996, *209*, 57–60.

[48] Ajit, D., Udan, M. L., Paranjape, G., Nichols, M. R., Amyloid-beta(1-42) fibrillar precursors are optimal for inducing tumor necrosis factor-alpha production in the THP-1 human monocytic cell line. *Biochemistry* 2009, *48*, 9011–9021.

